ASTRONOMICAL INSTITUTE
SLOVAK ACADEMY OF SCIENCES

# CONTRIBUTIONS OF THE ASTRONOMICAL OBSERVATORY SKALNATÉ PLESO

• VOLUME LI •

Number 2


June 2021

ISSN: 1336–0337 (on-line version)

CODEN: CAOPF8

Editorial Office: Astronomical Institute of the Slovak Academy of Sciences
SK - 059 60 Tatranská Lomnica, The Slovak Republic

# CONTENTS

## STARS

The Contributions of the Astronomical Observatory Skalnaté Pleso
are available in a full version
in the frame of ADS Abstract Service
and can be downloaded in a usual way from the URL address:

**https://ui.adsabs.harvard.edu/**

as well as from the web-site of
the Astronomical Institute of the Slovak Academy of Sciences
on the URL address:

**https://www.astro.sk/caosp/caosp.php**

The journal is covered/indexed by:

**Thomson Reuters services (ISI)**
Science Citation Index Expanded (also known as SciSearch®)
Journal Citation Reports/Science Edition

**SCOPUS**

Contrib. Astron. Obs. Skalnaté Pleso **51**, 103 – 117, (2021)
https://doi.org/10.31577/caosp.2021.51.2.103

# Photometry and spectroscopy of the new symbiotic star 2SXPS J173508.4-292958

**U. Munari[1], P. Valisa[2], A. Vagnozzi[2], S. Dallaporta[2], F.-J. Hambsch[2] and A. Frigo[2]**

[1] *INAF Padova Astronomical Observatory, I-36012 Asiago (VI), Italy*
[2] *ANS Collaboration, Astronomical Observatory, 36012 Asiago (VI), Italy*

Received: December 2, 2020; Accepted: December 21, 2020

**Abstract.** We present and discuss the results of our photometric and spectroscopic monitoring of 2SXPS J173508.4-292958 carried out from April to August 2020. This X-ray source, in the foreground with respect to the Galactic center, brightened in X-rays during 2020, prompting our follow-up optical observations. We found the star to contain a K4III giant with a modest but highly variable H$\alpha$ emission, composed by a $\sim$470 km s$^{-1}$ wide component with superimposed a narrow absorption, offset by a positive velocity with respect to the giant. No orbital motion is detected for the K4III, showing an heliocentric radial velocity stable at $-12\pm1$ km s$^{-1}$. No flickering in excess of 0.005 mag in $B$ band was observed at three separate visits of 2SXPS J173508.4-292958. While photometrically stable in 2016 through 2018, in 2019 the star developed a limited photometric variability, that in 2020 took the form of a sinusoidal modulation with a period of 38 days and an amplitude of 0.12 mag in $V$ band. We argue this variability cannot be ascribed to Roche-lobe filling by the K4III star. No correlation is observed between the photometric variability and the amount of emission in H$\alpha$, the latter probably originating directly from the accretion disk around the accreting companion. While no emission from dust is detected at mid-IR wavelengths, an excess in $U$-band is probably present and caused by direct emission from the accretion disk. We conclude that 2SXPS J173508.4-292958 is a new symbiotic star of the accreting-only variety (AO-SySt).

**Key words:** binaries: symbiotic

## 1. Introduction

Attention to the X–ray source 2SXPS J173508.4-292958 has been recently driven by a report from Heinke et al. (2020) about a brightening of the object they observed in X–rays with the Swift satellite in April 2020. Noting the positional coincidence with the cool 2MASS star 17350831-2929580 of Ks=7.4 mag, Heinke et al. suggested that 2SXPS J173508.4-292958 could be a previously unknown symbiotic star. The optical counterpart was quickly subjected to BVRI photometry and high- and low-resolution spectroscopy by Munari et al. (2020a) that found 2SXPS J173508.4-292958 to host a K4 III/II giant, with marked

near-UV excess and H$\alpha$ in emission, the latter showing a broad profile with a central absorption. Such properties confirm a probable symbiotic nature for 2SXPS J173508.4-292958 (for a recent global review of symbiotic stars see Munari 2019). In this paper we report about the results of our follow-up photometric and spectroscopic campaign to monitor 2SXPS J173508.4-292958 (2SXPS for short in the rest of this paper) during the period of seasonal visibility in 2020.

## 2. Observations

Our observations have been carried out primarily from Italy. At such northern latitudes, the $-29^\circ$ declination of 2SXPS implies a very short observing window, $\sim$2 hours around transit at meridian at just 15 to 20° above horizon. Such a short observing interval coupled with the large atmospheric extinction and seeing degradation led to a lower-than-usual S/N for our observations, and argued against employing the highest possible resolution in the spectroscopic observations.

### 2.1. $BVRI$ photometry

We have obtained optical photometry of 2SXPS in the Landolt photometric system from late April to early August 2020 with two telescopes operated by ANS Collaboration. ID 0310 is a 0.30m f/8 Richey-Chretien telescope located in Cembra (TN, Italy) and equipped with an SBIG ST-8 CCD camera, 1530×1020 array, 9 $\mu$m pixels $\equiv 0.77''$/pix, with a field of view of $19'\times13'$. ID 1301 is a 0.50m f/6 Ritchey-Chretien telescope located in Stroncone (TR, Italy). It feeds light to an SBIG STL1001E CCD Camera 1024×1024 array, 24 $\mu$m pixels $\equiv 1.60''$/pix, field of view of $28'\times28'$. Both telescopes adopt $BVR_CI_C$ photometric filters from Astrodon, in the version corrected for red-leak.

Data reduction has involved all the usual steps for bias, dark and flat with calibration images collected during the same observing nights. We adopted aperture photometry because the sparse field around 2SXPS did not required PSF-fitting procedures. The transformation from the local to the Landolt standard system was carried out via color equations calibrated on a photometric sequence recorded on the same frames as 2SXPS:

$$\begin{aligned} V &= v + \alpha_v \times (v-i) + \gamma_v \\ B-V &= \beta_{bv} \times (b-v) + \delta_{bv} \\ V-R &= \beta_{vr} \times (v-r) + \delta_{vr} \\ V-I &= \beta_{vi} \times (v-i) + \delta_{vi} \end{aligned}$$

where lowercase and uppercase letters denote values in the local and and in the standard system, respectively. The local photometric sequence has been extracted from APASS DR8 survey (Henden et al. 2016), ported to the Landolt

**Table 1.** Our BVRI photometry on the Landolt system of 2SXPS J173508.4-292958.

| HJD | date | B | err | V | err | R | err | I | err | ID |
|---|---|---|---|---|---|---|---|---|---|---|
| 8962.57973 | 2020-04-23.080 | 13.489 | 0.008 | 11.846 | 0.005 | 10.904 | 0.007 | 9.935 | 0.015 | 0310 |
| 8962.57973 | 2020-04-23.080 | 13.490 | 0.008 | 11.848 | 0.005 | 10.906 | 0.007 | 9.935 | 0.015 | 0310 |
| 8963.57773 | 2020-04-24.078 | 13.426 | 0.008 | 11.835 | 0.006 | 10.974 | 0.007 | 9.890 | 0.011 | 1301 |
| 8963.58953 | 2020-04-24.090 | 13.444 | 0.009 | 11.851 | 0.007 | 10.911 | 0.008 | 9.898 | 0.015 | 0310 |
| 8971.58456 | 2020-05-02.085 | 13.417 | 0.009 | 11.788 | 0.007 | 10.835 | 0.008 | 9.893 | 0.013 | 0310 |
| 8974.57796 | 2020-05-05.078 | 13.387 | 0.024 | 11.757 | 0.008 | 10.856 | 0.008 | 9.866 | 0.009 | 0310 |
| 8978.53534 | 2020-05-09.035 | 13.376 | 0.010 | 11.780 | 0.005 | 11.174 | 0.005 | 0.103 | 0.005 | 1301 |
| 8990.53842 | 2020-05-21.038 | 13.466 | 0.008 | 11.840 | 0.007 | 10.924 | 0.008 | 9.936 | 0.012 | 0310 |
| 8990.56051 | 2020-05-21.061 | 13.442 | 0.017 | 11.861 | 0.008 | | | 9.913 | 0.012 | 0310 |
| 8991.50080 | 2020-05-22.001 | 13.452 | 0.006 | 11.843 | 0.004 | 10.917 | 0.003 | 9.903 | 0.008 | 1301 |
| 8992.50328 | 2020-05-23.003 | 13.512 | 0.007 | 11.859 | 0.003 | 10.917 | 0.004 | 9.893 | 0.009 | 1301 |
| 8993.54900 | 2020-05-24.049 | 13.496 | 0.007 | 11.871 | 0.004 | 10.927 | 0.004 | 9.912 | 0.011 | 1301 |
| 8994.54993 | 2020-05-25.050 | 13.444 | 0.013 | 11.852 | 0.006 | 10.955 | 0.010 | 9.944 | 0.008 | 0310 |
| 8995.51675 | 2020-05-26.017 | 13.486 | 0.009 | 11.901 | 0.008 | 10.908 | 0.008 | 9.944 | 0.012 | 0310 |
| 8995.53700 | 2020-05-26.037 | 13.469 | 0.013 | 11.837 | 0.008 | | | 9.945 | 0.010 | 0310 |
| 8995.54481 | 2020-05-26.045 | | | 11.852 | 0.002 | 10.961 | 0.002 | 0.044 | 0.005 | 1301 |
| 8996.50775 | 2020-05-27.008 | 13.508 | 0.007 | 11.896 | 0.004 | 10.937 | 0.005 | 9.932 | 0.011 | 0310 |
| 8996.52131 | 2020-05-27.021 | | | 11.874 | 0.006 | | | 9.919 | 0.010 | 0310 |
| 8996.56371 | 2020-05-27.064 | 13.395 | 0.010 | 11.866 | 0.004 | 10.954 | 0.004 | 9.927 | 0.006 | 1301 |
| 8997.51757 | 2020-05-28.018 | 13.481 | 0.007 | 11.870 | 0.006 | 10.927 | 0.006 | 9.914 | 0.013 | 0310 |
| 8997.53240 | 2020-05-28.032 | 13.411 | 0.010 | 11.839 | 0.005 | 10.914 | 0.003 | 9.883 | 0.005 | 1301 |
| 8998.52015 | 2020-05-29.020 | 13.480 | 0.010 | 11.828 | 0.005 | 10.979 | 0.011 | 9.923 | 0.012 | 0310 |
| 9012.45686 | 2020-06-11.957 | 13.416 | 0.007 | 11.804 | 0.004 | 10.835 | 0.005 | 9.883 | 0.015 | 0310 |
| 9012.53045 | 2020-06-12.030 | 13.339 | 0.010 | 11.758 | 0.004 | 10.827 | 0.003 | 9.824 | 0.008 | 1301 |
| 9013.45632 | 2020-06-12.956 | 13.421 | 0.006 | 11.791 | 0.005 | 10.857 | 0.007 | 9.888 | 0.013 | 0310 |
| 9013.46770 | 2020-06-12.968 | 13.377 | 0.006 | 11.766 | 0.003 | 10.861 | 0.008 | 9.902 | 0.009 | 1301 |
| 9021.39395 | 2020-06-20.894 | 13.432 | 0.004 | 11.816 | 0.006 | 10.882 | 0.008 | 9.882 | 0.014 | 1301 |
| 9021.43568 | 2020-06-20.936 | 13.440 | 0.008 | 11.834 | 0.005 | 10.858 | 0.006 | 9.883 | 0.012 | 0310 |
| 9023.40886 | 2020-06-22.909 | 13.436 | 0.005 | 11.835 | 0.009 | 10.908 | 0.009 | 9.900 | 0.014 | 1301 |
| 9023.43529 | 2020-06-22.935 | 13.456 | 0.008 | 11.805 | 0.008 | 10.919 | 0.006 | 9.921 | 0.012 | 0310 |
| 9024.42908 | 2020-06-23.929 | 13.483 | 0.007 | 11.876 | 0.005 | 10.891 | 0.005 | 9.910 | 0.013 | 0310 |
| 9024.44579 | 2020-06-23.946 | 13.463 | 0.005 | 11.872 | 0.007 | 10.905 | 0.008 | 9.921 | 0.014 | 1301 |
| 9027.46236 | 2020-06-26.962 | 13.513 | 0.009 | 11.890 | 0.004 | 10.927 | 0.005 | 9.863 | 0.008 | 1301 |
| 9030.42147 | 2020-06-29.921 | 13.544 | 0.007 | 11.876 | 0.006 | 10.909 | 0.007 | 9.829 | 0.009 | 1301 |
| 9036.39575 | 2020-07-05.896 | | | 11.885 | 0.006 | | | 9.938 | 0.012 | 0310 |
| 9037.40316 | 2020-07-06.903 | 13.463 | 0.006 | 11.843 | 0.004 | 10.928 | 0.010 | 9.967 | 0.014 | 1301 |
| 9038.39037 | 2020-07-07.890 | 13.491 | 0.010 | 11.872 | 0.004 | 10.888 | 0.014 | 9.919 | 0.011 | 0310 |
| 9039.38832 | 2020-07-08.888 | 13.472 | 0.009 | 11.842 | 0.005 | 10.922 | 0.006 | 9.929 | 0.012 | 0310 |
| 9043.37997 | 2020-07-12.880 | 13.427 | 0.010 | 11.811 | 0.004 | | | 9.883 | 0.013 | 0310 |
| 9056.37435 | 2020-07-25.874 | | | 11.758 | 0.008 | | | 9.827 | 0.014 | 0310 |
| 9056.37609 | 2020-07-25.876 | 13.358 | 0.004 | 11.789 | 0.003 | 10.875 | 0.007 | 9.913 | 0.011 | 1301 |
| 9058.38020 | 2020-07-27.880 | 13.407 | 0.015 | 11.814 | 0.007 | 10.826 | 0.008 | 9.881 | 0.010 | 0310 |
| 9067.36391 | 2020-08-05.864 | 13.513 | 0.013 | 11.850 | 0.009 | | | 9.941 | 0.011 | 0310 |
| 9068.35588 | 2020-08-06.856 | 13.484 | 0.012 | 11.866 | 0.004 | 10.926 | 0.005 | 9.879 | 0.007 | 1301 |

system via the transformations calibrated by Munari et al. (2014). Our photometry of 2SXPS is listed in Table 1. The quoted errors are the quadratic sum of the Poissonian error on the variable and the error in the transformation to the standard system via the above color equations.

### 2.2. Spectroscopy

Low resolution spectra of 2SXPS have been obtained with a Shelyak LHIRES spectrograph + 300 ln/mm grating mounted on the 0.50 Ritchey-Chretien tele-

scope operated for ANS Collaboration in Stroncone (TR, Italy). The CCD Camera is an ATIK 460EX (2749×2199 pixels, 4.5 $\mu$m in size). A slit width of 30 $\mu$m (=2.0 arcsec) has been adopted. Table 2 presents a log of these low-res observations.

Echelle high resolution spectra of 2SXPS have been obtained with the 0.84m telescope operated by ANS Collaboration in Varese (Italy), and equipped with a mark.III Multi-Mode Spectrograph from Astrolight Instruments. The detector is a SBIG ST10XME CCD camera (2192×1472 array, 6.8 $\mu$m pixel, KAF-3200ME chip with micro-lenses to boost the quantum efficiency). In the high resolution mode, an R2 Echelle grating of 79 ln/mm is used in conjunction with an equilateral 60° prims made in high dispersion N-SF11 flint glass, for a final 18,000 resolving power with a 2arcsec slit width. For 2SXPS observations a binning 2x2 was adopted leading to a resolving power 10,000.

The spectroscopic observations at both telescopes were obtained in long-slit mode, with the slit always rotated to the parallactic angle and widened to 2arcsec on the sky. All data have been similarly reduced within IRAF, carefully involving all steps connected with correction for bias, dark and flat, sky subtraction, wavelength calibration and heliocentric correction. The low-res spectra have been flux calibrated using similar observations of the nearby spectrophotometric standard HR 6698 observed immediately before or after 2SXPS.

**Table 2.** Log of spectroscopic observations of 2SXPS J173508.4-292958.

| *low-resolution* | | | | | *Echelle* | | | | |
|---|---|---|---|---|---|---|---|---|---|
| 2020 | | UT | JD (-2450000) | expt (sec) | 2020 | | UT | JD (-2450000) | expt (sec) |
| Apr | 24 | 01:38 | 8963.572 | 9000 | Apr | 23 | 02:25 | 8962.601 | 3600 |
| May | 03 | 00:21 | 8972.519 | 3600 | | 24 | 02:30 | 8963.604 | 3600 |
| | 22 | 00:41 | 8991.534 | 5400 | May | 21 | 01:28 | 8990.561 | 4500 |
| | 24 | 00:15 | 8993.516 | 4500 | Jul | 29 | 20:58 | 9060.374 | 3600 |
| | 27 | 00:14 | 8996.515 | 2700 | Aug | 05 | 20:40 | 9067.361 | 4500 |
| Jun | 11 | 23:40 | 9012.492 | 7200 | | 09 | 20:15 | 9071.344 | 3600 |
| | 12 | 22:50 | 9013.457 | 7200 | | 20 | 19:55 | 9082.330 | 2700 |
| | 20 | 20:45 | 9021.370 | 4500 | | | | | |
| | 22 | 21:02 | 9023.382 | 3600 | | | | | |
| | 23 | 22:00 | 9024.422 | 4500 | | | | | |
| | 25 | 23:15 | 9026.474 | 7200 | | | | | |
| | 29 | 21:28 | 9030.400 | 3600 | | | | | |
| Jul | 12 | 21:16 | 9043.391 | 3600 | | | | | |
| | 25 | 20:21 | 9056.352 | 4500 | | | | | |
| Aug | 06 | 19:48 | 9068.329 | 3600 | | | | | |
| | 20 | 19:07 | 9082.299 | 2700 | | | | | |

## 3. Results

### 3.1. Spectral classification, energy distribution, and radial velocities

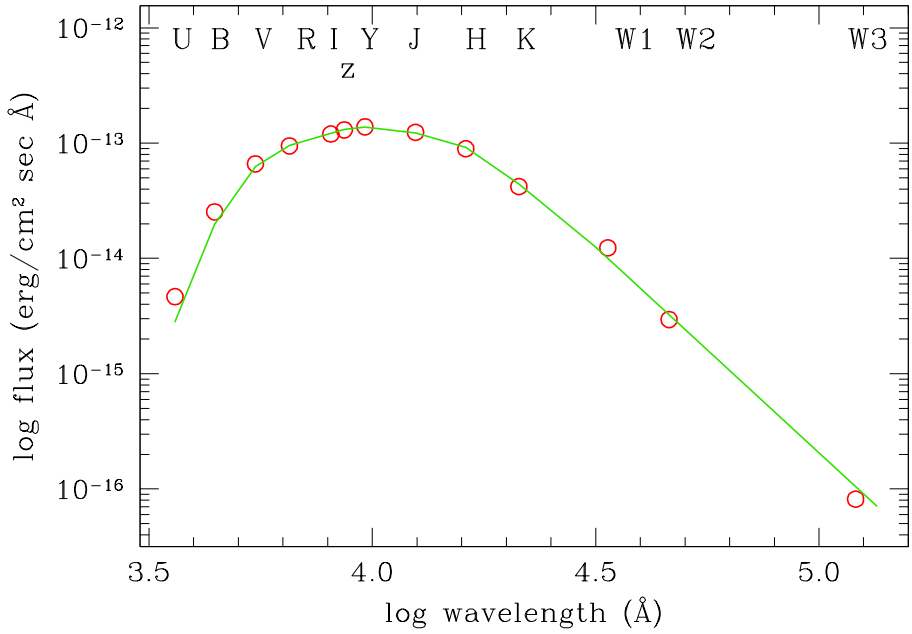


**Figure 1.** The observed energy distribution of 2SXPS J173508.4-292958 from our BVRIzY observations complemented with JHKs from 2MASS (Cutri et al. 2003), W1,W2,W3 from AllWISE (Cutri et al. 2014), and U band from Heinke et al. (2020). The green line is the intrinsic energy distribution of a K4III star from Koornneef (1983), Cousins (1980) and Fitzgerald (1970) subjected to an $E_{B-V}$=0.375 following the reddening law of Fitzpatrick (1999).

Even if projected close to the Galactic Center, 2SXPS is in the foreground at 1.50 kpc distance according to Gaia eDR3 parallax 0.6685±0.0197 mas (Gaia Collaboration 2020). The distance would be minimally affected, to 1.53 kpc, by the application of the mean −0.017mas offset derived by Lindegren et al. (2020) to affect globally the eDR3 parallaxes (they reported this bias to depend in a non-trivial way on - at least - the magnitude, colour, and ecliptic latitude of the source, with different dependencies that apply to the five- and six-parameter solutions in eDR3).

From Green et al. (2019) 3D extinction maps, 2SXPS should suffer from a modest E(B-V)=0.375. We have dereddened accordingly our BVRI photometry combined with 2MASS JHKs data and found an excellent match with the spec-

tral energy distribution of a K4III giant (Fig. 1). Fitting instead with K3III or K5III distributions would require to change E(B-V) to 0.49 or 0.28, respectively. Combining distance, reddening and observed V=11.825, an absolute magnitude M(V)=−0.55 is derived, intermediate between K4III and K4III/II luminosity classes for which Sowell et al. (2007) list M(V)=+0.20 and M(V)=−1.00, respectively.

The AllWISE mid-IR data in Fig. 1 exclude the presence of circumstellar dust warmer than ∼200 K. Any remnant blown-off by the progenitor of the present-day degenerate companion to the K4III has therefore already dispersed at a great distance from the central binary.

The SED in Fig. 1 is suggestive of an excess flux at the shortest wavelengths, amounting to 0.29 mag at U band. A word of caution is however in order considering that the U-band *Swift* observation from Heinke et al. (2020) in Fig. 1 is *not* contemporaneous with the BVRIzY data, and 2SXPS is moderately variable (see below). So the apparent excess at the shortest wavelengths of Fig. 1 may be (in part or entirely) an artifact. Such an ultraviolet excess is frequently seen in symbiotic binaries of the accretion-only variety, and probably originates from the accretion disk around the companion to the cool giant (Mukai et al. 2016, Munari et al. 2020b). A significant contribution to the UV excess can be also provided by nebular emission from ionized gas located somewhere else in the binary system (Skopal 2005a,b), ionized by either the hard radiation emitted from the accretion disk and its central star or from some other mechanism, including wind collision. For simplicity, in this paper we attribute the UV excess to the accretion disk, including cumulatively in it also the contribution by any nebular region distinct from the disk itself.

The K4III classification for 2SXPS agrees with our low resolution spectra. Their average is plotted in Fig. 2 and compared with spectra of standards for spectral types K3III, K4III and K5III selected from the compilation by Yamashita and Nariai (1977) and observed along 2SXPS with the same spectrograph set-up. These nearby K giants trace the metallicity and chemical partition of the Solar neighborhod. The presence of H$\alpha$ in emission in 2SXPS is rather obvious. The very large airmass affecting all our observations of 2SXPS marks the spectrum in Fig. 2 with signatures of telluric absorption red-ward of the NaI doublet at 5893 Å, the strongest feature being the $O_2$ band at 6285 Å. The BaII feature at 6496 Å shows the same strength in 2SXPS and the field K giants of Fig. 2, suggesting a normal abundance (for a discussion of Barium enhanced stars vs. symbiotic stars see Jorissen 2003).

Radial velocities have been obtained from the Echelle spectra by cross-correlation (fxcor task in IRAF) with spectra of the IAU radial velocity standard HR 6859 obtained immediately before and after those of 2SXPS on each visit. This standard is rather convenient: it is located a short angular distance from 2SXPS at RA=18:21:48 DEC=−29:49:18 (minimizing differential spectrograph flexures), it is very bright at V=2.7 mag, and its K2III spectral type is an excellent proxy for that of 2SXPS. We adopted the $-20.0\pm0.0$ km s$^{-1}$ heliocentric

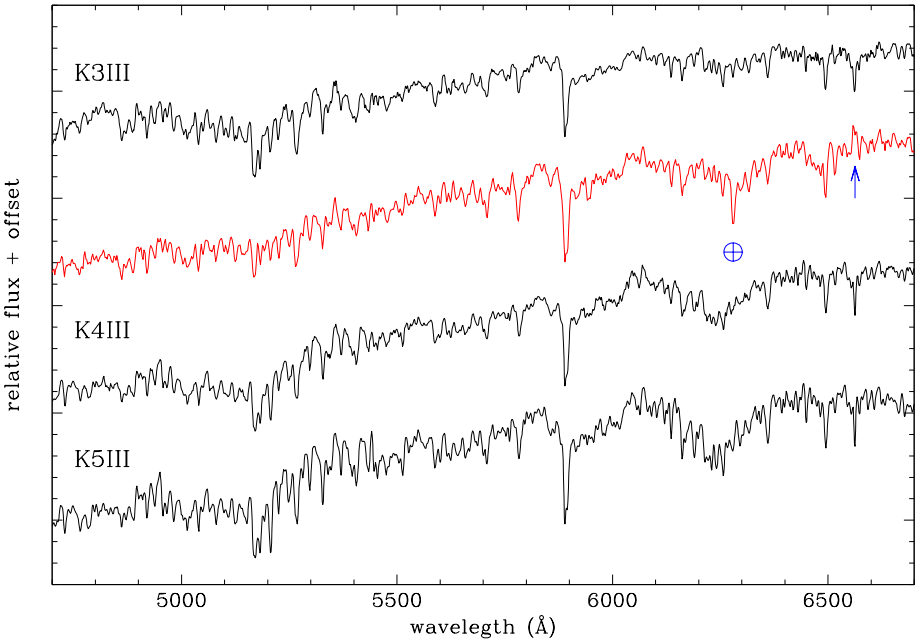


**Figure 2.** The low resolution spectrum of 2SXPS J173508.4-292958 compared with those of K3III, K4III and K5III spectral standards observed along with it. The strong telluric $O_2$ band at 6285 Å is marked, and the arrow points to H$\alpha$ in obvious emission.

**Table 3.** Heliocentric radial velocities of the K-giant in 2SXPS J173508.4-292958 obtained with the Varese 0.84m telescope.

| | date | $RV_\odot$ (km/s) | err (km/s) |
|---|---|---|---|
| 2020 | Apr 23/24 | −11 | 1.5 |
| 2020 | May 21 | −15 | 3 |
| 2020 | Aug 05 | −13 | 1.5 |
| 2020 | Aug 09 | −12 | 1.5 |
| 2020 | Aug 20 | −12 | 2 |

velocity listed in the "Standard Radial Velocity Stars" section of the Nautical Almanac. The epoch radial velocities so obtained for 2SXPS are listed in Table 3. They are fully compatible with a constant heliocentric radial velocity of $-12\pm1$ km s$^{-1}$ for 2SXPS during the four months span of our observations. This suggests that the orbital period is either rather long (and as a consequence the amplitude of orbital motion quite small) and/or the viewing angle to 2SXPS

is oriented high above the orbital plane. The tangential velocity of 2SXPS is similarly low at $-26$ km s$^{-1}$ (from Gaia eDR3 parallax and proper motions), for a combined space velocity of 29 km s$^{-1}$.

### 3.2. The variable and structured emission in H$\alpha$

Supporting the association of the K4III giant with the X–ray source 2SXPS is the presence on optical spectra of emission in H$\alpha$, not expected in normal and single K4III stars belonging to the field.

In the left panel of Fig. 3 we present small portions around H$\alpha$ from a sample of our low-resolution spectra (those with the highest S/N). The flux and equivalent width of H$\alpha$ are observed to change by a large amount over the course of our observations; no correlation is noted (see phases marked on the spectra) with the low-amplitude (0.12 mag), 38-day sinusoidal variability exhibited by 2SXPS, and presumably associated with the K4III giant (see sect. 3.4 an Eq. 1 below). The absence of correlation, and the low temperature characterizing a K4III giant, suggest the accretion disk around the companion as the origin of the H$\alpha$ emission.

The H$\alpha$ profile as recorded on our Echelle spectra is presented on the right panel of Fig. 3. It is composed by a broad emission, about 470 km s$^{-1}$ of width at half intensity, on which it is superimposed a narrow absorption component (only slightly wider than the instrumental PSF), which heliocentric velocity averaged over all spectra is $-4$ km s$^{-1}$. While the observed velocity of the K4III giant is consistent with a constant value, the velocity of the narrow absorption component could vary over the range $-10$ to 0 km s$^{-1}$. Our spectra lack however the S/N required for a firm conclusion about that.

One thing about the narrow absorption seems however well established: its velocity is *positive* with respect to the K4III giant, so it seems unlikely it may form in the gentle wind out-flowing from it and engulfing the whole binary system. A typical shift $\Delta$vel $\approx -10/-20$ km s$^{-1}$ is generally observed in symbiotic stars for the narrow absorption superimposed to the H$\alpha$ emission, matching the typical wind velocity of field cool giants (Munari et al. 2020b, Shagatova et al. 2020). This leaves open the possibility that the narrow absorption component seen in 2SXPS may form elsewhere in the binary system (as the accretion disk itself or an atmosphere engulfing it), or in alternative its appearance is spurious and the H$\alpha$ profile is actually composed by two separate emission components. The latter could be expected for an accretion disk seen at high inclination angle (e.g. Horne and Marsh 1986), but this condition seems to contrast with the limited (or null) orbital motion exhibited by the K4III giant over the four months of our observations.

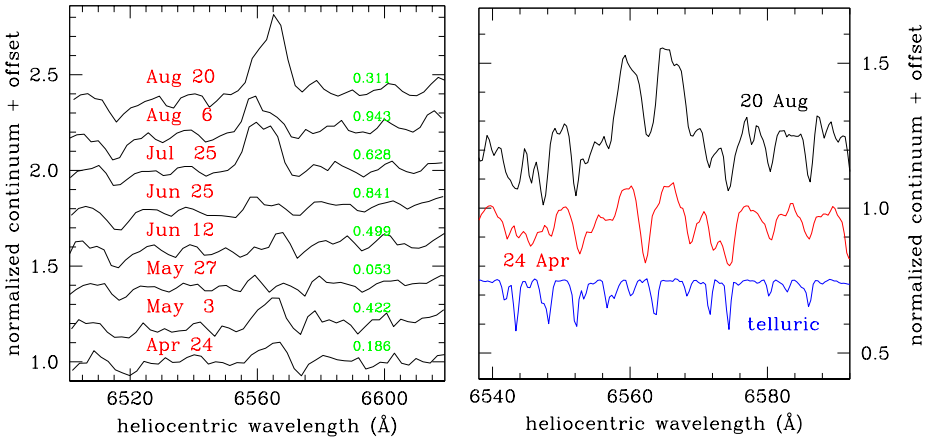


**Figure 3.** The variable H$\alpha$ emission observed in 2SXPS J173508.4-292958 during 2020. *Left panel*: a strong variation in intensity in recorded on our low-res spectra. *Right panel*: on Echelle spectra the profile turns out to be characterized by a broad emission component with superimposed a narrow absorption. For reference, the spectrum at the bottom show the telluric absorption lines in the region as derived from observations of a telluric divider observed along the program star.

### 3.3. No flickering observed

We carried out a search for flickering at optical wavelengths as an indication of on-going accretion. To search for flickering we used a 50cm telescope, with a 40arcmin corrected field of view and quality photometric filters, operated robotically for ANS Collaboration in Atacama (San Pedro Martir, Chile). We observed in $B$-band with 1-min integration time, with interspersed observations in $V$-band serving to construct the $B-V$ color base for the transformation from the instantaneous local photometric system to the Landolt's standard one. The same local photometric sequence and data reduction procedures as used for the long term $BVRI$ monitoring, were adopted.

About 50 field stars close on the image to 2SXPS, of a similar magnitude and well isolated from neighboring stars were also measured on all recorded images in exactly the same way as 2SXPS. The photometry of these 50 field stars was then inspected looking for those with a $B-V$ color as close as possible to 2SXPS. Four such stars were found, which serve as samplers of the observational noise above which the flickering has to be detected.

A first run, 70min in duration, was carried out from Sept 2.971 to 3.018 UT, 2020. The results are presented in Fig. 4: the dispersion of $B$-band measurements for 2SXPS is the same as for the four field stars of the same color and magnitude, and if any flickering is present, its amplitude does not exceed 0.005 mag. Other two runs, each one lasting 35min were carried out from Oct 24.980 to 25.003,

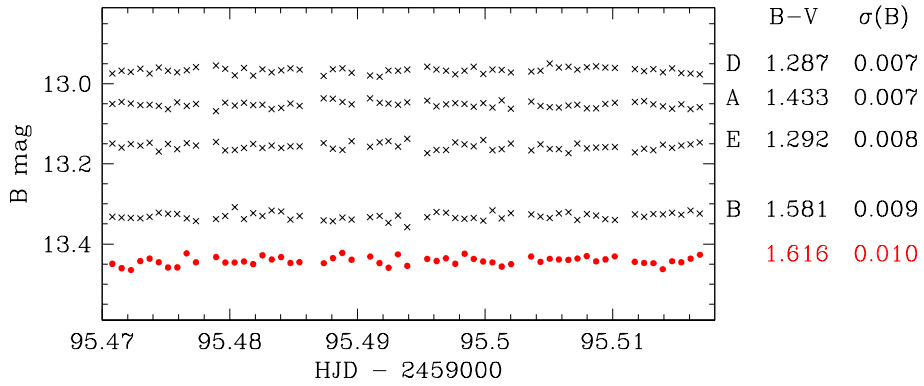


**Figure 4.** Results from a 70min run in $B$ band in search for flickering from 2SXPS J173508.4-292958 (red dots). The regular gaps in the data mark epochs when $V$-band exposures have been obtained to allow the transformation to the standard system. The corresponding data for four field stars of similar color and magnitude are presented as crosses. The progression from $\sigma$=0.007 for field star D to $\sigma$=0.010 for 2SXPS is accounted for by the $\Delta B\sim$0.5mag difference, and exclude the presence of any flickering with an amplitude in excess of 0.005 mag.

and from Oct 26.981 to 27.003 UT, 2020. They confirmed the findings for the early September run, with no flickering being detected.

We have seen above how large is the variability displayed by H$\alpha$ emission. It probably parallels a similarly large variability of the accretion rate onto the compact object in 2SXPS. Therefore, the absence of flickering on early September and late October observations does not necessarily imply it is always absent. Unfortunately, at the time of flickering observations, the object was no more observable from Italy, and therefore we have no contemporaneous spectroscopy to compare the absence of flickering to the amount of emission in H$\alpha$.

### 3.4. Photometric evolution

Our $BVRI$ photometry from Table 1 is plotted in Fig. 5. The $V$ band light-curve is characterized by a mean 11.825 mag value, and a sinusoidal modulation with a period of 38 days and an amplitude of 0.12 mag, with the following ephemeris providing times of mimina:

$$\min(\mathrm{V}) = 2458994.5(\pm 1) + 38(\pm 0.5) \times E \qquad (1)$$

The colors do not appear to change along the cycle. As illustrated by the SED in Fig. 1, the emission at optical wavelengths is dominated by the K4III giant, so the sinusoidal variability probably originates from it, either in the form of some pulsation or the rotation of a spotted surface.

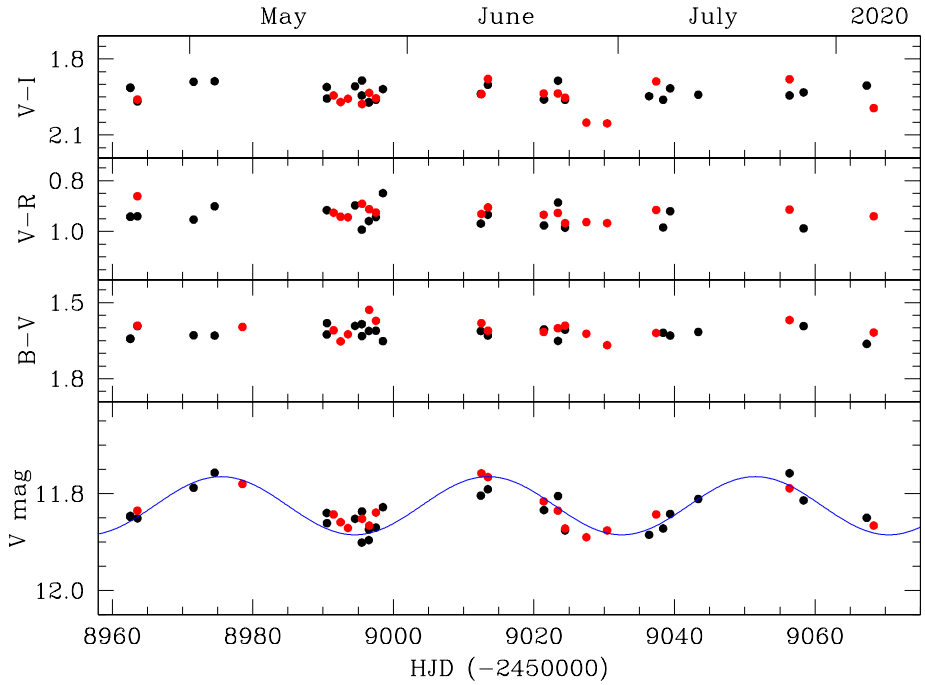


**Figure 5.** Our April-to-August 2020 light-curve of 2SXPS J173508.4-292958 built from data in Table 1 (red dots mark the observations obtained with ANS Collaboration telescope ID 0310, and black dots those with telescope ID 1301). The sinusoid going through the $V$-band data has minima according to Ephemeris (1), an amplitude of 0.12 mag and a period of 38 days.

The sinusoidal variability could instead point to an ellipsoidal deformation of the K4III, should the latter fill its Roche lobe, in which case the orbital period would be twice the photometric one, or 76 days. The typical mass of a field K4III is listed as 1.2 $M_\odot$ by Drilling and Landolt (2000). Assuming 1.0 $M_\odot$ for the companion, this leads to a semi-major axis for the binary system of 98 $R_\odot$. The relation between mass ratio $q$, orbital separation $a$, and Roche lobe radius $R_{RL}$ as given by Eggleton (1983) is

$$\frac{R_{RL}}{a} = \frac{0.49q^{2/3}}{0.6q^{2/3} + \ln(1 + q^{1/3})} \tag{2}$$

and returns a radius of 39 $R_\odot$ for the K4III, twice the tabulated values of $\sim$20 $R_\odot$ (Drilling and Landolt 2000). The discrepancy would persist also for different assumption on the mass of the companion: 0.5 $M_\odot$ leads to 41 $R_\odot$ and

2.5 $M_\odot$ to 37 $R_\odot$. Therefore, the origin of the observed sinusoidal light-curve is probably other that Roche-lobe filling.

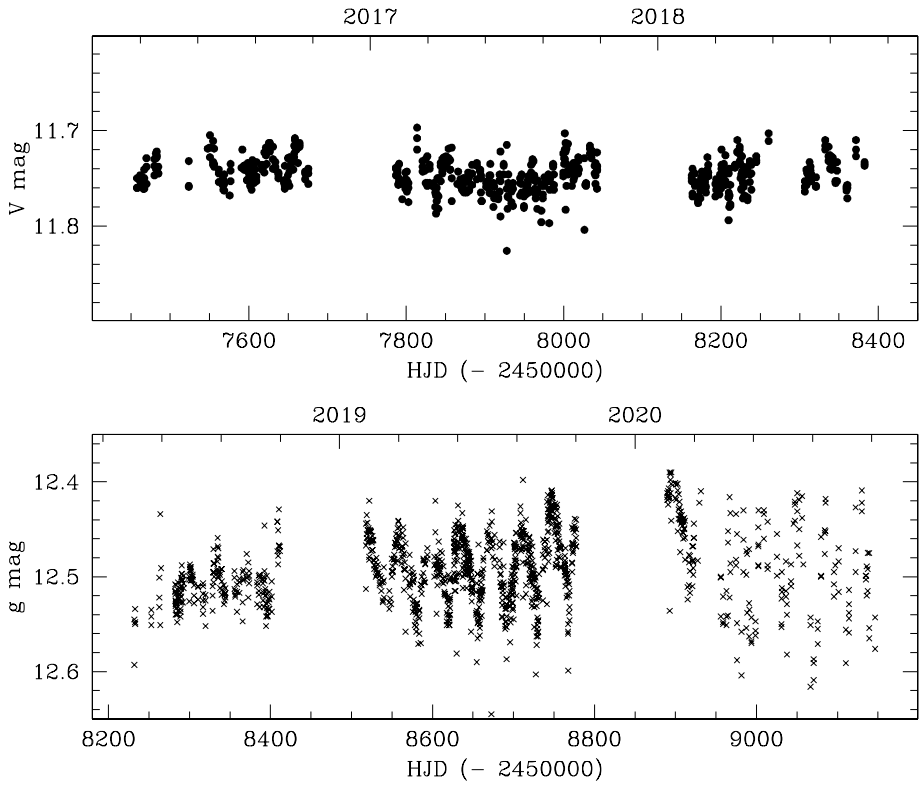


**Figure 6.** Long-term light-curve of 2SXPS J173508.4-292958 built from ASAS-SN sky-patrol data in $V$ and $g$ bands.

In support of this conclusion comes the absence of detectable radial velocity changes in Table 3. A 76-day period would correspond to an orbital velocity of the K4III of 30 km $s^{-1}$ for a 0.5 $M_\odot$ companion and 38 km $s^{-1}$ for 2.5 $M_\odot$. The maximum photometric amplitude (for edge-on systems) of the ellipsoidal modulation is 0.25/0.30 mag. An amplitude of 0.12 mag for 2SXPS requires a significant orbital inclination, such that the amplitude of radial velocity variations would be at least 10 km $s^{-1}$, incompatible with results from Table 3.

The nail in the coffin about ellipsoidal modulation is however the fact that the sinusoidal variability is not always present but highly variable with time, as discussed in the following section.

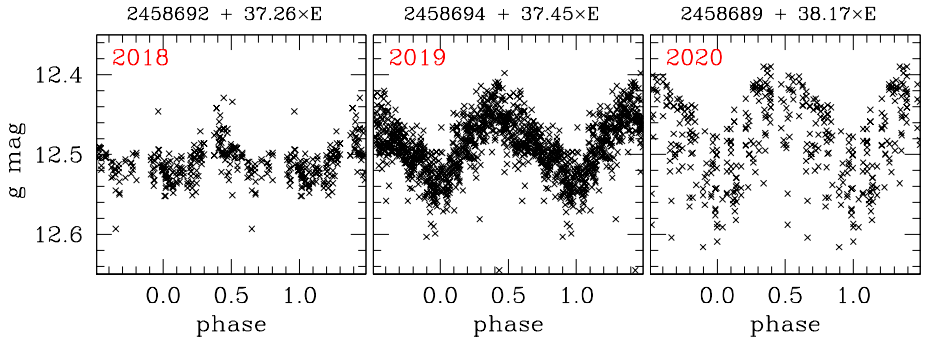


**Figure 7.** Phased light-curves for the modulated part of Figure 6.

### 3.5. Long-term light-curve

To reconstruct a longer term light-curve of 2SXPS we have downloaded ASAS-SN all-sky patrol data (Shappee et al. 2014, Kochanek et al. 2017) and plotted them in Fig. 6. 2SXPS was observed by ASAS-SN with a $V$-filter over 2016-2018 and with a $g$-filter during 2018-2020.

The median value of the 2016-2018 ASAS-SN $V$ band data in Fugure 6 is 0.076 mag brighter than our data in 2020. We do not regard this as significative: ASAS-SN data are just differential magnitudes with respect to *not-transformed* data for field stars, while our photometry is fully transformed to Landolt's system of equatorial standards (cf. sect. 2.1). The rather red color of 2SXPS, much redder than typical field stars, can easily account for the offset affecting ASAS-SN data.

The ASAS-SN light-curve in Fig. 6 shows a stable 2SXPS during 2016-2018, and appearance of the sinusoidal modulation only in 2019, which extended to 2020 with a lower degree of coherence. The phased light-curves of 2SXPS from ASAS-SN data for 2018, 2019 and 2020 is presented in Fig. 7, with the best-fit ephemeris given at the top of the panels. The differences between them are marginally within uncertainties.

While certainly arguing against an interpretation in terms of ellipsoidal distortion of the K4III giant, the light-curves of Fig. 5, 6 and 7 do not disentangle a specific cause for the variability observed in 2SXPS, although some kind of pulsation could be a viable explanation.

## 4. Conclusions

Our observations suggest 2SXPS to be a previously unknown symbiotic star, of the accreting-only variety (AO-SySt). The low space velocity, absence of cool circumstellar dust, solar-like metallicity and lack of enhancement in Barium set

2SXPS aside from other symbiotic stars of the *yellow* class (i.e. those harbouring a cool giant of the F,G,K spectral types). As typical of AO-SySt systems, the signature for 2SXPS of on-going accretion onto a degenerate companion are feeble (weak and structure emission in H$\alpha$, just a hint of near-UV excess emission) and highly variable in time, so that the AO-SySt nature may be not recognized at all times from optical observations alone. The star clearly deserves further observations, especially accurate radial velocities over a long time interval in order to derive the orbital period, orbital inclination and an estimate for the mass of the unseen companion.

## References

Cousins A. W. J., 1980, SAAOC, 1

Cutri R. M., Skrutskie M. F., van Dyk S., Beichman C. A., Carpenter J. M., Chester T., Cambresy L., et al., 2003, yCat, II/246

Cutri R. M., et al., 2014, yCat, II/328

Drilling J. S., Landolt A. U., 2000, in Allen's Astrophysical Quantities, 4th ed., A.N. Cox ed., pag. 381, Springer-Verlag (New York)

Eggleton P. P., 1983, ApJ, 268, 368. doi:10.1086/160960

Fitzgerald M. P., 1970, A&A, 4, 234

Fitzpatrick E. L., 1999, PASP, 111, 63. doi:10.1086/316293

Gaia Collaboration, 2020, yCat, I/350

Green G. M., Schlafly E., Zucker C., Speagle J. S., Finkbeiner D., 2019, ApJ, 887, 93. doi:10.3847/1538-4357/ab5362

Heinke C. O., Rivera Sandoval L., Maccarone T. J., Kennea J., Bahramian A., Strader J., Sivakoff G. R., 2020, ATel, 13648

Henden A. A., Templeton M., Terrell D., Smith T. C., Levine S., Welch D., 2016, yCat, II/336

Horne K., Marsh T. R., 1986, MNRAS, 218, 761. doi:10.1093/mnras/218.4.761

Jorissen A., 2003, ASPC, 303, 25

Kochanek C. S., Shappee B. J., Stanek K. Z., Holoien T. W.-S., Thompson T. A., Prieto J. L., Dong S., et al., 2017, PASP, 129, 104502. doi:10.1088/1538-3873/aa80d9

Koornneef J., 1983, A&A, 500, 247

Lindegren L., Bastian U., Biermann M., Bombrun A., de Torres A., Gerlach E., Geyer R., et al., 2020, arXiv, arXiv:2012.01742

Mukai K., Luna G. J. M., Cusumano G., Segreto A., Munari U., Sokoloski J. L., Lucy A. B., et al., 2016, MNRAS, 461, L1. doi:10.1093/mnrasl/slw087

Munari U., 2019, in The Impact of Binary Stars on Stellar Evolution, G. Beccari and M.J. Boffin eds., Cambridge Univ. Press., Cambridge Astrophysical Series vol. 54, pag. 77 (arXiv:1909.01389)

Munari U., Henden A., Frigo A., Dallaporta S., 2014, JAD, 20, 4

Munari U., Valisa P., Dallaporta S., Vagnozzi A., Andreoli V., Castellani F., 2020a, ATel, 13660

Munari, U., Traven, G., Masetti, N. et al., 2020, MNRAS, submitted

Shagatova N., Skopal A., Shugarov S. Y., Komžík R., Kundra E., Teyssier F., 2020, arXiv, arXiv:2012.08417

Shappee B. J., Prieto J. L., Grupe D., Kochanek C. S., Stanek K. Z., De Rosa G., Mathur S., et al., 2014, ApJ, 788, 48. doi:10.1088/0004-637X/788/1/48

Skopal A., 2005a, A&A, 440, 995. doi:10.1051/0004-6361:20034262

Skopal A., 2005b, ASPC, 330, 463

Sowell J. R., Trippe M., Caballero-Nieves S. M., Houk N., 2007, AJ, 134, 1089. doi:10.1086/520060

Yamashita Y., Nariai K., 1977, An Atlas of Representative Stellar Spectra, University of Tokyo Press

Contrib. Astron. Obs. Skalnaté Pleso **51**, 118 – 131, (2021)
https://doi.org/10.31577/caosp.2021.51.2.118

# V355 And: a neglected detached binary in a multiple star system

**B. Özkardeş**[1,2]

[1] *Department of Space Science and Technologies, Faculty of Arts and Sciences, Çanakkale Onsekiz Mart University, Terzioğlu Kampüsü, TR-17020, Çanakkale, Turkey, (E-mail: burcu@comu.edu.tr)*

[2] *Çanakkale Onsekiz Mart University, Astrophysics Research Center and Ulupınar Observatory, TR-17100, Çanakkale, Turkey*

Received: October 9, 2020; Accepted: December 28, 2020

**Abstract.** The analysis of light curves (from TESS, ASAS–SN and KWS databases) of the eclipsing binary V355 And is presented for the first time. The *O-C* diagram was constructed using all available times of minimum light together with the ones determined in this study, and the revised ephemeris was obtained. The final photometric model describes V355 And as an Algol-like type binary star with a detached configuration. Absolute parameters of the components of the system were found to be: masses, $M_1$=1.56 ± 0.01 $M_\odot$ and $M_2$=1.38 ± 0.01 $M_\odot$, radii, $R_1$=1.70 ± 0.03 $R_\odot$ and $R_2$=1.38 ± 0.03 $R_\odot$, and effective temperatures, $T_1$=6650 ± 200 K and $T_2$=6235 ± 201 K. Considering interstellar extinction the distance to V355 And was computed as 117 ± 7 pc. The evolutionary state of V355 And is also discussed using the Geneva stellar models.

**Key words:** Stars: binaries: eclipsing; Stars: absolute parameters; Stars: Individual V355 And

## 1. Introduction

Eclipsing binary systems are important celestial objects in astrophysics in determining the astrophysical parameters of stars in our galaxy, the Milky Way, and nearby galaxies and understanding stellar evolutionary status. Since the proximity and ellipsoidal effects are not important in detached binary systems, their absolute parameters can be derived more accurately from the solutions of light and radial velocity curves. This paper focuses on the neglected eclipsing binary V355 And. The primary objectives of the present study are to determine the absolute dimensions of V355 And and to examine the evolutionary state of the system's components. Literature-based studies of this neglected binary star are summarized below.

V355 And is an Algol-type binary star and a component of the visual binary WDS 00442–4614. The eclipsing nature and multiplicity of the system were

discovered by the Hipparcos satellite (ESA, 1997). The system has a fainter ($\Delta V_{Hip} \simeq 1^m.17$) component at a separation of 1.41 arcsec and a position angle of 5.5 deg. The target system V355 And is one of the poorly studied eclipsing binary stars. Kazarovets et al. (1999) gave the GCVS name and variability type of the system in their 74th name-list of variable stars. Tikkanen (2002) published the complete visual light curve of V355 And and revealed the light elements to be $T_0$=2452295.088(8) and $P$=4.71841(2). Imbert (2006) determined the spectroscopic orbits of 25 binary stars, including the double-lined system V355 And, using 1402 *Coravel* radial velocity measurements. Zasche et al. (2009) presented a new catalog of visual double systems containing eclipsing binaries as one component. For V355 And, they suggested the visual orbit's period to be in the order of 3000 yr according to the orbital coverage. Hubscher (2015) recorded one minimum light time in the *I*–filter for the system. Some photometric properties of the multiple system V355 And are given in various catalogues (e.g. Malkov et al., 2006; McDonald et al., 2012; Avvakumova et al., 2013; Paunzen, 2015; Soubiran et al., 2016). The fundamental data for V355 And is given in Table 1.

**Table 1.** Fundamental data based on the ASAS–SN database for V355 And.

| Star Name | ASASSN–*V* J004411.33+461407.2 |
|---|---|
| LCID | 51037 |
| RA, DEC | 11.0472, 46.2353 |
| Epoch (HJD) | 2457747.80809 |
| *V* mag | 7.97 |
| Amplitude | 0.73 |
| Type | VAR |

## 2. O-C analysis

### 2.1. Data

For V355 And, there are few times of minimum light in the literature: Tikkanen (2002) observed the system visually and obtained 5 minima times. In the *O-C* Gateway archive[1], 4 minima times of the eclipsing binary V355 And are recorded. In this study, 9 minima times of the system were obtained from the photometric light curves of the SuperWASP (Wide Angle Search for Planets; Butters et al., 2010) and TESS (Transiting Exoplanet Survey Satellite; Ricker et al., 2015) surveys. Newly determined minima times were computed with the software Minima Vers.27 published by B. Nelson[2] using the Kwee & van Woer-

[1] http://var2.astro.cz/ocgate/index.php?lang=en

[2] https://www.variablestarssouth.org/software-by-bob-nelson/

den (1956) method. All minima times in HJD were converted to $BJD_{TDB}$ using the HJD2BJD calculator[3] (Eastman et al., 2010) because the calculated times of minima from TESS observations were in the $BJD_{TDB}$ time system. Minima times of V355 And are tabulated in Table 2.

**Table 2.** Minima times of V355 And.

| $BJD_{TDB}$(+2400000) | Type | Method | Reference |
|---|---|---|---|
| 52271.5000±0.0210 | p | visual | |
| 52276.2170±0.0160 | p | visual | |
| 52283.2910±0.0070 | p | visual | Tikkanen (2002) |
| 52295.0900±0.0080 | p | visual | |
| 52309.2420±0.0110 | s | visual | |
| 56928.5218±0.0033 | p | CCD | |
| 57256.4517±0.0064 | s | CCD | $O-C$ Gateway |
| 57992.5188±0.0015 | s | CCD | |
| 58379.4208±0.0015 | s | CCD | |
| 54418.3577±0.0004 | p | CCD | SuperWASP |
| 54373.5245±0.0004 | s | CCD | |
| 58768.6916±0.0001 | p | CCD | |
| 58778.1289±0.0002 | p | CCD | |
| 58782.8474±0.0001 | p | CCD | |
| 58766.3361±0.0002 | s | CCD | TESS |
| 58771.0540±0.0001 | s | CCD | |
| 58780.4909±0.0001 | s | CCD | |
| 58785.2092±0.0001 | s | CCD | |

### 2.2. New light elements

We can examine whether the orbital period of a binary system has changed using the *O-C* diagram. In the case of V355 And, the *O-C* values of the minima times listed in Table 2 were calculated using $T_0$=2458768.6916 (from TESS observations) and $P$=4.71841 (from Tikkanen, 2002), and thus the *O-C* diagram of the system was created. A linear regression of all *O-C* values was performed to obtain the revised ephemeris, given in equation (1). The residuals are plotted in Fig. 1. In this figure, it is clearly seen that the period of the system has been constant throughout the time interval of 18 years.

$$Min\ I\ (BJD_{\rm TDB}) = 2458768.6924(\pm0.0011) + 4^d.7183707(\pm0.0000013) \times E, \quad (1)$$

where the values in brackets are the uncertainties.

[3]http://astroutils.astronomy.ohio-state.edu/time/hjd2bjd.html

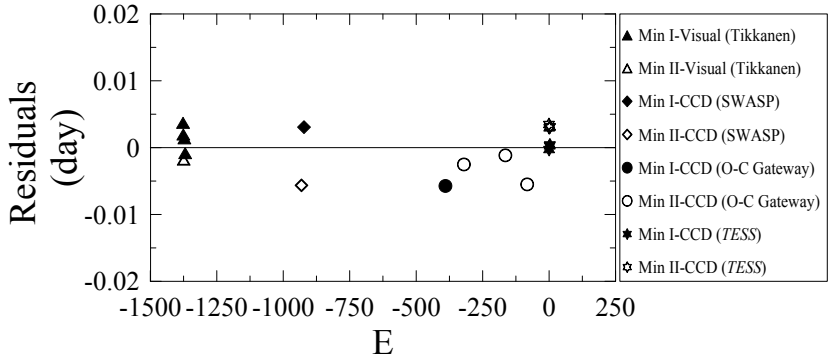


**Figure 1.** A plot of *O–C* residuals versus the ephemeris used in equation (1).

## 3. Light curve modeling

### 3.1. Data

The neglected binary V355 And was observed by five different photometric surveys: The All-Sky Automated Survey for Supernovae (ASAS–SN; Shappee et al., 2014; Kochanek et al., 2017; Jayasinghe et al., 2018), Kamogata/Kiso/Kyoto Wide-field Survey (KWS; Maehara, 2014), Hipparcos, SuperWASP and TESS. The photometric light curves observed by the TESS[4], ASAS–SN[5] and KWS[6] were analyzed, while the Hipparcos and SuperWASP light curves were not solved because of the inadequate phase covering and more scattered data.

The main purpose of TESS is to explore planetary transits by scanning the chosen sky over a period of two years. TESS observational data comes from sectors that cover a 24°x90° region in the sky. The observations of 32 sectors in total have been completed so far. TESS observations of V355 And ($T_{mag}$=7.42, TIC 601366244) were made in 120 s cadence during Sector 17 starting in October 2019. In this study, Simple Aperture Photometry (SAP) Flux data with QUALITY=0 of V355 And, which consists of 12,613 photometric points for the system, was converted into magnitude values. The average values per each three data points were used to generate the normalized data, thus nearly 4200 normal points in total. The photometric phases of the TESS light curve were computed using equation (1).

The ASAS–SN project aims to survey the whole sky up to 18th magnitude and focuses on the discovery of bright nearby supernovae. In the ASAS–SN Variable Stars database 666,502 light curves are available, including the *V*–band light curve of the target binary V355 And obtained between October

[4]https://mast.stsci.edu/portal/Mashup/Clients/Mast/Portal.html
[5]https://asas-sn.osu.edu/
[6]http://kws.cetus-net.org/ maehara/VSdata.py

2013 and January 2018. The ASAS–SN light curve of V355 And is composed of about 1800 data points in $V$ mag. The outliers with $\sigma \geq 0.0004$, where $\sigma = \frac{error\ of\ observation\ point}{observation\ point}$, were removed from the ASAS–SN data. The remaining data points, ∼1480, were processed in the analysis. Using equation (1), the phases of the ASAS–SN light curve were calculated.

KWS is designed for the automated wide-field optical survey of bright transits and variable stars via a small CCD camera and lens to achieve a photometric precision of $< 5\%$ for stars with $V$–band magnitude between 5 and 11. KWS observations of V355 And were made between December 2010 and January 2020, and nearly 1200 data points were obtained in total in the $V$ and $I_c$ filters. The scattered data points with $\sigma \geq 0.00095$ for $V$ and $\sigma \geq 0.00013$ for $I_c$ were removed from the KWS data, thus a total of ∼800 data points remained for the analysis. Equation (1) was used for phasing the KWS–$VI_c$ light curves.

The spectroscopic orbital parameters of the system given by Imbert (2006) are tabulated in Table 3. The spectroscopic mass ratio ($q = \frac{K_1}{K_2}$) of V355 And is calculated to be 0.88 based on this table. Public data of the radial velocity curves of the eclipsing pair can be extracted from the webpage[7] of SB9 (Pourbaix et al., 2004).

**Table 3.** Spectroscopic orbital parameters of V355 And from Imbert (2006).

| Parameters | Unit | Primary | Secondary |
|---|---|---|---|
| T0 | HJD | 48929.67±0.007 | |
| Period | day | 4.71835±0.00002 | |
| e | – | 0 (fixed) | |
| $\omega$ | deg | 0 (fixed) | |
| K | km/s | 85.01±0.28 | 96.59±0.30 |
| $V_\gamma$ | km/s | 6.93±0.17 | |
| asin(i) | km | $5.52 \times 10^6 \pm 0.02 \times 10^6$ | $6.27 \times 10^6 \pm 0.02 \times 10^6$ |
| $m\sin^3(i)$ | $M_\odot$ | 1.56±0.01 | 1.38±0.01 |

### 3.2. Analysis

If both a light curve and radial velocity curves of an eclipsing binary system are obtained, the absolute parameters of that system can be determined more precisely. The Wilson-Devinney (WD) code (Wilson & Devinney, 1971), appended with the Monte Carlo (MC) algorithm (Zola et al., 2010), was used for the light curve modeling. In the first step, due to its high inherent accuracy (each datum on the order of 0.0001 mag), the TESS light curve of V355 And was solved. The MC procedure outlined by Zola et al. (2010) was followed, and the spectroscopic mass ratio value was kept fixed. In the second step, ASAS–SN and

[7] https://sb9.astro.ulb.ac.be/

KWS light curves were solved. The ASAS–SN and KWS light curves both have lower photometric accuracy and show more scattering at their maximum levels (see Fig. 2). On the other hand, there are not enough observation points in the depths of the minima of KWS light curves. As it is well known, the depths of minima of a given light curve are important factors in determining the surface potential parameters (then the fractional radii) of component stars. Therefore, in the solution of ASAS–SN and KWS light curves, these surface potential parameters ($\Omega_1$, $\Omega_2$) were fixed at the values obtained from the solution of the TESS light curve, and the other parameters were adjusted.

The following parameters were adopted and fixed during all iterations. The temperature of the primary component was fixed at 6650 K corresponding to the F5 spectral type given by the Hipparcos catalogue using Drilling & Landolt (2000)'s calibration for MK spectral types. The bolometric gravity-darkening exponents ($g_1$=$g_2$=0.32) and albedos ($A_1$=$A_2$=0.5) of the components were set at their theoretical values as suitable for the spectral type of component stars, following Lucy (1967) and Ruciński (1969), respectively. The square-root limb-darkening law was adopted with limb-darkening coefficients from the calibration tables of Claret & Bloemen (2011) and Claret et al. (2013), depending on the filter wavelengths and temperatures of the primary and secondary components. Besides synchronous rotation of the components, a circular orbit for the systems was also assumed.

The free parameters in the light curve fitting were the orbital inclination ($i$), phase-shift ($\phi$), temperature of the secondary component ($T_2$), non-dimensional surface potential parameters of components ($\Omega_1$ and $\Omega_2$), luminosity of the primary ($L_1$) and third light contribution ($\frac{L_3}{L_{total}}$). In the MC process, an assumed range within realistic bounds for each free parameter should be defined. In the analysis, the search ranges of the adjusted parameters are given in Table 4.

The parameters of the WD+MC solution are listed in Table 4 with the errors corresponding to a 90% confidence level. The best theoretical fits of the WD+MC modeling program are compared with the observed light curves in Fig. 2. The 2D plot of the parameter space for degeneracies between the chosen five parameters ($i$, $T_2$, $\Omega_1$, $\Omega_2$ and $L_3$) are shown in Fig. 3 using MC confidence levels. There are considerable degeneracies between $\Omega_1$ and $\Omega_2$ and between $i$ and $L_3$, while no degeneracies are seen between $i$ and $T_2$, $i$ and $\Omega_1$ and $i$ and $\Omega_2$. Such degeneracies between the geometric and physical parameters were found in some detached binaries (see Garcia et al., 2014; Sürgit et al., 2017).

**Table 4.** Selected search ranges of adjusted parameters in the WD+MC method.

| System | $i$ (deg) | $\phi$ | $T_2$ (K) | $\Omega_1$ and $\Omega_1$ | $L_1$ | $\frac{L_3}{L_{total}}$ |
|---|---|---|---|---|---|---|
| V355 And | 70–90 | -0.01–0.01 | 5500–6600 | 9.0–14.0 | 2.0–12.0 | 0.1–0.50 |

**Table 5.** Results of the analysis of light curves of V355 And.

| Parameters | TESS | ASAS-SN | KWS |
|---|---|---|---|
| $i\,(^\circ)$ | 88.1±0.2 | 87.5±0.2 | 88.1±0.2 |
| $\phi$ | -0.0006±0.0001 | -0.0007±0.0001 | -0.0007±0.0001 |
| $T_1\,(K)$ | 6650 (fixed) | 6650 | 6650 |
| $T_2\,(K)$ | 6414±12 | 6237±14 | 6297±23 |
| $q = M_2/M_1$ | 0.88 (fixed) | 0.88 | 0.88 |
| $\Omega_1$ | 10.867±0.109 | 10.867 | 10.867 |
| $\Omega_2$ | 11.838±0.191 | 11.838 | 11.838 |
| $r_1\,(mean)$ | 0.100±0.001 | 0.100 | 0.100 |
| $r_2\,(mean)$ | 0.082±0.001 | 0.082 | 0.082 |
| $L_1/L_{total}$ -$TESS$ | 0.45±0.02 | – | – |
| $L_1/L_{total}$ -$V$ | – | 0.46±0.01 | 0.45±0.02 |
| $L_1/L_{total}$ -$I_c$ | – | – | 0.46±0.01 |
| $L_3/L_{total}$ -$TESS$ | 0.29±0.02 | – | – |
| $L_3/L_{total}$ -$V$ | – | 0.30±0.01 | 0.28±0.01 |
| $L_3/L_{total}$ -$I_c$ | – | – | 0.28±0.01 |
| $\sum W(O-C)^2$ -$RV1$ | 0.0003 | 0.0003 | 0.0003 |
| $\sum W(O-C)^2$ -$RV2$ | 0.0003 | 0.0003 | 0.0003 |
| $\sum W(O-C)^2$ -$LC-TESS$ | 0.0194 | – | – |
| $\sum W(O-C)^2$ -$LC-V$ | – | 0.2548 | 0.2843 |
| $\sum W(O-C)^2$ -$LC-I_c$ | – | – | 0.1731 |

## 4. Results and discussion

A detailed photometric data analysis of V355 And was performed in this study for the first time. The best-fitting model reveals that V355 And has a detached configuration, and the primary and secondary components fill 34% and 31% of their Roche limiting lobes, respectively. In the following subsections, the obtained absolute parameters and evolutionary status of the system are given.

### 4.1. Absolute dimensions

The absolute dimensions of V355 And were calculated from the combination of the TESS light curve solution and the RV curve solution, and are given in Table 6 with their uncertainties. The solar values, $T_{eff}$=5771.8±0.7 K, $M_{bol}$=4.7554±0.0004 mag and $g$=27423.2±7.9 cm/s$^2$, taken from Pecaut & Mamajek (2013), were used in the computations.

The uncertainty of 20 K in the temperature of the secondary component, seen in Table 5, corresponds to the 1-$\sigma$ formal error resulting from the WD+MC analysis. The standard error of the secondary component's temperature has been corrected to 201 K by adopting the standard error of 200 K in the temperature of the primary component given in Table 6. The Bolometric corrections (BC)

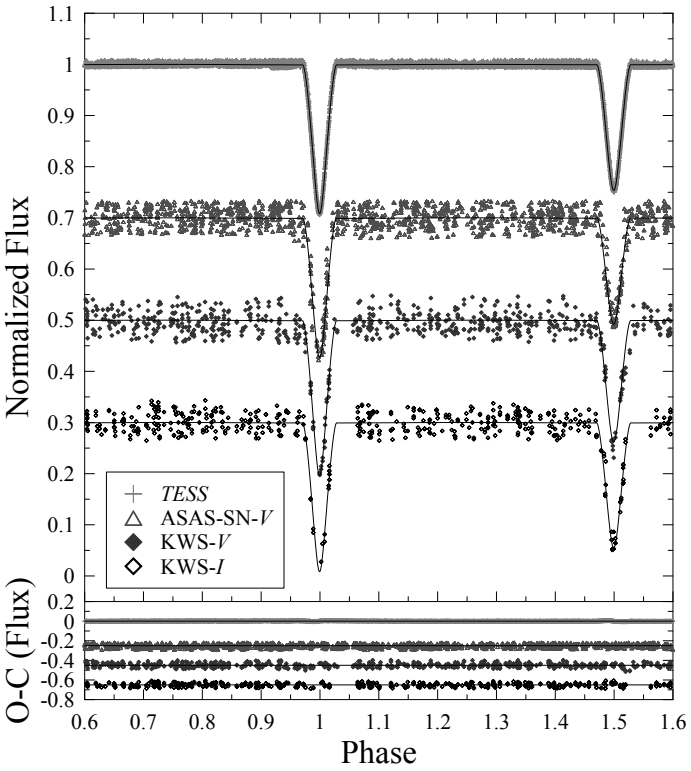


**Figure 2.** Comparison between the theoretical (solid lines) and TESS (top), ASAS-SN–$V$ (middle) and KWS–$VI_c$ light curves (bottom) of V355 And. The residuals of the WD+MC model fitting are shown in the bottom panel.

of the primary and secondary components were chosen from the tabulation of Flower (1996) to be $BC_1$=0.016 and $BC_2$=-0.017, respectively, according to the computed effective temperatures of the components. The absolute magnitudes of both components were then obtained.

Through the well-known equation $E(B-V)= (B-V)–(B-V)_0$, the color excess of the system was determined as 0.017, where the de-reddened color index $(B-V)_0$ was computed using the absolute magnitude calibrations for detached binaries given by Bilir et al. (2008), while the $(B-V)$ value of the system was taken from the APASS catalogue[8]. The interstellar extinction value $A_\nu$ in the $V$ passband was computed as 0.052 mag by means of the well-known formula $A_V = 3.1 \times E(B-V)$. Finally, the distance to V355 And of 117±7 pc was derived from the distance modulus formula. Additionally, the distance of the

[8]APASS Catalogue: The AAVSO Photometric All-Sky Survey, http://www.aavso.org/apass.

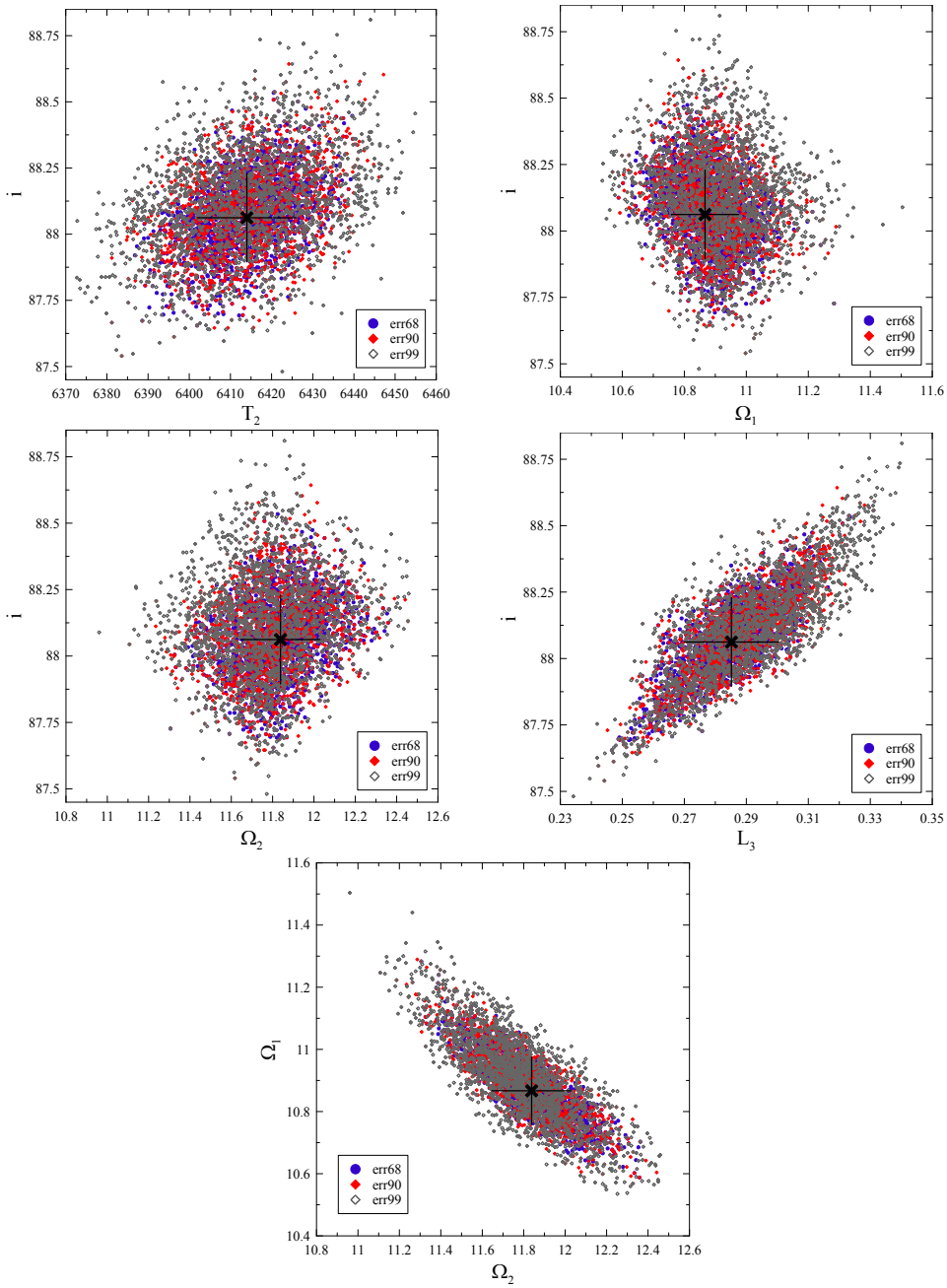


**Figure 3.** Degeneracies of the selected parameters, ($i$, $T_2$, $\Omega_1$, $\Omega_2$ and $L_3$), for the WD+MC search best fit solution using three confidence levels (68%, 90%, and 99%). Confidence levels are represented by blue-filled circles, red diamonds and grey diamonds. The best-fit solution is represented by the cross symbol with error bars selected from a 90% confidence level.

system was calculated to be 117.9±2.0 pc according to the *Gaia* DR2 parallax (Gaia Collaboration et al., 2018). It is clearly seen that the determined distance is in good agreement when compared with the *Gaia* distance.

**Table 6.** Absolute parameters of the components of V355 And.

| Parameters | Unit | Primary | Secondary |
|---|---|---|---|
| $A$ | $R_\odot$ | 16.94±0.03 | |
| $P_{orb}$ | days | 4.7183808±0.0000001) | |
| $M$ | $M_\odot$ | 1.56±0.01 | 1.38±0.01 |
| $R$ | $R_\odot$ | 1.70±0.03 | 1.38±0.03 |
| log $g$ | cgs | 4.17±0.02 | 4.29±0.01 |
| $T$ | K | 6650±200 | 6235±201 |
| $M_{bol}$ | mag | 2.99±0.16 | 3.59±0.14 |
| $M_V$ | mag | 2.97±0.16 | 3.61±0.14 |
| $L$ | $L_\odot$ | 5.10±0.77 | 2.92±0.37 |
| $M_V$ | mag | 2.10±0.13 | |
| $BC$ | mag | 0.016 | -0.017 |
| $d$ | pc | 117±7 | |

### 4.2. Evolutionary status

A comparison of the measured physical parameters of a star with predictions from theoretical models can be made by means of the Hertzsprung–Russell (HR) diagram. According to the iron number abundance, [Fe/H]=0.17, given by Nordström et al. (2004) and Holmberg et al. (2009), the metallicity value was computed to be 0.021 using the relation between Z and [Fe/H] in the logarithmic scale[9]. Therefore, the locations of the components of V355 And were plotted on the log $T_{eff}$–log $(L/L_\odot)$ diagram (see Fig. 4), namely the HR diagram, using the Geneva stellar evolution models[10] (Mowlavi et al., 2012) for the metallicity Z=0.02. Trials were made for other Z values (Z=0.14 and Z=0.03); however, as it can be seen in Fig. 4, the theoretical evolution model at Z=0.02 is the most suitable for the masses of both components of the system. In addition, we also tried to predict the age of V355 And using the evolutionary isochrones for Z=0.02 adopted from Mowlavi et al. (2012). Consequently, with respect to the HR diagram, it can be said that the components of V355 And are main-sequence stars at the age of $\sim$ 1.26 Gyr.

[9]https://people.umass.edu/wqd/astro640/ToO.pdf

[10]https://www.unige.ch/sciences/astro/evolution/en/database/syclist/

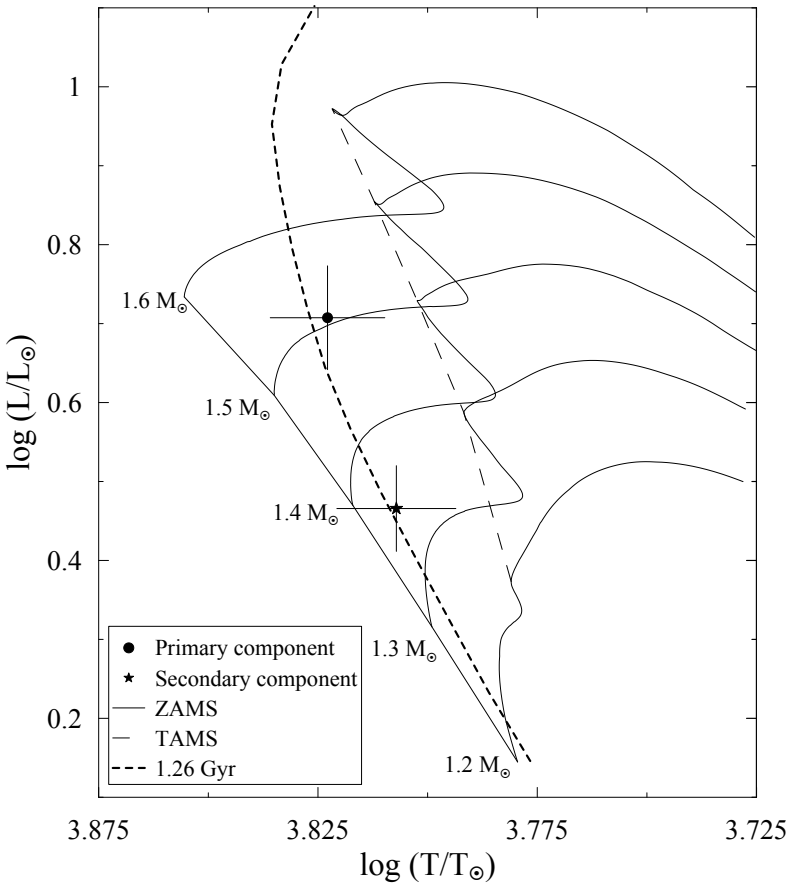


**Figure 4.** Locations of primary and secondary components of V355 And in the logarithmic temperature-luminosity plane according to Geneva stellar evolutionary models. ZAMS, TAMS and evolutionary tracks were taken from Mowlavi et al. (2012) for the metallicity of Z=0.02. Lines drawn vertically and horizontally denote error bars of the measured parameters. The isochrone for the estimated age of the system at 1.26 Gyr is represented by a dashed line. In the HR diagram the numbers added to the left of ZAMS indicate initial masses.

**Acknowledgements.** This paper includes data collected by the TESS mission, which are publicly available from the Mikulski Archive for Space Telescopes (MAST). The author would like to thank Prof. A. Erdem for his advice and comments, and Prof. S. Zola for his help in using the W–D FORTRAN code with modern limb-darkening coefficients. The author would like to thank the anonymous referee who provided valuable comments for improving the manuscript. The author also thanks Mr. G.H. Lee for checking the English.

## References

Avvakumova, E. A., Malkov, O. Y., & Kniazev, A. Y., Eclipsing variables: Catalogue and classification. 2013, *Astronomische Nachrichten*, **334**, 860, DOI: 10.1002/asna.201311942

Bilir, S., Ak, T., Soydugan, E., et al., New absolute magnitude calibrations for detached binaries. 2008, *Astronomische Nachrichten*, **329**, 835, DOI: 10.1002/asna.200811002

Butters, O. W., West, R. G., Anderson, D. R., et al., The first WASP public data release. 2010, *Astronomy and Astrophysics*, **520**, L10, DOI: 10.1051/0004-6361/201015655

Claret, A. & Bloemen, S., Gravity and limb-darkening coefficients for the Kepler, CoRoT, Spitzer, uvby, UBVRIJHK, and Sloan photometric systems. 2011, *Astronomy and Astrophysics*, **529**, A75, DOI: 10.1051/0004-6361/201116451

Claret, A., Hauschildt, P. H., & Witte, S., New limb-darkening coefficients for Phoenix/1d model atmospheres. II. Calculations for 5000 K $\leq$ $T_{eff}$ $\leq$ 10 000 K Kepler, CoRot, Spitzer, uvby, UBVRIJHK, Sloan, and 2MASS photometric systems. 2013, *Astronomy and Astrophysics*, **552**, A16, DOI: 10.1051/0004-6361/201220942

Drilling, J. S. & Landolt, A. U., Normal Stars. 2000, in *Allen's astrophysical quantities*, ed. A. N. Cox (Springer-Verlag New York), 381–396

Eastman, J., Siverd, R., & Gaudi, B. S., Achieving Better Than 1 Minute Accuracy in the Heliocentric and Barycentric Julian Dates. 2010, *Publications of the ASP*, **122**, 935, DOI: 10.1086/655938

ESA, VizieR Online Data Catalog: The Hipparcos and Tycho Catalogues (ESA 1997). 1997, *VizieR Online Data Catalog*, I/239

Flower, P. J., Transformations from Theoretical Hertzsprung-Russell Diagrams to Color-Magnitude Diagrams: Effective Temperatures, B-V Colors, and Bolometric Corrections. 1996, *Astrophysical Journal*, **469**, 355, DOI: 10.1086/177785

Gaia Collaboration, Brown, A. G. A., Vallenari, A., et al., Gaia Data Release 2. Summary of the contents and survey properties. 2018, *Astronomy and Astrophysics*, **616**, A1, DOI: 10.1051/0004-6361/201833051

Garcia, E. V., Stassun, K. G., Pavlovski, K., et al., A Strict Test of Stellar Evolution Models: The Absolute Dimensions of the Massive Benchmark Eclipsing Binary V578 Mon. 2014, *Astronomical Journal*, **148**, 39, DOI: 10.1088/0004-6256/148/3/39

Holmberg, J., Nordström, B., & Andersen, J., The Geneva-Copenhagen survey of the solar neighbourhood. III. Improved distances, ages, and kinematics. 2009, *Astronomy and Astrophysics*, **501**, 941, DOI: 10.1051/0004-6361/200811191

Hubscher, J., BAV-Results of observations - Photoelectric Minima of Selected Eclipsing Binaries and Maxima of Pulsating Stars. 2015, *Information Bulletin on Variable Stars*, **6152**, 1

Imbert, M., Vitesses Radiales, Elements Orbitaux et Modeles Pour 25 Systemes Doubles Spectroscopiques. 2006, *Romanian Astronomical Journal*, **16**, 3

Jayasinghe, T., Kochanek, C. S., Stanek, K. Z., et al., The ASAS-SN catalogue of variable stars I: The Serendipitous Survey. 2018, *Monthly Notices of the RAS*, **477**, 3145, DOI: 10.1093/mnras/sty838

Kazarovets, E. V., Samus, N. N., Durlevich, O. V., et al., The 74th Special Name-list of Variable Stars. 1999, *Information Bulletin on Variable Stars*, **4659**, 1

Kochanek, C. S., Shappee, B. J., Stanek, K. Z., et al., The All-Sky Automated Survey for Supernovae (ASAS-SN) Light Curve Server v1.0. 2017, *Publications of the ASP*, **129**, 104502, DOI: 10.1088/1538-3873/aa80d9

Kwee, K. K. & van Woerden, H., A method for computing accurately the epoch of minimum of an eclipsing variable. 1956, *Bulletin Astronomical Institute of the Netherlands*, **12**, 327

Lucy, L. B., Gravity-Darkening for Stars with Convective Envelopes. 1967, *Zeitschrift fuer Astrophysik*, **65**, 89

Maehara, H., Automated Wide-field Survey for Transient Objects with a Small Telescope. 2014, *JAXA research and development report*, **JAXA-RR-13-010**, 119

Malkov, O. Y., Oblak, E., Snegireva, E. A., & Torra, J., A catalogue of eclipsing variables. 2006, *Astronomy and Astrophysics*, **446**, 785, DOI: 10.1051/0004-6361:20053137

McDonald, I., Zijlstra, A. A., & Boyer, M. L., Fundamental parameters and infrared excesses of Hipparcos stars. 2012, *Monthly Notices of the RAS*, **427**, 343, DOI: 10.1111/j.1365-2966.2012.21873.x

Mowlavi, N., Eggenberger, P., Meynet, G., et al., Stellar mass and age determinations . I. Grids of stellar models from Z = 0.006 to 0.04 and M = 0.5 to 3.5 M. 2012, *Astronomy and Astrophysics*, **541**, A41, DOI: 10.1051/0004-6361/201117749

Nordström, B., Mayor, M., Andersen, J., et al., The Geneva-Copenhagen survey of the Solar neighbourhood. Ages, metallicities, and kinematic properties of ∼14 000 F and G dwarfs. 2004, *Astronomy and Astrophysics*, **418**, 989, DOI: 10.1051/0004-6361:20035959

Paunzen, E., A new catalogue of Strömgren-Crawford uvby$\beta$ photometry. 2015, *Astronomy and Astrophysics*, **580**, A23, DOI: 10.1051/0004-6361/201526413

Pecaut, M. J. & Mamajek, E. E., Intrinsic Colors, Temperatures, and Bolometric Corrections of Pre-main-sequence Stars. 2013, *Astrophysical Journal, Supplement*, **208**, 9, DOI: 10.1088/0067-0049/208/1/9

Pourbaix, D., Tokovinin, A. A., Batten, A. H., et al., $S_{B^9}$: The ninth catalogue of spectroscopic binary orbits. 2004, *Astronomy and Astrophysics*, **424**, 727, DOI: 10.1051/0004-6361:20041213

Ricker, G. R., Winn, J. N., Vanderspek, R., et al., Transiting Exoplanet Survey Satellite (TESS). 2015, *Journal of Astronomical Telescopes, Instruments, and Systems*, **1**, 014003, DOI: 10.1117/1.JATIS.1.1.014003

Ruciński, S. M., The Proximity Effects in Close Binary Systems. II. The Bolometric Reflection Effect for Stars with Deep Convective Envelopes. 1969, *Acta Astronomica*, **19**, 245

Shappee, B. J., Prieto, J. L., Grupe, D., et al., The Man behind the Curtain: X-Rays Drive the UV through NIR Variability in the 2013 Active Galactic Nucleus Outburst in NGC 2617. 2014, *Astrophysical Journal*, **788**, 48, DOI: 10.1088/0004-637X/788/1/48

Soubiran, C., Le Campion, J.-F., Brouillet, N., & Chemin, L., The PASTEL catalogue: 2016 version. 2016, *Astronomy and Astrophysics*, **591**, A118, DOI: 10.1051/0004-6361/201628497

Sürgit, D., Erdem, A., Engelbrecht, C. A., van Heerden, H. P., & Manick, R., Absolute parameters of detached binaries in the southern sky - III: HO Tel. 2017, *New Astronomy*, **54**, 109, DOI: 10.1016/j.newast.2017.01.013

Tikkanen, A., 160. list of minima of eclipsing binaries. 2002, *Bulletin der Bedeckungsveraenderlichen-Beobachter der Schweizerischen Astronomischen Gesellschaft*, **127**, 1

Wilson, R. E. & Devinney, E. J., Realization of Accurate Close-Binary Light Curves: Application to MR Cygni. 1971, *Astrophysical Journal*, **166**, 605, DOI: 10.1086/150986

Zasche, P., Wolf, M., Hartkopf, W. I., et al., A Catalog of Visual Double and Multiple Stars With Eclipsing Components. 2009, *Astronomical Journal*, **138**, 664, DOI: 10.1088/0004-6256/138/2/664

Zola, S., Gazeas, K., Kreiner, J. M., et al., Physical parameters of components in close binary systems - VII. 2010, *Monthly Notices of the RAS*, **408**, 464, DOI: 10.1111/j.1365-2966.2010.17129.x

Contrib. Astron. Obs. Skalnaté Pleso **51**, 132 – 137, (2021)
https://doi.org/10.31577/caosp.2021.51.2.132

# New SU UMa-type star ZTF18abdlzhd in the Zwicky Transient Facility data

**S.V. Antipin**[1], **A.M. Zubareva**[2,1], **A.A. Belinski**[1], **M.A. Burlak**[1], **N.P. Ikonnikova**[1], **K.L. Malanchev**[3,1], **M.V. Kornilov**[1,4] **and E.O. Mishin**[1]

[1] *Sternberg Astronomical Institute, M.V. Lomonosov Moscow State University, Universitetskij pr., 13, Moscow, 119234, Russia, (E-mail: serge_ant@inbox.ru)*

[2] *Institute of Astronomy of the Russian Academy of Sciences, Pyatnitskaya str., 48, Moscow, 119017, Russia*

[3] *Department of Astronomy, University of Illinois at Urbana-Champaign, 1002 West Green Street, Urbana, IL 61801, USA*

[4] *National Research University Higher School of Economics, Staraya Basmannaya str., 21/4, Moscow, 105066, Russia*

Received: December 04, 2020; Accepted: February 11, 2021

**Abstract.** We carried out a search for unknown dwarf novae in a public data release of the Zwicky Transient Facility survey and suspected that the object ZTF18abdlzhd is a SU UMa-type star. Performed multicolor CCD observations permit us to follow its fading from an outburst in August and an entire superoutburst in October 2020. The duration of the superoutburst is 13 days. We detected superhumps with period P = $0^{d}.06918(3)$ that are characteristic of UGSU type stars.

**Key words:** stars – photometry – dwarf novae – ZTF18abdlzhd

## 1. Introduction

Cataclysmic variables provide opportunities to observe various accretion-related phenomena in a setting of close binary systems. A white dwarf primary is receiving matter via the inner Lagrangian point (L1) from a low-mass secondary star that fills up its Roche lobe. Dwarf novae are a subclass of cataclysmic variables where the stream of matter forms an accretion disk around the white dwarf and the disk alters between hot (high accretion rate) and cold (low accretion rate) states resulting in recurrent dramatic changes in brightness.

SU UMa-type dwarf novae are known to increase their brightness by several magnitudes for days, after which they get back to the quiescent state for a while. Two kinds of outbursts are found in these systems, distinguished by the outburst amplitude and duration. Short low-amplitude outbursts are called normal, and long ones having greater amplitudes and a "plateau" phase, are

known as superoutbursts. In the course of a superoutburst, periodic brightness variations called "superhumps" occur. They are characterized by amplitudes up to 0.3 mag and have periods longer than the orbital period of a system by several percent. See more detailed information on Dwarf Novae in Warner (1995), and specifically on UGSU-type stars in Kato et al. (2009).

We revealed the object in Zwicky Transient Facility Data Release 3 (Bellm et al., 2019) during the dedicated search of dwarf novae. We downloaded ZTF DR3 light curves from the IRSA IPAC server[1]. Then we selected all $zr$ (ZTF Sloan $r$ band, see Fig. 2 from Bellm et al. (2019)) light curves with the following restrictions: the peak magnitude is brighter than 19.5 mag, the amplitude is at least 1 mag, the duration is between 10 and 30 days, and the number of observed nights is at least 10. Only good weather-condition observations were considered. This search yielded us 15 out of 3 billion ZTF DR3 objects.

A visual analysis of light curves was performed with the SNAD ZTF web-viewer[2] (Malanchev et al., in prep.[3]) and the object ZTF18abdlzhd was found as the only reliable UGSU candidate.

The outburst light curve based on ZTF data is shown in Fig. 1.

## 2. Observations

CCD photometry of ZTF18abdlzhd ($\alpha = 23^h15^m30\overset{s}{.}841, \delta = +57°08'46\overset{''}{.}98$, J2000) carried out in August and October 2020 permit us to follow the end of the fading stage of one outburst and a full superoutburst of this dwarf nova. We monitored the field of the variable with the new automated 60-cm telescope of the Caucasus Mountain Observatory of SAI MSU. The ASA RC600 60-cm reflector was installed at the Caucasus observatory supported by M.V. Lomonosov Moscow State University Program of Development. It is equipped with an Andor iKon-L (DZ936N-BV) 2048 × 2048 CCD-camera and a set of filters (see Berdnikov et al., 2020). Sloan $g$, $r$, $i$ (Fukugita et al., 1996) and Johnson-Cusins $B$, $V$, $R_c$, $I_c$ bands were used to explore the behaviour of ZTF18abdlzhd. Observations in $g$, $r$, $i$ were obtained on August 19–23, 2020 (JD2459081–85, 4 nights), and CCD frames in $B$, $V$, $R_c$, $I_c$ were taken on October 10–26, 2020 (JD2459133–149, 15 nights). The observational log is given in Table 1. The exposure times varied from 120 seconds during the outburst to 600 seconds in minimum brightness of the object.

To perform aperture photometry and magnitude calibration, we used VaST[4] software (Sokolovsky & Lebedev, 2018). We derived magnitudes of an ensemble of comparison stars within the field of view from the APASS ($B$, $V$, $R_c$, $I_c$) and the PanSTARRS1 ($g$, $r$, $i$) survey (Chambers et al., 2016).

[1] https://irsa.ipac.caltech.edu/data/ZTF/lc_dr3/

[2] https://ztf.snad.space

[3] https://arxiv.org/abs/2012.01419

[4] https://scan.sai.msu.ru/vast

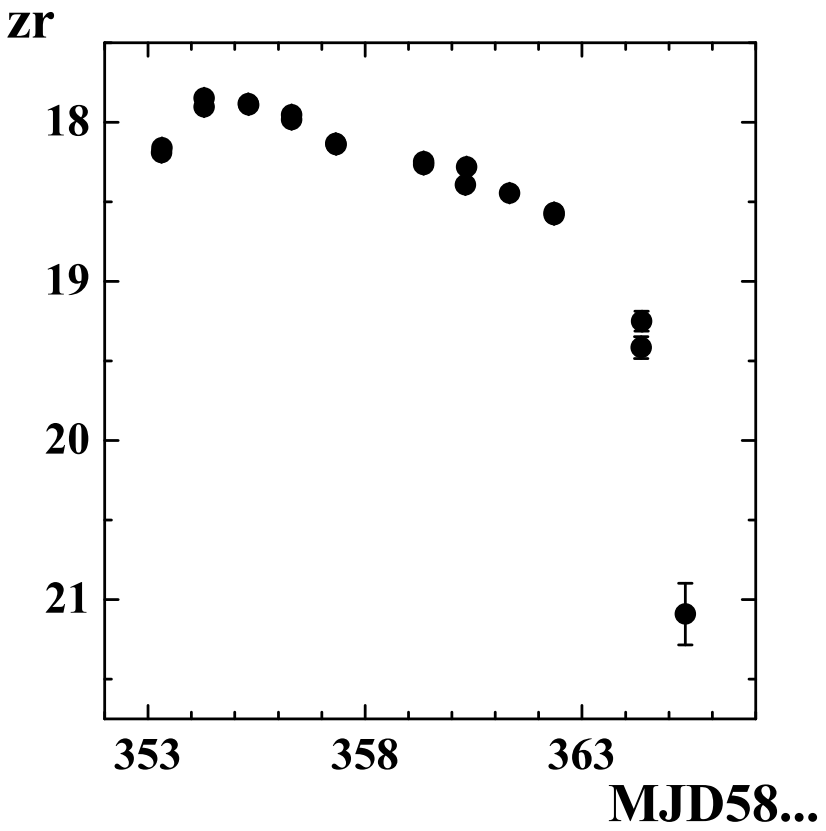


**Figure 1.** ZTF18abdlzhd outburst light curve from ZTF survey data. *zr* is for ZTF *r* band whose transmission curve is depicted in Fig.2 in Bellm et al. (2019).

## 3. Results

Our data cover two outbursts of ZTF18abdlzhd. Unfortunately, we have no opportunity to classify the type of the August outburst (normal or superoutburst, see the left panel of Fig. 2) because the observations reveal only the final stage of the event.

On October 10, 2020, we found the variable in its bright state again. The brightness of the variable star increased to the next night of observations, so we can say that we detected the dwarf nova at the beginning of an outburst. The total duration of this outburst is 13 days which is very similar to the event found in ZTF data (cf. Fig. 1 and the right panel of Fig. 2).

ZTF18abdlzhd reached the maximum brightness on October, 11, $R_c = 17.49$ mag. Immediately after the superoutburst, the star faded to $R_c = 21.8$ mag. In

**Table 1.** Observational log.

| JD | Date | Number of frames (Band) |
|---|---|---|
| 2459081 | August 19, 2020 | 3 ($g$), 23 ($r$), 2 ($i$) |
| 2459082 | August 20, 2020 | 1 ($g$), 1 ($r$), 1 ($i$) |
| 2459084 | August 22, 2020 | 1 ($r$) |
| 2459085 | August 23, 2020 | 1 ($r$) |
| 2459133 | October 10, 2020 | 5 ($B$), 5 ($V$), 5 ($R_c$), 5 ($I_c$) |
| 2459134 | October 11, 2020 | 2 ($B$), 2 ($V$), 2 ($R_c$), 2 ($I_c$) |
| 2459135 | October 12, 2020 | 2 ($B$), 2 ($V$), 2 ($R_c$), 2 ($I_c$) |
| 2459136 | October 13, 2020 | 2 ($B$), 2 ($V$), 2 ($R_c$), 2 ($I_c$) |
| 2459137 | October 14, 2020 | 1 ($B$), 1 ($V$), 73 ($R_c$), 1 ($I_c$) |
| 2459138 | October 15, 2020 | 45 ($R_c$) |
| 2459139 | October 16, 2020 | 43 ($R_c$) |
| 2459140 | October 17, 2020 | 2 ($B$), 2 ($V$), 2 ($R_c$), 2 ($I_c$) |
| 2459141 | October 18, 2020 | 2 ($B$), 2 ($V$), 2 ($R_c$), 2 ($I_c$) |
| 2459144 | October 21, 2020 | 1 ($B$), 1 ($V$), 1 ($R_c$), 1 ($I_c$) |
| 2459145 | October 22, 2020 | 1 ($B$) |
| 2459146 | October 23, 2020 | 6 ($R_c$) |
| 2459147 | October 24, 2020 | 1 ($R_c$) |
| 2459148 | October 25, 2020 | 1 ($R_c$) |
| 2459149 | October 26, 2020 | 1 ($R_c$) |

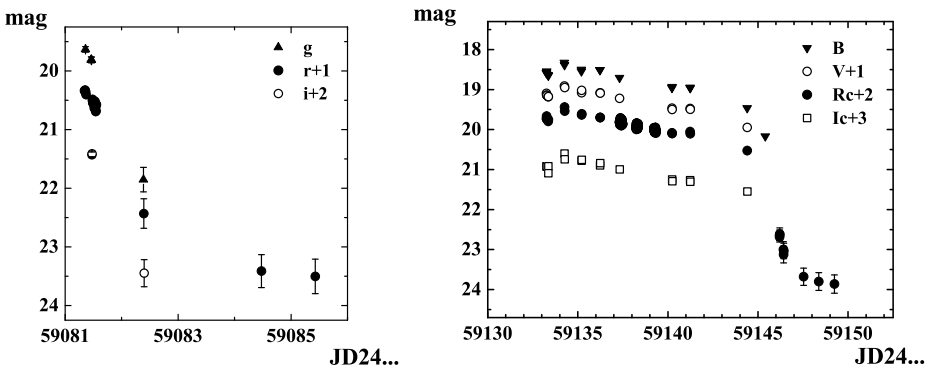


**Figure 2.** ZTF18abdlzhd. The fading stage of the August outburst (left panel) and the superoutburst of October 2020 (right panel).

the next few days, the dwarf nova passed beyond the detection limit (about 22.0 mag in $R_c$-band at 600 s exposure). Thus, the variability amplitude is greater than 4.5 mag. We found ZTF18abdlzhd in PanSTARRS DR1 (object ID 176573488784746366) at $r = 22.096 \pm 0.196$ mag (Chambers et al., 2016)).

Color indices remain constant during the plateau phase of the outburst and are equal to $B - V = 0.46 \pm 0.02$, $V - R_c = 0.41 \pm 0.02$ and $V - I_c = 0.23 \pm 0.03$.

During the maximum of the October 2020 outburst we found a periodic brightness variability – superhumps – which are a distinctive feature of a superoutburst (see Fig. 3). The most of our observations in the plateau phase of this superoutburst were obtained in $R_c$ band – 161 frames for three nights covered with photometry densely (see Table 1). For this set we removed a linear trend from the brightness measurements before running the period search for which WinEfk software[5] developed by Dr. V.P. Goranskij was applied. The corresponding periodogram and the phased light curve of the superhumps are given in Fig. 4. The ephemeris is as follows:

$$JD_{max} = 2459137.4314 + 0.06918(3) \times E.$$

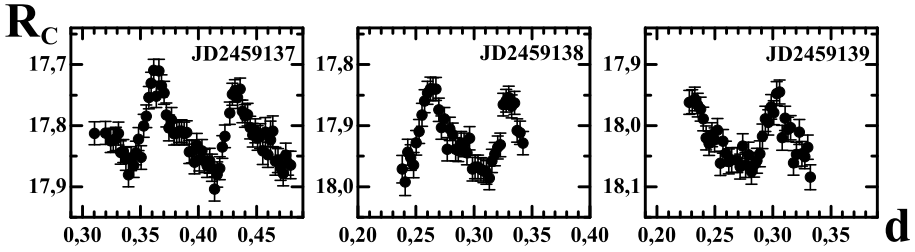


**Figure 3.** Individual light curves of ZTF18abdlzhd for three nights in maximum of the superoutburst (October 14, 15 and 16, 2020).

## 4. Conclusion

Based on the ZTF survey data, we suspected that object ZTF18abdlzhd is a UGSU-type star. Our CCD observations allow us to confirm this assumption. The duration of the October 2020 superoutburst was 13 days. We found a superhump period $P = 0^{d}.06918(3)$.

**Acknowledgements.** The authors are grateful for partial support from M.V. Lomonosov Moscow State University Program of Development. This research has been

[5]http://www.vgoranskij.net/software/

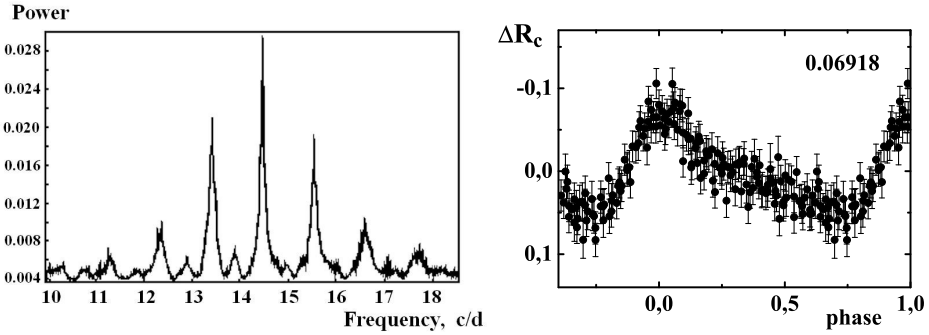


**Figure 4.** Left panel: the periodogram for three nights of observations shown in Fig. 3. Maximum peak corresponds to the frequency 14.455(6) c/d and period 0.06918(3) days. Right panel: the corresponding phased light curve of superhumps.

supported by the Interdisciplinary Scientific and Educational School of Moscow University "Fundamental and Applied Space Research". K.L.M. and M.V.K. are supported by RFBR grant 20-02-00779 for the preparing ZTF data and the revealing of the object. The study was made possible through the use of the AAVSO Photometric All-Sky Survey (APASS), funded by the Robert Martin Ayers Sciences Fund and NSF AST-1412587.

## References

Bellm, E. C., Kulkarni, S. R., Graham, M. J., et al., The Zwicky Transient Facility: System Overview, Performance, and First Results. 2019, *Publications of the ASP*, **131**, 018002, DOI: 10.1088/1538-3873/aaecbe

Berdnikov, L. N., Belinskii, A. A., Shatskii, N. I., et al., $BVI_c$ Observations and Search for Evolutionary Variations in the Cepheid V811 Oph Period. 2020, *Astronomy Reports*, **64**, 310, DOI: 10.1134/S1063772920040010

Chambers, K. C., Magnier, E. A., Metcalfe, N., et al., The Pan-STARRS1 Surveys. 2016, *arXiv e-prints*, arXiv:1612.05560

Fukugita, M., Ichikawa, T., Gunn, J. E., et al., The Sloan Digital Sky Survey Photometric System. 1996, *Astronomical Journal*, **111**, 1748, DOI: 10.1086/117915

Kato, T., Imada, A., Uemura, M., et al., Survey of Period Variations of Superhumps in SU UMa-Type Dwarf Novae. 2009, *Publications of the ASJ*, **61**, S395, DOI: 10.1093/pasj/61.sp2.S395

Sokolovsky, K. V. & Lebedev, A. A., VaST: A variability search toolkit. 2018, *Astronomy and Computing*, **22**, 28, DOI: 10.1016/j.ascom.2017.12.001

Warner, B., Cataclysmic variable stars. 1995, *Cambridge Astrophysics Series*, **28**

Contrib. Astron. Obs. Skalnaté Pleso **51**, 138 – 162, (2021)
https://doi.org/10.31577/caosp.2021.51.2.138

# MASTER OT J172758.09+380021.5: a peculiar ER UMa-type dwarf nova, probably a missed nova in the recent past

**E. Pavlenko[1], T. Kato[2], K. Antonyuk[1], N. Pit[1], L. Keir[3], S. Udovichenko[3], P. Dubovský[4], A. Sosnovskij[1], O. Antonyuk[1], V. Shimansky[5,6], M. Gabdeev[5,6,7], F. Rakhmatullaeva[8], G. Kokhirova[8], S. Belan[1], A. Simon[9], A. Baklanov[1], N. Kojiguchi[2] and V. Godunova[10]**

[1] *Federal State Budget Scientific Institution "Crimean Astrophysical Observatory of RAS", Nauchny, 298409, Republic of Crimea, (E-mail: eppavlenko@gmail.com)*

[2] *Department of Astronomy, Kyoto University, Kyoto 606-8502, Japan*

[3] *Astronomical Observatory, I. I. Mechnikov Odessa National University, Odessa oblast, Ukraine*

[4] *Vihorlat Observatory, Mierova 4, 06601 Humenne, Slovakia*

[5] *Kazan (Volga region) Federal University, Kazan, 420008, Kremlyovskaya 18, Russia*

[6] *Special Astrophysical Observatory, 369167, Nizhnij Arkhyz, Karachai-Cherkessian Republic, Russia*

[7] *Tatarstan Academy of Science Institute of Advanced Studies, 4221, Levobulachnaya St. 36 A, Kazan, Tatarstan republic, Russia*

[8] *Institute of Astrophysics of the Academy of Sciences of the Republic of Tajikistan, Bukhoro 22, Dushanbe, 734042, Tajikistan*

[9] *Astronomy and Space Physics Department, Taras Shevshenko National University of Kyiv, Volodymyrska str. 60, Kyiv, 01601, Ukraine*

[10] *ICAMER Oservatory of NAS of Ukraine, 27 Acad. Zabolotnogo str., 03143 Kyiv, Ukraine*

Received: November 5, 2020; Accepted: February 25, 2021

**Abstract.** A CCD photometry of the dwarf nova MASTER OT J172758.09 +380021.5 was carried out in 2019 during 134 nights. Observations covered three superoutbursts, five normal outbursts and quiescence between them. The available ASASSN and ZTF data for 2014 – 2020 were also examined. Spectral observations were done in 2020 when the object was in quiescence. Spectra and photometry revealed that the star is an H-rich active ER UMa-type dwarf nova with a highly variable supercycle (time interval between two successive superoutbursts) of $\sim 50 - 100$ d that implies a high and variable mass-transfer rate. MASTER OT J172758.09+380021.5 demonstrated peculiar behaviour: short-lasted superoutbursts (a week); a slow superoutburst decline and cases

of rebrightenings; low frequency (from none to a few) of the normal outbursts during the supercycle. In 2019 a mean period of positive superhumps was found to be 0.05829 d during the superoutbursts. Late superhumps with a mean period of 0.057915 d which lasted about $\sim$ 20 d after the end of superoutburst and were replaced by an orbital period of 0.057026 d or its orbital-negative superhump beat period were detected. An absence of eclipse in the orbital light curve and its moderate amplitude are consistent with the orbital inclination of about 40° found from spectroscopy. The blue peaks of the *V-Ic* and *B-Rc* colour indices of superhumps during the superoutburst coincided with minima of the light curves, while *B-Rc* of the late superhumps coincided with a rising branch of the light curves. We found that a low mass ratio $q = 0.08$ could explain most of the peculiarities of MASTER OT J172758.09+380021.5. The mass-transfer rate should be accordingly higher than what is expected from gravitational radiation only, this assumes the object is in a post-nova state and underwent a nova eruption relatively recently – hundreds of years ago. This object would provide probably the first observational evidence that a nova eruption can occur even in CVs near the period minimum.

**Key words:** stars: MASTER OT J172758.09+380021.5 – dwarf novae – activity

## 1. Introduction

Cataclysmic variables (CVs) are close binary systems in which a white dwarf (WD) accretes matter from a late-type donor star that fills its Roche lobe. Accretion is either disc-like or pole-on if a WD is non-magnetic or magnetic one, respectively. The orbital periods of CVs are limited by a rather blurry border of about 12 hours and by a strong period minimum at 78 min (Hellier, 2001). There is a so-called orbital period gap between 2.15 and 3.18 hours (Knigge, 2006) with a significant deficit of non-magnetic CVs. Non-magnetic CVs in the period gap and below it up to the period minimum are the SU UMa-type stars (Warner, 1995). These binaries are the H-rich stars approaching during their evolution to the period minimum or passed it ("period bouncers"), further evolution of period bouncers takes place with an increase of the orbital period. 56 system are known at present which have shorter periods than the period minimum. They are the He-rich AM CVn stars (Green et al., 2018) evolving with a decrease of the period. CVs on a way to AM CVn stars are called "EI Psc-type stars" (Kato et al., 2016a), they exhibit both H and He and are located near the period minimum. Another subgroup of SU UMa-stars, namely WZ-type stars, could also be found close to the period minimum (Kato, 2015). Transfer of matter from the late-type companion leads to thermal instability of the accretion disk and causes its outburst - a dwarf nova (DN) event (Osaki, 1996). SU UMa stars display two types of outbursts: the normal outbursts that last 2-5 days and brighter and longer superoutbursts lasting up to several weeks.

During the superoutbursts periodic brightness variations (positive superhumps) with periods of a few percent longer than the orbital period are present.

These superhumps, as it was shown by Whitehurst (1988); Osaki (1989); Hirose & Osaki (1990); Lubow (1991), are the consequence of tidal instability resulting from the 3:1 resonance in the accretion disc. This can only happen for the SU UMa-type stars with a mass ratio $q = M_2/M_1 \leq 0.3$, where $M_2$ and $M_1$ are the masses of the donor and WD stars, respectively.

Kato et al. (2009) introduced three stages in the positive superhump evolution: Stage A has longer superhump periods and growth of superhump amplitudes; superhump periods during Stage B could systematically decrease/increase or be stable with a decrease of their amplitudes; Stage C has shorter superhump periods.

Some of the DNe display so-called late superhumps (Vogt, 1983). They have a similar period **as** positive superhumps, but have phases shifted by a half of this period. One explanation of this phenomenon is that they arise from a hot spot on an elliptical disc (Osaki, 1985).

Contrary to the positive superhumps, the negative superhumps have periods a few percents shorter than the orbital one. Negative superhumps mostly appear in quiescence independently on the mass ratio (Montgomery, 2010; Pavlenko et al., 2019) and probably are caused by nodal precession of a tilted accretion disk (Warner, 2003). Osaki & Kato (2014) suggested that decrease of the frequency of the normal outbursts in some DNe resulting in a transition from a short (S) cycle to a long (L) one (designations of cycles, i.e., the interval between two successive outbursts, is taken from Smak (1985)) could be caused by a transition of a disc from coplanar with an orbital plane to a tilted to the orbital plane and the subsequent appearance of nodal precession and negative superhumps. This suggestion was confirmed for NY Her (Sosnovskij et al., 2017), V1504 Cyg (Osaki & Kato, 2013) and V503 Cyg (Pavlenko et al., 2019).

WZ-type stars have in average a lowest mass transfer rate and rare outbursts that occur every several years - decades and actually are the superoutbursts with no normal outbursts with rare exceptions (Kato, 2015). One of the outstanding features of WZ Sge-type stars is rebrightenings, which are outbursts that appear after the plateau of the superoutburst during the superoutburst decline (Kato, 2015). WZ-type stars display a long-lasting approach to the quiescence. The superhumps during this stage (late-stage superhumps) could be observable, indicating that the disc in this stage is still thermally and tidally unstable.

About 25 years ago a special sub-group of SU UMa stars, ER UMa-type stars (Kato & Kunjaya, 1995; Nogami et al., 1995), was distinguished among the DNe as having an extremely highest frequency of superoutbursts (every 20-50 days).

DN MASTER OT J172758.09+380021.5 (hereafter MASTER 1727) was discovered by Denisenko et al. (2014) in an outburst at $V = 14^m.3$. Thorstensen et al. (2016) obtained spectrum in quiescence at $V \sim 18^m.5$. It showed very strong, relatively narrow single-peaked emission lines of H. The emission-line velocities indicated an orbital period of 82.14(6) minutes. The authors predicted the superhumps detection in the nearest future. Indeed, superhumps were dis-

covered in the 2019 superoutburst (see vsnet-alerts 22236 and 23335)[1], where the superhump period was reported to be 0.0565(1) d and 0.05803(1) d, respectively. K. Naoto previously suggested that this object might be the EI Psc-type candidate (vsnet-alert 23720). According to the available ASASSN (Shappee et al., 2014) light curve[2] one could suggest a rather short supercycle (interval between two successive superoutbursts) of $\sim 50 - 60$ d and unusually low frequency of normal outbursts between them within JD 2458415 – 2458650.

In this paper, we present a spectral and photometric study of MASTER 1727 at different stages of its activity based on our observations in 2019 – 2020 and on the ASASSN and ZTF[3] (Masci et al., 2019) database in 2014 – 2019.

## 2. Observations and data reduction

Spectral observations were carried out at the 6-m telescope of SAO RAS on 29 April 2020 using the SCORPIO reducer with a long slit mode. We used the volume holographic grating with 1200 lines per mm (VPHG1200G) and the 1" slit. We obtained the spectra in the range $\lambda\lambda = 3900 - 5700$ Å with the resolution of 5.5 Å. Five consecutive exposures with a total duration of 25 minutes were obtained. For the wavelength and flux calibration we used the HeNeAr lamp and a spectrophotometric standard. The observed data reduction was performed with standard methods under the IDL[4] environment. Bright sky background, light clouds and seeing of stars about 2.5" provided the resulting S/N ratio $\sim 40$.

Photometric observations were carried out in 2019 during 134 nights (174 independed runs of observations) from June 25 to November 5 in the Crimean Astrophysical Observatory, Vihorlat Observatory, and in Observatories of Mayaki, Sanglokh and Terskol (see the log of observations given that is available in an electronic form). Most of the observations were done in white light (without any filter) but several observations close to the Johnson-Cousins *B, V, Rc* and *Ic* system were obtained. We used the comparison star 1280-0316078 of the USNO B1.0 catalogue. Depending on astroclimatic conditions (i.e. sky background, light absorption in the atmosphere and seeing), telescope and brightness of the object, exposure time varied and provided $S/N = 20-200$. We used the MAXIM DL package for aperture photometry after standard data processing (i.e., debiasing, dark subtracting, flat-fielding).

For further analyses of the time series we used the Stellingwerf method implemented in the ISDA package (Pel't, 1980) and used the O-C analysis for the times of light curves maxima. For this and analysis of multicolour observations, we used the MCV program (Andronov & Baklanov, 2004).

[1] https://groups.yahoo.com/neo/groups/cvnet-outburst/
[2] http://cv.asassn.astronomy.ohio-state.edu/
[3] https://lasair.roe.ac.uk/
[4] http://www.ittvis.com/idl

## 3. Results

### 3.1. Spectrum in the 2020 quiescence

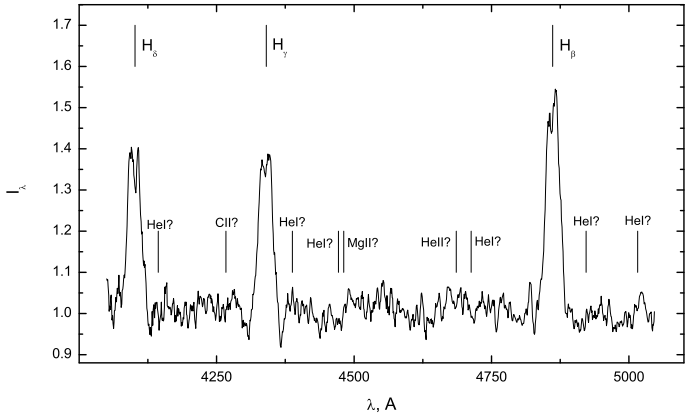


**Figure 1.** Spectrum of MASTER 1727 in the 2020 quiescence.

In the spectrum, double-peaked emission lines of the Balmer series with a $FWHM = 23 - 27$ $\mathring{A}$ are observed (see Fig. 1). The lines of neutral and ionized He are not found with exception of a weak emission near 5015 Å, which probably is an artefact of sky lines subtraction. Besides of these lines, the CII and Mg II ions are also absent in the spectrum. Peak-to-peak distances in the HI ($\Delta\lambda = 13.2 - 13.9$ Å) correspond to rotational velocity of the outer radius of the accretion disc $Vsin(i) = 410 - 450$ km/s. Assuming the WD Roche-lobe radius $R_L = 0.4R_\odot$, its mass $M_1 = 0.75M_\odot$ and the ratio of the outer radius of the accretion disk to the Roche-lobe size equal to 0.8, one could estimate the orbital inclination $i = 40^\circ \pm 2^\circ$.

According to the theoretical calculations of Paczynski (1977), the size of this radius is limited by the tidal effect of the secondary component and is about 0.8 $R_L^1$. To find the value of $R_L^1$ we applied the method for estimating the masses of the components of the close binaries developed by Borisov et al. (2017). The WD mass corresponds to $M_1 = 0.75M_\odot$, the average mass of the primary component WD (Ritter & Kolb, 2011). For a large set of mass ratios of the components $q = M_2/M_1$, we calculated the mass of the secondary component $M_2$ and the size of its Roche lobe according to the Eggleton formula (Eggleton, 1983):

$$R_L^2 = \frac{0.49q^{2/3}}{0.6q^{2/3} + \ln(1 + q^{1/3})}, \quad 0 < q < \infty \tag{1}$$

We estimated the radius of the secondary component $R_2$ for each value of its mass based on the results of evolutionary calculations of Baraffe et al. (2003) and

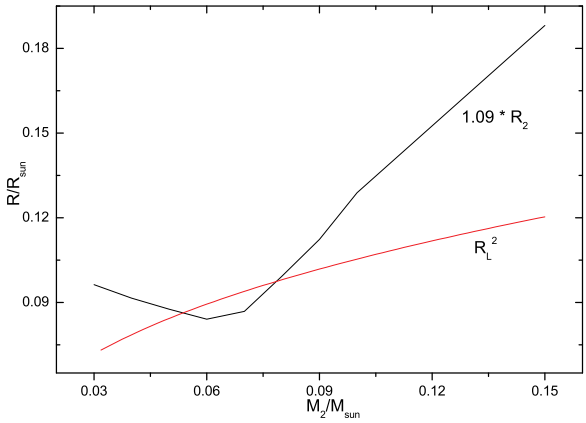


**Figure 2.** Dependences of the secondary star radius $R_2$ and its Roche-lobe radius $R_L^2$ on its mass $M_2$.

Girardi et al. (2000) for the low-mass dwarfs. The resulting dependences of $R_2$ and $R_L^2$ on $M_2$ were compared (see Fig. 2) taking into account the assumption that for systems with stable accretion the following condition is valid:

$$R_L^2 = 1.05 - 1.09 \sim R_2 \tag{2}$$

For $M_2 = 0.070 M_\odot \pm 0.005 M_\odot$, ensuring the fulfillment of the condition, we calculated by the formula (Eggleton, 1983) Roche-lobe radius of the primary component $R_L^1 = 0.347 R_\odot \pm 0.030 R_\odot$ and the outer radius of the accretion disk $R_{AD} = 0.28 R_\odot \pm 0.03 R_\odot$. Comparing the Keplerian velocity at this radius $V = 690$ km/s with the observed values presented above we can find the angle of inclination of the orbit is $i = 41^\circ \pm 5^\circ$.

### 3.2. A long-term light curve

In this subsection, we consider supercycles, cycles and morphology of superoutbursts based on our data obtained in 2019 and on the available ASASSN and ZTF data obtained in 2014 -2019.

#### 3.2.1. 2019 light curve

The overall 2019 light curve of Master 1727 is shown in Fig. 3. It is constructed using our and part of ASASSN data. It covered three superoutbursts with the amplitude of $\sim 4^m$ and four normal outbursts. All superoutbursts displayed an unusually short duration of about one week. This is shorter than a range of

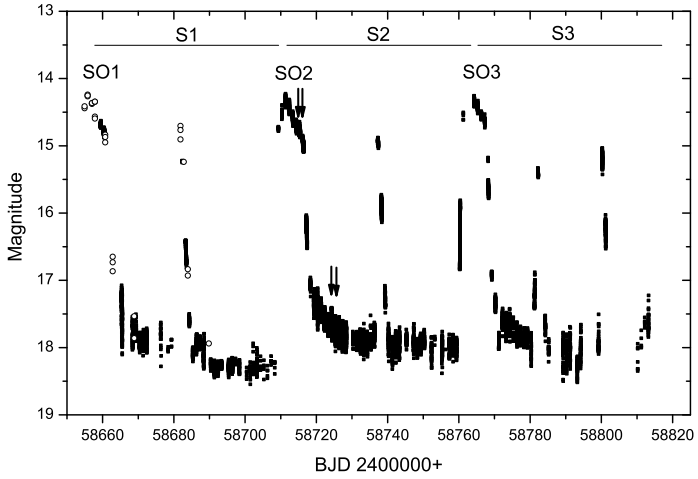


**Figure 3.** An overall 2019 light curve of MASTER 1727. SO1, SO2 and SO3 denote the number of superoutbursts while S1, S2 and S3 denote the number of supercycles. Our and ASASSN data are marked by black and open circles, respectively. Arrows indicate the time of colourimetric observations.

typical H-rich DNe (Warner, 1995) with exception of the 6-d duration in RZ LMi (Robertson et al., 1995), though there are a few He-rich AM CVn systems (Cannizzo & Ramsay, 2019) with a duration of superoutbursts less than 10 days. The superoutburst plateau of MASTER 1727+38 declined with a rate of $\sim 0.136$ mag/d. Then the superoutburst displayed rapid decay of $\sim$2.5 mag in two days, subsequent slow return to quiescence that lasted up to the beginning of the next superoutburst, and a short supercycle of 52 d. The normal outbursts lasted about two days. There was only one normal outburst just in the middle between superoutbursts, this activity repeated for two neighbour supercycles. However, the next supercycle included at least two normal outbursts. The appearance of outbursts during a slow approaching of superoutbursts to quiescence looks like rebrightenings often seen in the WZ Sge-type stars (Kato, 2015).

### 3.2.2. ASASSN and ZTF 2014 – 2019 light curve

It was possible to explore the outburst activity of MASTER 1727 on the $\sim$5.5-year scale (2014 – 2019) using the available ASASSN and ZTF data (see Fig. 4). Contrary to our observations, we cannot immediately identify a type of all bright events (whether they are normal outbursts or superoutbursts) for this data. Moreover, in the case of the the superoutburst, maximum of brightness potentially could refer to any moment within the 7-day plateau. Probably all the data of $14^m - 14.5^m$ refer to the superoutbursts. The impression from the visual inspection of the data is that the supercycle is not constant on a 5.5-year

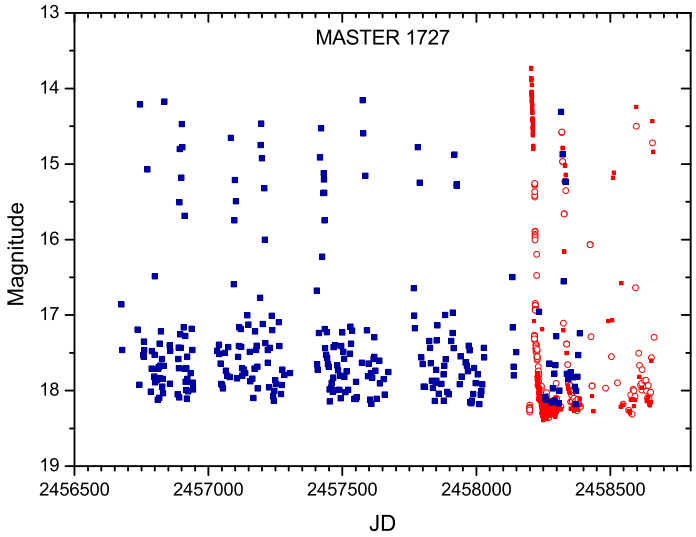


**Figure 4.** The ∼5.5-year light curve. ASASSN and ZTF data are shown by blue and red colours, respectively.

scale. Due to the short duration of the superoutburst, risk of missing it in a not very dense observation series makes it difficult to accurately determine the supercycle length. Nevertheless, denser observations (also taking into account our data) allow us to conclude that the supercycle could change in a range of 52 - 110 d during 1.5 years at least in 2018 - 2019. Note that no normal outbursts occurred during the 110-d supercycle. Of all the data on a 5.5-year scale, six events with a complex profile can be distinguished (Fig.5). The most striking among them are the fifth and sixth events. The fifth event obviously is the superoutburst with two rebrightenings. A plateau of this superoutburst lasted a ∼week. The sixth event could be understood as a superoutburst lasting 6 – 9 d and the subsequent rebrightening with an unusually long (∼6 d) rising branch. The first – fourth events probably can also be related to superhumps with rebrightenings.

### 3.3. Superhumps during 2019 SO2 superoutburst

Due to the fact that the SO2 superoutburst plateau was closely covered by observations, we calculated its mean superhump period. A periodogram indicates the most significant period of 0.05803(4) d among the one-day aliased peaks (see Fig. 6) that we attribute to the positive superhump period. Its mean the profile is asymmetric one with an amplitude of about $0^m.1$. Over a course of all superoutbursts and in more detail during the SO2 superoutburst (Fig.8), the original amplitudes of superhumps decrease from $0^m.15$ to $0^m.05$ This means that su-

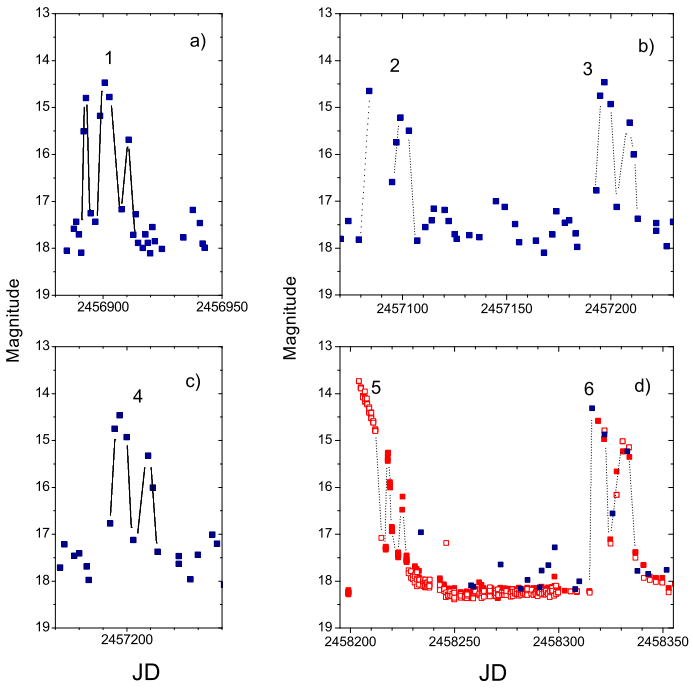


**Figure 5.** Fragments (a, b, c, d) of the long-term light curve displaying complex morphology of the outburst profile. The first event probably associates with a normal outburst + superoutburst + rebrightening, the second – fourth events and the sixth one with the superoutburst + rebrightening and the fifth event with the superoutburst and two rebrightenings. ASASSN and ZTF data are shown by blue and red colours, respectively.

perhumps were already fully grown since the superoutburst maxima (stage B) and stage A was probably too brief (a day or so) to be catched by us.

The periodic light variations with a period close to a superhump period continued over the quiescence between superoutbursts during every supercycle. The times of maxima for nightly light curves were defined wherever possible (see Tab. 1) and (O-C)s were calculated using the zero epoch of BJD 2458710.346 and the period of 0.0580294 d. The O-C for the superhumps maxima of the SO2 superoutburst displayed a possibly slight increase of the mean period.

### 3.4. Periodicity in quiescence

Starting with BJD 2458717, which was ∼ a middle of the fast SO2 superoutburst decline, the (O-C)s displayed a clear jump by a half the period of positive superhumps. This event looked like classical late superhumps (Vogt, 1983; Kato

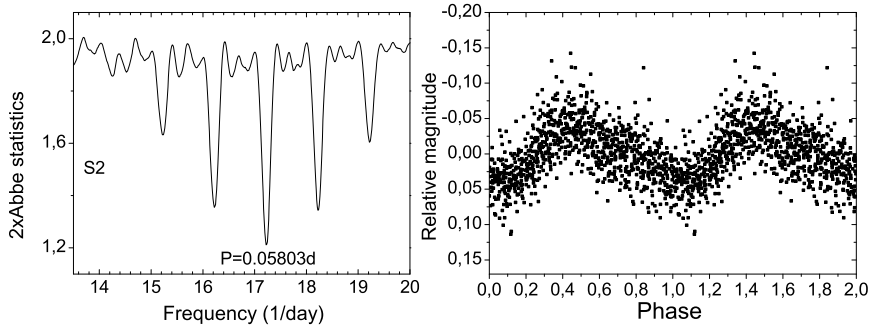


**Figure 6.** Left: a periodogram for the S2 superoutburst plateau in the vicinity of the superhump period. A corresponding zero epoch is 2458711.29888. The most significant peak indicates the period of 0.05803(4) d. Right: data folded on this period.

et al., 2002; Uemura et al., 2002) that is shown in Fig.7 and Fig.8. Further (O-C)s decreased up to the next superoutburst that means that the corresponding period was shorter than superhumps in the superoutburst. Simultaneously the mean amplitude of this periodicity grew from $0^m.05$ to $0^m.35$ up to the onset of the normal outburst. After that, the cycle-to-cycle amplitudes varied around the mean amplitude of $\sim 0^m.15$ up to the end of the supercycle.

It seems that the O-C behaviour repeated from supercycle to supercycle. To study the nature of periods in quiescence we combined the O-C for all S1, S2 and S3 supercycles by choosing the zero-point as the onset of the corresponding superoutburst. Despite poorer statistics for S1 and S3 supercycles, the O-C behaviours are consistent with each other. We have identified three stages in the O-C behaviour: a stage of the superoutburst plateau Sa, quiescence Sb that is limited by the end of the superoutburst and the normal outburst, and quiescence Sc between the end of the normal outburst and the next superoutburst (see Fig. 9). Limited and uneven coverage of the superhump plateau does not enable us to define the evolution of superhumps during stage B. The mean period at this stage is 0.058029 d. The stages Sb and Sc could be fitted by the linear trends which refer to two periods of 0.057938 d and 0.057611 d, respectively. Alternatively, Sb+Sc stages could be approximated by a parabola. The scattering around linear fits seems to be slightly less than around the parabola, so the version of two periods in quiescence is more reliable.

We performed a periodogram analysis for the data at Sb and Sc stages using data of the S2 supercycle only (Fig. 10). The periods at these stages were 0.057915(10) d and 0.057026(10) d, respectively. One could see a good agreement of the O-C and periodogram analyses for the period at the Sb stage. The mean period at the stage Sb is 0.00011 d less than the mean period at the Sa stage. We suggest that this is a period of late superhumps that lasted about 20 d up to

**Table 1.** Times of nightly light curves maxima of the MASTER J1727 in 2019.

| BJD 2458000+ | Error | BJD 2458000+ | Error | BJD 2458000+ | Error | BJD 2458000+ | Error |
|---|---|---|---|---|---|---|---|
| 659.457 | 0.003 | 715.212 | 0.003 | 722.318 | 0.004 | 733.324 | 0.003 |
| 659.517 | 0.003 | 715.270 | 0.002 | 722.324 | 0.003 | 736.332 | 0.005 |
| 660.333 | 0.004 | 715.330 | 0.005 | 722.325 | 0.002 | 736.343 | 0.004 |
| 660.395 | 0.003 | 715.331 | 0.002 | 722.381 | 0.002 | 738.264 | 0.005 |
| 660.456 | 0.002 | 715.332 | 0.003 | 722.441 | 0.003 | 743.298 | 0.006 |
| 665.356 | 0.004 | 715.389 | 0.003 | 723.252 | 0.002 | 745.245 | 0.007 |
| 665.419 | 0.003 | 715.445 | 0.004 | 723.311 | 0.003 | 747.293 | 0.005 |
| 668.377 | 0.003 | 716.144 | 0.003 | 723.375 | 0.003 | 748.328 | 0.006 |
| 668.432 | 0.003 | 716.202 | 0.003 | 724.298 | 0.002 | 749.230 | 0.004 |
| 669.415 | 0.003 | 716.316 | 0.002 | 724.359 | 0.002 | 749.290 | 0.005 |
| 670.400 | 0.003 | 716.317 | 0.003 | 724.414 | 0.002 | 749.325 | 0.006 |
| 670.456 | 0.003 | 716.318 | 0.005 | 725.279 | 0.002 | 752.311 | 0.003 |
| 671.380 | 0.008 | 716.375 | 0.003 | 725.279 | 0.003 | 755.317 | 0.004 |
| 671.503 | 0.005 | 716.376 | 0.002 | 725.336 | 0.002 | 759.315 | 0.003 |
| 672.400 | 0.003 | 716.435 | 0.003 | 725.390 | 0.004 | 760.297 | 0.005 |
| 683.319 | 0.01 | 717.160 | 0.003 | 725.396 | 0.002 | 764.296 | 0.004 |
| 683.445 | 0.008 | 717.225 | 0.004 | 726.319 | 0.003 | 765.213 | 0.003 |
| 686.347 | 0.005 | 717.396 | 0.003 | 727.255 | 0.002 | 766.265 | 0.005 |
| 686.410 | 0.007 | 718.317 | 0.003 | 727.310 | 0.008 | 770.243 | 0.005 |
| 691.390 | 0.01 | 719.300 | 0.004 | 727.314 | 0.004 | 770.295 | 0.005 |
| 710.346 | 0.002 | 719.301 | 0.003 | 727.368 | 0.008 | 772.288 | 0.004 |
| 711.331 | 0.002 | 719.421 | 0.003 | 727.373 | 0.004 | 772.261 | 0.004 |
| 712.311 | 0.002 | 720.292 | 0.004 | 728.293 | 0.004 | 773.263 | 0.004 |
| 712.311 | 0.003 | 720.295 | 0.003 | 728.296 | 0.004 | 774.251 | 0.002 |
| 712.370 | 0.005 | 720.356 | 0.005 | 728.347 | 0.004 | 776.276 | 0.005 |
| 713.360 | 0.005 | 720.360 | 0.003 | 728.352 | 0.003 | 778.241 | 0.002 |
| 713.412 | 0.003 | 720.361 | 0.003 | 730.253 | 0.003 | 779.232 | 0.002 |
| 714.288 | 0.003 | 721.280 | 0.003 | 730.269 | 0.004 | 781.246 | 0.003 |
| 714.342 | 0.005 | 721.281 | 0.002 | 731.309 | 0.003 | 782.185 | 0.003 |
| 714.343 | 0.004 | 721.332 | 0.003 | 731.368 | 0.003 | 782.223 | 0.004 |
| 714.398 | 0.002 | 721.334 | 0.003 | 731.368 | 0.003 | 791.258 | 0.005 |
| 714.402 | 0.003 | 721.394 | 0.005 | 732.344 | 0.002 | 800.220 | 0.005 |
| 714.460 | 0.003 | 722.268 | 0.002 | 732.400 | 0.003 | 801.192 | 0.005 |

the start of a normal outburst. Note that IY UMa (Patterson et al., 2000) also displayed the period of late superhumps that was slightly shorter than during the superoutburst plateau. As for the Sc stage, the O-C also yields confirmation of the period obtained from the periodogram analysis but with less accuracy (probably because of an insufficient number of the O-C data). We adopt the 0.057026(9) d for the orbital period.

According to Hellier (2001) an expected fractional period deficit $\epsilon^-$ of nega-

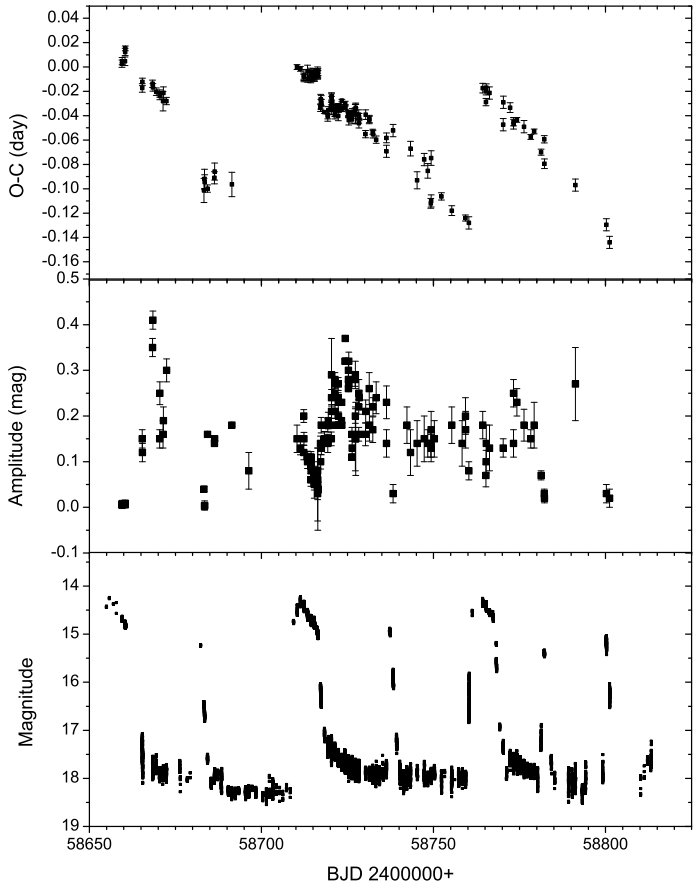


**Figure 7.** From top to bottom: O-C for maxima; amplitudes and an overall light curve during three S1, S2 and S3 supercycles.

tive superhumps is $\sim 0.5 \times \epsilon^+$ (here $\epsilon^+$ is a fractional period excess). In our case $\epsilon^-$ should be $\sim$ -0.0087 and the period of negative superhumps has to be about 0.0565 d (frequency 17.70 $d^{-1}$). No prominent peak at this frequency for both the superoutburst and the quiescence was found. There is only a week signal at this frequency during the stage C that we cannot take into account due to its low significance. Instead, a period of 0.057026(9) d within errors coincides with the orbital period 0.057042(42) d that was obtained from spectroscopy (Thorstensen et al., 2016). The mean light curve does not contain the eclipse and has a relatively low amplitude (about $0^m.1$). This does not contradict the moderate inclination of the orbit ($i = 40^\circ \pm 2^\circ$) that we obtained from spectroscopy.

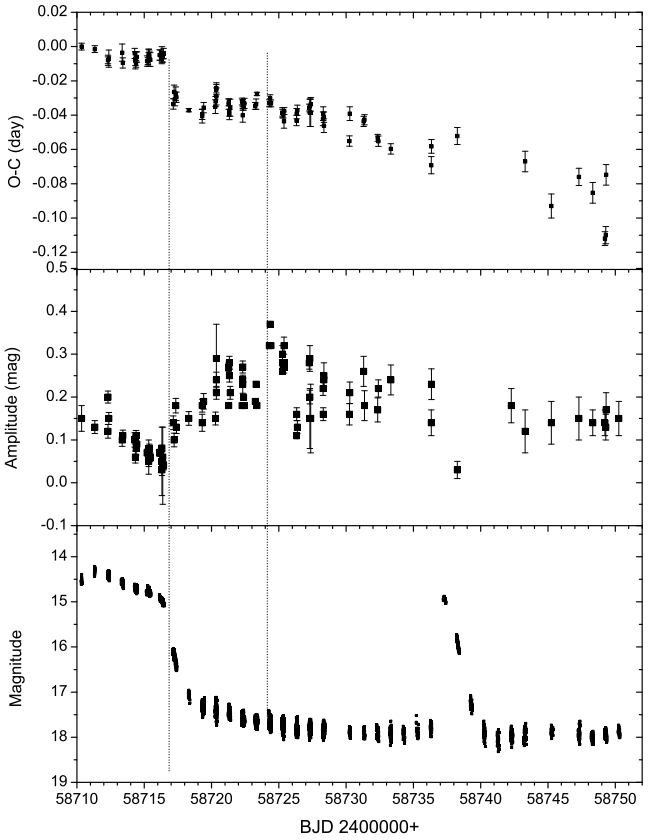


**Figure 8.** The same as in Fig. 7, but for the part of the S2 supercycle only.

Despite the insufficiently dense rows of the ASASSN and ZTF data for each night, a large number of nights in the quiescent state following the fifth superoutburst made it possible to search for periodicities in this quiescence. We have done this for data of a slow decline (JD 2458227 – 2458250) and quiescence (JD 2458253 – 2458315) separately. A result is presented in Fig.11.

A periodogram for the slow superoutburst decline revealed a most significant period of 0.057929(7) d. It coincides, within accuracy, with the period of late superhumps 0.057915(10) d found in 2019. Among the day-aliased peaks of periodogram for quiescent data one peak points to a period of 0.057797(3) d that is close to but is slightly less then the period of the late superhumps. In the case of our observations in 2019, where the second half of the supercycle was presented by orbital variations, the ZTF periodogram does not show this period. Possibly a period of late superhumps acted in quiescence and was somewhat smaller than during a slow fading, or there was cross-contamination of the late

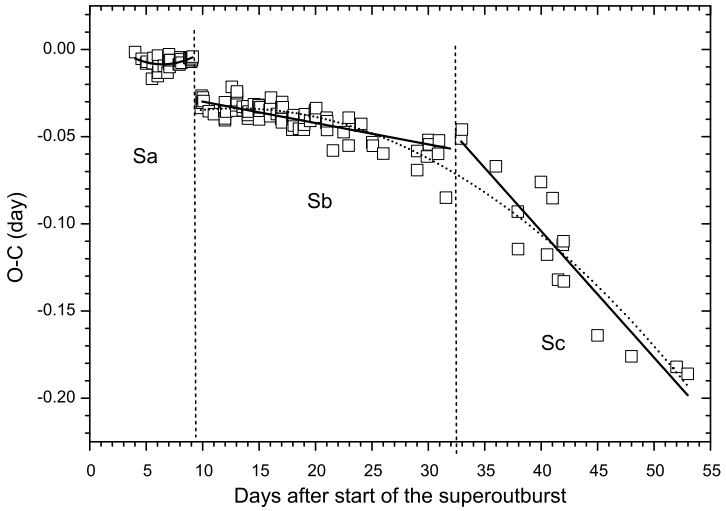


**Figure 9.** O-C combined for three S1, S2 and S3 supercycles. Sa, Sb and Sc mean three stages of combined supercycles: Sa means a plateau of the superoutburst, Sb and Sc are the parts of supposed late superhumps. The dashed curve is the best parabolic fit of (O-C)s behaviour at $Sb + Sc$ stages; solid lines are the best fits of (O-C)s at Sb and Sc stages separately.

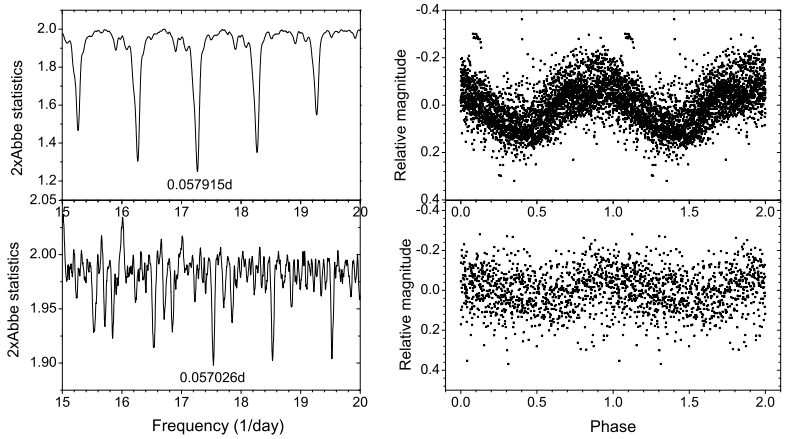


**Figure 10.** Left from top to bottom: periodograms for data in the S2 quiescence before the normal outburst and after it; Right from top to bottom: data folded with the most significant periods 0.057915 d and zero epoch 2458725.253; 0.057026 d and zero epoch 2458740.252, respectively.

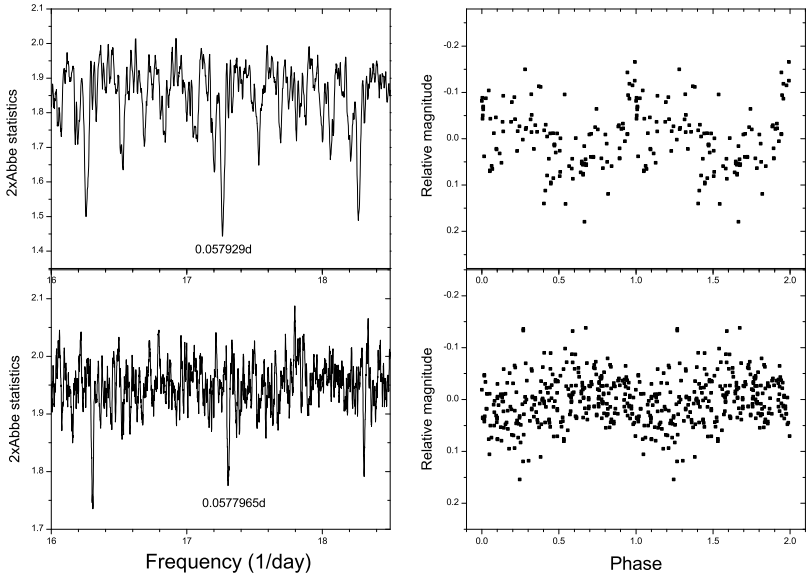


**Figure 11.** Left from top to bottom: a periodogram for data of a slow superoutburst 6 decline and the subsequent quiescence; right from top to bottom: data folded on the periods of 0.057929 d and 0.0577965 d, respectively.

superhumps, orbital periodicity, potential negative superhumps or some of them (the negative superhumps could be good candidates to an additional periodicity in the quiescence taking into account that this supercycle does not contain normal outbursts, so we can consider it as an L-type supercycle). The negative fractional period excess is poorly defined on the empirical diagram "orbital period – $\epsilon^-$" (Hellier, 2001) for the shortest orbital periods. The extrapolation of the data suggests an expected $\epsilon^-$ in a region from -0.008 to -0.02. In the case of the orbital frequency $F_{orb} = 17.536$, a frequency of variations in quiescence $F_q = 17.302$ could be a beat (side-band) frequency $F_{sb} = 2F_{orb} - F_n$ for $\epsilon^- = -0.013$ and the frequency of negative superhump $F_n = 17.767$.

### 3.5. Color indices

The multicolour *V, Ic* and *B, Rc* observations of superhumps were done for two nights of the S2 superoutburst plateau and those of *B, Rc* were done during the slow S2 superoutburst decline close to quiescence. As it follows from Fig. 12, colour indices are the phase-dependent ones and their dependence is different for different stages of outburst activity. During the S2 superoutburst, the bluest peak of the *V-Ic* and *B-Rc* coincided with a maximum of the light curve, while during a slow approach to quiescence it was slightly shifted and coincided with

a rising branch of the light curve. The amplitudes of colour curves were $\sim 0^m.08$ during the superoutburst and $\sim 0^m.1 - 0^m.2$ close to quiescence. Similar behaviour of the superhumps colour indices was reported for several SU UMa stars (see a brief review by Pavlenko et al. (2020).

### 3.6. Mass ratio from photometry

With known orbital and positive superhumps periods, one could calculate the fractional period excess $\epsilon^+$ at stage B of the superoutburst

$$\epsilon^+ = (Psh - Porb)/Porb, \tag{3}$$

where $Psh$ and $Porb$ are positive superhump and orbital periods, $q = M_2/M_1$, $M_2$ and $M_1$ are the masses of the donor and the primary components, respectively. We obtained $\epsilon^+ = 0.0173$ for the stage B.

With a known orbital period and $\epsilon$ we can estimate the mass ratio $q(\epsilon^+)$. According to Kato & Osaki (2013), the real $q$ one could obtain with the period of superhumps that is detected at stage A of the superoutburst, which is unknown in our case. As we pointed in Section 5, stage A was not recorded in any of the superoutbursts: it is seen from Fig. 7 and Fig. 8 that the onset of the superoutburst is already accompanied with fully grown superhumps. The only thing that can be said is that a potential stage A lasted no more than a day. However, we could estimate expected $\epsilon^*$ at stage A using the relation of Kato & Osaki (2013),

$$\epsilon^* = 0.012(2) + 1.04(8)\epsilon^+, \tag{4}$$

where $\epsilon^*$ and $\epsilon^+$ are the fractional period excesses at stage A and B, respectively. We found $\epsilon^* = 0.030$. Then, according to Table 1 from Kato & Osaki (2013), we obtain $q = 0.081$ and assuming $M_1 = 0.75 M_\odot$, we have $M_2 = 0.061 M_\odot$.

This result is in a good agreement with the estimate for the mass described in Section 3 and places MASTER 1727 near a low-mass bound of the H-rich SU UMa stars (Fig. 13).

## 4. Discussion: MASTER 1727 as a peculiar ER UMa-type star

In the 90s the known supercycles of SU UMa-type stars were mainly between ∼100 and ∼500 days (Kato et al., 1999). A special group of four objects with supercycles of 19 – 44 d, called ER UMa-type stars (Nogami et al., 2003), stood out among them. At that time, no new SU UMa type-stars were known between these two groups. Over time, information began to appear about both new stars of the ER UMa-type and stars with supercycles less than 100 d ("active novae"). Moreover, as it turned out, ER UMa itself displayed a change of its supercycle (Zemko et al., 2013) in a range of 42-60 d. A modern histogram of the supercycles of SU UMa-stars distribution is presented in Fig. 14. This

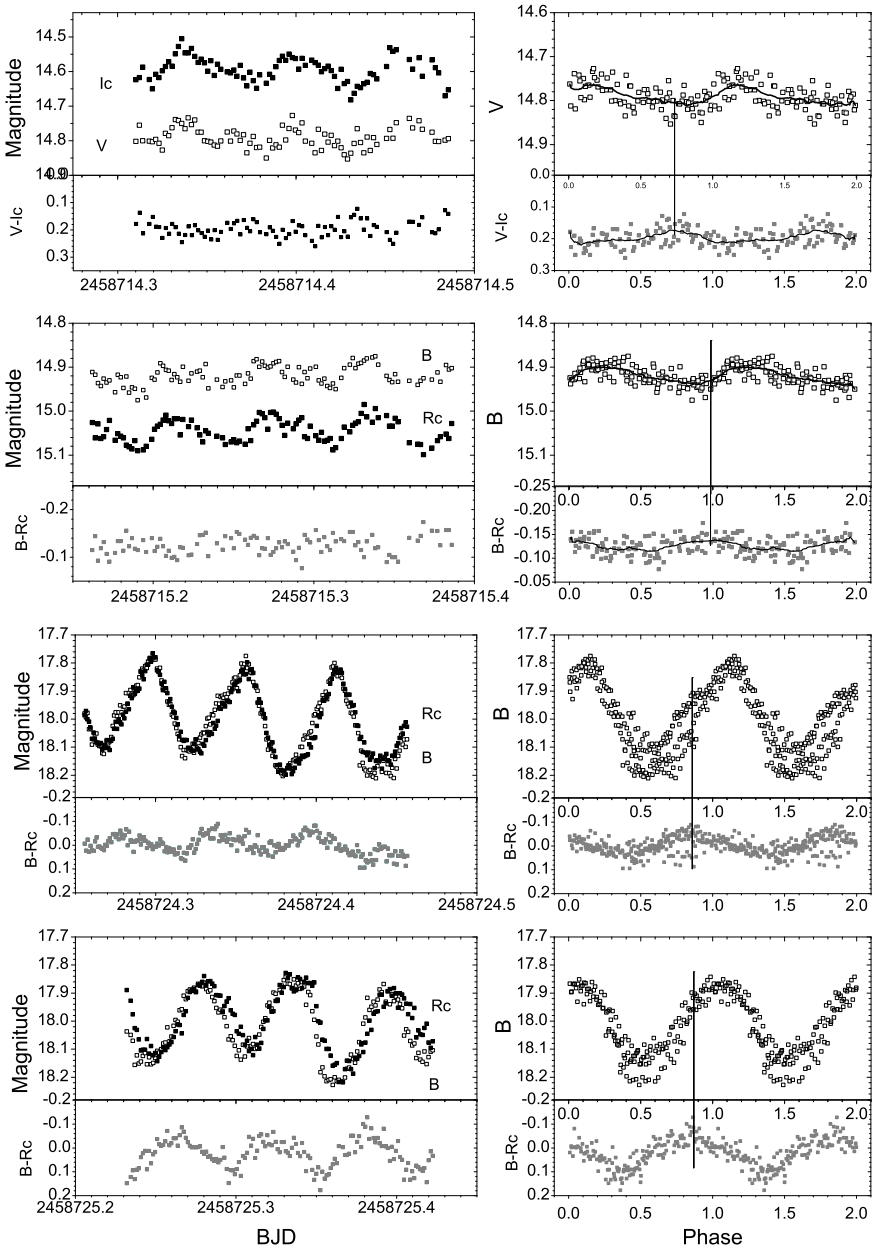


**Figure 12.** Left from top to bottom: original light and colour indices curves for the data of the S2 superoutburst plateau (BJD 2458714 and 2458715 ) and two consecutive nights close to quiescence (BJD 2458724 and 2458725). Right from top to bottom: folded light (*V* and *Ic*, *B* and *Rc*) and instrumental colour indices (*V-Ic* and *B-Rc*) on the 0.058029 d period with the zero epoch BJD 2458724.0. The dotted line is plotted through the *B-Rc* maximum. The smoothed line is drawn through the *V, V-Ic*, and *B, B-Rc* light and colour indices curves, respectively.

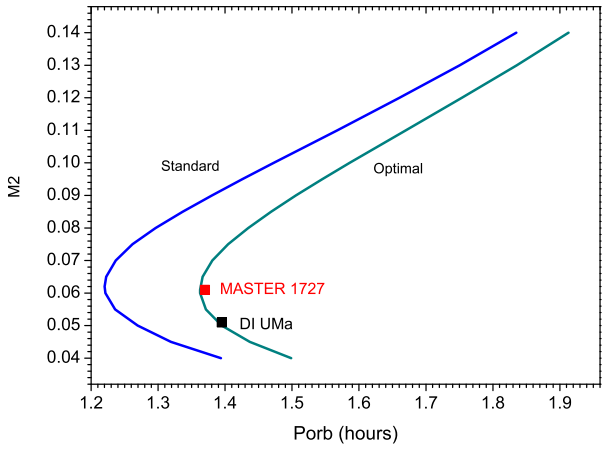


**Figure 13.** Dependence of the mass of the secondary $M_2$, expressed in units of the solar masses, on the orbital period. For DI UMa we used $P_{orb}$ = 0.054564 d (Fried et al., 1999) and re-estimated $q$ = 0.068 and $M_2 = 0.051 M_\odot$ obtained by the same method as for MASTER 1727. Tracks of standard and optional evolution according to Knigge et al. (2011) are marked by blue and dark cyan lines, respectively. The position of DI UMa and MASTER 1727 is shown.

distribution is a bimodal one. The largest number of supercycles falls on 250-400 days (the primary maximum). A smaller, almost flat secondary maximum falls on the interval of 40-160 days and ER UMa-type stars no longer look like a separate group in this distribution.

A short ∼50-d supercycle length could define MASTER 1727 as an ER UMa-type DN. Also, like other ER UMa-type stars, MASTER 1727 displays amplitudes of superhumps that are largest in the earliest stage of the superoutburst; similarly to RZ LMi (Osaki, 1995b), it has an extremely short superoutburst duration.

Besides of MASTER 1727, there are two other known ER UMa-type objects around the period minimum, RZ LMi (Nogami et al., 1995) and DI UMa (Kato et al., 1996). MASTER 1727 is the next after DI UMa object on the standard CV evolutionary path. The evolutionary state of RZ LMi may be different (Kato et al., 2016b).

According to light curve simulations based on the thermal-tidal instability model of SU UMa stars (Osaki, 1995a), the ER UMa-type stars have a high rate of mass transfer, about ∼ 10 times higher than that expected from the CV evolution. In our case, for the shortest supercycle of about 50 d, two possibilities correspond to the mass-transfer rate of 4 or 7 $\dot{M}$, where $\dot{M}$ is the mass-transfer rate in units of $10^{16}$ $gs^{-1}$ for the disk radius 0.35a, where a is the binary separation.

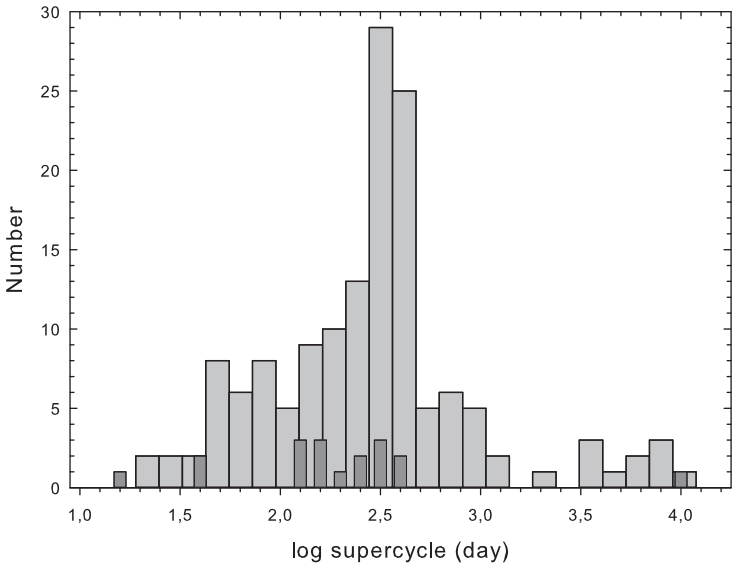


**Figure 14.** A histogram of supercycles distribution for the SU UMa-type CVs based on the avalable data taken from Ritter & Kolb (2003), edition 7.24; Pavlenko et al. (2019); Antonyuk & Pavlenko (2013). Data from Kato et al. (1999) are marked by dark rectangles.

The low mass ratio (and, hence, a small mass of the secondary) is a key parameter that may explain the peculiarities of MASTER 1727. A small mass of the secondary causes the weaker tidal torques compared to the usual SU UMa-type stars (Osaki, 1995b). The weak tidal torques lead to an increase in the radius of the accretion disc at the end of the superoutburst and a reduction in its duration since a smaller angular momentum will be removed during the superoutburst. This could explain a shortening of a supercycle because it takes a shorter time to replenish the angular momentum reservoir in the disc. Osaki (1995b) showed that dependence of a number of normal outbursts on supercycle for ordinary and ER UMa-type DNe (i.e. for DNe with low and high $\dot{M}$) is the opposite: while this number is inversely proportional to the supercycle for stars with low and moderate $\dot{M}$, it is proportional to the supercycle for stars with high $\dot{M}$.

A big radius of the disk could provide the possibility of accumulation of cold matter in the outer parts of the accretion disc beyond the 3:1 resonance that may be the cause of rebrightenings. Note that the colour indices behaviour of MASTER 1727 during the superoutburst is also similar to that in WZ Sge-type stars (see e.g. Imada et al. (2018); Neustroev et al. (2017)). A strong variations

in $\dot{M}$ probably may modify a morphology of the superoutburst from a "clear" superoutburst to a superoutburst with rebrightenings.

The supercycle variation of MASTER 1727 deserves special attention. According to Osaki (1995b), a two-fold increase in the supercycle corresponds to a $\sim$ two-fold decrease of $\dot{M}$. There are several known examples with variable supercycles in active novae where the supercycle changes in a form of secular increase and/or quasi-periodic oscillations as was shown by Kato (2001), Otulakowska-Hypka & Olech (2014), Zemko et al. (2013). Generally, the nature of these variations is still an open question. However, the tendency of the secular increase in the supercycle, which means a gradual increase in $\dot{M}$, suggests that these objects (at least some of them) could experience a transition between DNe and nova-likes. Thus Kato et al. (2016b) applied this idea for a systematic increase of the supercycle length in RZ LMi.

There are several known postnovae stars of different evolution status (i.e., orbital periods) showing some activity that is probably caused by a high mass transfer rate after the nova explosion. Thus in the renown classical Nova Cygni 1975 (V1500 Cyg), which is an asynchronous polar with the orbital period of 0.14d, a strong eruption heated the WD up to the $\sim$100 000 K (Schmidt et al., 1995). The hot WD irradiated the secondary and formed a radiation-driven wind (Katz, 1991), which during the first three years after the eruption could have an even stronger decelerating effect on the orbital motion of the WD than the magnetic field. The observational evidence of this was shown by Pavlenko & Malanushenko (1995). At present (45 years after the WD eruption) the white dwarf is still hot and produces $\sim$1.5-mag reflection effect of the secondary (Pavlenko et al., 2018).

It was shown by Patterson et al. (2020) that the mass-transfer rate in recurrent novae T Pyx and IM Nor is unnaturally high for their state of evolution (orbital periods are 0.076 d and 0.103 d, respectively) and supposed that it is caused by a strong and long-lasting irradiation effect of the secondary component powered by a WD eruption.

MASTER 1727, with an orbital period of 0.057 d and mass ratio 0.08 is a low-q extension of ER UMa stars. The mass-transfer rate should be accordingly higher than what is expected from gravitational radiation only. The only currently known mechanism could be a post-nova state. They suggest that the object underwent a nova eruption relatively recently – hundreds of years ago. (Note that checking the DASCH archive[5] did not reveal a nova outburst over the past $\sim$100 years). This object would provide the evidence that a nova eruption can occur even if CVs are near the period minimum (probably the first observational evidence for that).

[5]http://dasch.rc.fas.harvard.edu/

## 5. Summary

– The spectrum of MASTER J1727 that was obtained in 2020 quiescence contained H lines and no He lines;

– The continuous photometry in 2019 over $\sim$ 160 d revealed a supercycle length to be 52 d, but the supercycle variability was found from 50 to 100 d on the $\sim$5.5-year scale. This implies as high as two times variations in the mass ratio;

– We found a mean period of positive superhumps to be 0.058029 d during a rather short 7-d superoutburst plateau;

– Late superhumps with a slightly shorter period of 0.057915 d were detected after the superoutburst. They lasted about 20 d up to the start of a normal outburst;

– In 2019 we found the orbital period of 0.057026 d during quiescence after the normal outburst and established its identity with those found earlier by spectroscopy (Thorstensen et al., 2016); the absence of an eclipse in the orbital light curve and its moderate amplitude is consistent with the orbital inclination of about 40° that we found from spectral observations;

– A blue peak of *V-Ic* and *B-Rc* colour indices coincides with a minimum of the superhump light curve during the superoutburst and those of *B-Rc* colour-index coincides with a rising branch of the late superhumps in quiescence;

– We estimated a low mass ratio of 0.08 and a small mass of the secondary $\sim$0.06 M$\odot$ that could explain most of the observed peculiarities of MASTER J1727 in the frame of thermal-tidal instability of accretion discs;

– The high mass-transfer rate indicates that in the relatively recent history, the MASTER J1727 could undergo a nova eruption. If so, it means that an eruption can occur even if the star is near the period minimum.

**Acknowledgements.** We are grateful to the anonymous referee for the valuable comments which helped to improve this paper. Elena Pavlenko is grateful to Nikolaus Vogt for the valuable discussion about the MASTER 1727 at the "Compact White Dwarf Binaries" Conference held in Erevan (2019) and Natali Katysheva for careful reading of the manuscript. Observations with the SAO RAS telescopes are supported by the Ministry of Science and Higher Education of the Russian Federation (including agreement No 05.619.21.0016, project ID RFMEFI61919X0016); Observations with CrAO RAS telescopes are supported by the grant of RSF (project number 19-72-10063). The work of Shimansky was funded by RFBR, project number 18-42-160003. The work of Maksim Gabdeev was funded by the subsidy 671-2020-0052 allocated to the Kazan Federal University for the state assignment in the sphere of scientific activities and was funded by RFBR, project number 19-32-60021. The work of Dubovský was supported by the Slovak Research and Development Agency under contract No. APVV-15-0458.

## References

Andronov, I. L. & Baklanov, A. V., Algorithm of the artificial comparison star for the CCD photometry. 2004, *Astronomical School's Report*, **5**, 264, DOI: 10.18372/2411-6602.05.1264

Antonyuk, O. I. & Pavlenko, E. P., Peculiarities of the SU UMa-Type Dwarf Nova V1504 Cyg Behavior in 1994 - 2012 Years. 2013, *Astrophysics*, **56**, 539, DOI: 10.1007/s10511-013-9306-5

Baraffe, I., Chabrier, G., Barman, T. S., Allard, F., & Hauschildt, P. H., Evolutionary models for cool brown dwarfs and extrasolar giant planets. The case of HD 209458. 2003, *Astronomy and Astrophysics*, **402**, 701, DOI: 10.1051/0004-6361:20030252

Borisov, N. V., Gabdeev, M. M., Shimansky, V. V., Katysheva, N. A., & Shugarov, S. Y., Spectral and photometric studies of polar CRTS CSS 130604 J 215427+155714. 2017, *Astrophysical Bulletin*, **72**, 184, DOI: 10.1134/S1990341317020092

Cannizzo, J. K. & Ramsay, G., The Superoutburst Duration versus Orbital Period Relation for AM CVn Stars. 2019, *Astronomical Journal*, **157**, 130, DOI: 10.3847/1538-3881/ab04ac

Denisenko, D., Lipunov, V., Gorbovskoy, E., et al., New Bright CV detected by MASTER. 2014, *The Astronomer's Telegram*, **5724**, 1

Eggleton, P. P., Aproximations to the radii of Roche lobes. 1983, *Astrophysical Journal*, **268**, 368, DOI: 10.1086/160960

Fried, R. E., Kemp, J., Patterson, J., et al., Superhumps in Cataclysmic Binaries. XVI. DI Ursae Majoris. 1999, *Publications of the ASP*, **111**, 1275, DOI: 10.1086/316433

Girardi, L., Bressan, A., Bertelli, G., & Chiosi, C., Evolutionary tracks and isochrones for low- and intermediate-mass stars: From 0.15 to 7 $M_{sun}$, and from Z=0.0004 to 0.03. 2000, *Astronomy and Astrophysics, Supplement*, **141**, 371, DOI: 10.1051/aas:2000126

Green, M. J., Marsh, T. R., Steeghs, D. T. H., et al., High-speed photometry of Gaia14aae: an eclipsing AM CVn that challenges formation models. 2018, *Monthly Notices of the RAS*, **476**, 1663, DOI: 10.1093/mnras/sty299

Hellier, C. 2001, *Cataclysmic Variable Stars* (Springer)

Hirose, M. & Osaki, Y., Hydrodynamic Simulations of Accretion Disks in Cataclysmic Variables: Superhump Phenomenon in SU UMa Stars. 1990, *Publications of the ASJ*, **42**, 135

Imada, A., Yanagisawa, K., & Kawai, N., On the colour variations of negative superhumps. 2018, *Publications of the ASJ*, **70**, L4, DOI: 10.1093/pasj/psy068

Kato, T., Changing Supercycle of the ER UMa-Type Star V1159 Ori. 2001, *Publications of the ASJ*, **53**, L17, DOI: 10.1093/pasj/53.4.L17

Kato, T., WZ Sge-type dwarf novae. 2015, *Publications of the ASJ*, **67**, 108, DOI: 10.1093/pasj/psv077

Kato, T., Hambsch, F.-J., Monard, B., et al., Survey of period variations of superhumps in SU UMa-type dwarf novae. VIII. The eighth year (2015-2016). 2016a, *Publications of the ASJ*, **68**, 65, DOI: 10.1093/pasj/psw064

Kato, T., Imada, A., Uemura, M., et al., Survey of Period Variations of Superhumps in SU UMa-Type Dwarf Novae. 2009, *Publications of the ASJ*, **61**, S395, DOI: 10.1093/pasj/61.sp2.S395

Kato, T., Ishioka, R., Isogai, K., et al., RZ Leonis Minoris bridging between ER Ursae Majoris-type dwarf nova and nova-like system. 2016b, *Publications of the ASJ*, **68**, 107, DOI: 10.1093/pasj/psw101

Kato, T. & Kunjaya, C., Discovery of a Peculiar SU UMa-Type Dwarf Nova ER Ursae Majoris. 1995, *Publications of the ASJ*, **47**, 163

Kato, T., Nogami, D., & Baba, H., DI Ursae Majoris: Discovery of an Extreme ER UMa-Type Dwarf Nova with the Shortest Orbital Period. 1996, *Publications of the ASJ*, **48**, L93, DOI: 10.1093/pasj/48.5.L93

Kato, T., Nogami, D., Baba, H., et al., Observation of ER UMa Stars. 1999, in *Disk Instabilities in Close Binary Systems*, ed. S. Mineshige & J. C. Wheeler, 45

Kato, T. & Osaki, Y., New Method of Estimating Binary's Mass Ratios by Using Superhumps. 2013, *Publications of the ASJ*, **65**, 115, DOI: 10.1093/pasj/65.6.115

Kato, T., Stubbings, R., Nelson, P., et al., The nature of V359 Centauri revealed: New long-period SU UMa-type dwarf nova. 2002, *Astronomy and Astrophysics*, **395**, 541, DOI: 10.1051/0004-6361:20021267

Katz, J. I., V1500 Cygni: A Prediction. 1991, *Astrophysical Journal, Letters*, **374**, L59, DOI: 10.1086/186071

Knigge, C., The donor stars of cataclysmic variables. 2006, *Monthly Notices of the RAS*, **373**, 484, DOI: 10.1111/j.1365-2966.2006.11096.x

Knigge, C., Baraffe, I., & Patterson, J., The Evolution of Cataclysmic Variables as Revealed by Their Donor Stars. 2011, *Astrophysical Journal, Supplement*, **194**, 28, DOI: 10.1088/0067-0049/194/2/28

Lubow, S. H., Simulations of Tidally Driven Eccentric Instabilities with Application to Superhumps. 1991, *Astrophysical Journal*, **381**, 268, DOI: 10.1086/170648

Masci, F. J., Laher, R. R., Rusholme, B., et al., The Zwicky Transient Facility: Data Processing, Products, and Archive. 2019, *Publications of the ASP*, **131**, 018003, DOI: 10.1088/1538-3873/aae8ac

Montgomery, M. M., Does an Average White Dwarf Have Enough Mass to Prevent Accretion Disk Tilt? 2010, in American Institute of Physics Conference Series, Vol. **1273**, *American Institute of Physics Conference Series*, ed. K. Werner & T. Rauch, 358–361

Neustroev, V. V., Marsh, T. R., Zharikov, S. V., et al., The remarkable outburst of the highly evolved post-period-minimum dwarf nova SSS J122221.7-311525? 2017, *Monthly Notices of the RAS*, **467**, 597, DOI: 10.1093/mnras/stx084

Nogami, D., Kato, T., Masuda, S., et al., Photometric Observations of an Extreme ER UMa Star, RZ Leonis Minoris. 1995, *Publications of the ASJ*, **47**, 897

Nogami, D., Uemura, M., Ishioka, R., et al., In-the-gap SU UMa-type dwarf nova, Var73 Dra with a supercycle of about 60 days. 2003, *Astronomy and Astrophysics*, **404**, 1067, DOI: 10.1051/0004-6361:20030509

Osaki, Y., Irradiation-induced mass-overflow instability as a possible cause of superoutbursts in SU UMa stars. 1985, *Astronomy and Astrophysics*, **144**, 369

Osaki, Y., A model for the superoutburst phenomenon of SU Ursae MAjoris stars. 1989, *Publications of the ASJ*, **41**, 1005

Osaki, Y., A Model for a Peculiar SU Ursae Majoris-Type Dwarf Nova ER Ursae Majoris. 1995a, *Publications of the ASJ*, **47**, L11

Osaki, Y., Why Does RZ Leonis Minoris, an Unusual SU UMa Star, Have Such a Short Supercycle? 1995b, *Publications of the ASJ*, **47**, L25

Osaki, Y., Dwarf-Nova Outbursts. 1996, *Publications of the ASP*, **108**, 39, DOI: 10.1086/133689

Osaki, Y. & Kato, T., Study of Superoutbursts and Superhumps in SU UMa Stars by the Kepler Light Curves of V344 Lyrae and V1504 Cygni. 2013, *Publications of the ASJ*, **65**, 95, DOI: 10.1093/pasj/65.5.95

Osaki, Y. & Kato, T., A further study of superoutbursts and superhumps in SU UMa stars by the Kepler light curves of V1504 Cygni and V344 Lyrae. 2014, *Publications of the ASJ*, **66**, 15, DOI: 10.1093/pasj/pst015

Otulakowska-Hypka, M. & Olech, A., Increasing Supercycle Lengths of Active SU UMa-type Dwarf Novae. 2014, in Astronomical Society of the Pacific Conference Series, Vol. **490**, *Stellar Novae: Past and Future Decades*, ed. P. A. Woudt & V. A. R. M. Ribeiro, 385

Paczynski, B., A model of accretion disks in close binaries. 1977, *Astrophysical Journal*, **216**, 822, DOI: 10.1086/155526

Patterson, J., Kemp, J., Jensen, L., et al., Superhumps in Cataclysmic Binaries. XVIII. IY Ursae Majoris. 2000, *Publications of the ASP*, **112**, 1567, DOI: 10.1086/317724

Patterson, J., Kemp, J., Monard, B., et al., IM Normae: The Death Spiral of a Cataclysmic Variable? 2020, *arXiv e-prints*, arXiv:2010.07812

Pavlenko, E., Antonyuk, K., Pit, N., et al., Evolution of negative superhumps. 2019, in *Compact White Dwarf Binaries*, ed. G. H. Tovmassian & B. T. Gansicke, 39

Pavlenko, E. P. & Malanushenko, V. P., The Peculiarity of V1500 Cyg Syncronization. 1995, in Astrophysics and Space Science Library, Dordrecht Kluwer Academic Publishers, Vol. **205**, *Cataclysmic Variables*, ed. A. Bianchini, M. della Valle, & M. Orio, 172

Pavlenko, E. P., Mason, P. A., Sosnovskij, A. A., et al., Asynchronous polar V1500 Cyg: orbital, spin, and beat periods. 2018, *Monthly Notices of the RAS*, **479**, 341, DOI: 10.1093/mnras/sty1494

Pavlenko, E. P., Sosnovskij, A. A., Antoniuk, K. A., et al., Humps and Superhumps in the SU UMa-Type Dwarf Nova System IRXS J161659.5+620014. 2020, *Astrophysics*, DOI: 10.1007/s10511-020-09653-0

Pel't, Y. 1980, *Frequency analysis of astronomical time series.* (Valgus, Tallin)

Ritter, H. & Kolb, U., Catalogue of cataclysmic binaries, low-mass X-ray binaries and related objects (Seventh edition). 2003, *Astronomy and Astrophysics*, **404**, 301, DOI: 10.1051/0004-6361:20030330

Ritter, H. & Kolb, U., VizieR Online Data Catalog: Cataclysmic Binaries, LMXBs, and related objects (Ritter+, 2004). 2011, *VizieR Online Data Catalog*, B/cb

Robertson, J. W., Honeycutt, R. K., & Turner, G. W., RZ Leonis Minoris, PG 0943+521, and V1159 Orionis: Three Cataclysmic Variables with Similar and Unusual Outburst Behavior. 1995, *Publications of the ASP*, **107**, 443, DOI: 10.1086/133572

Schmidt, G. D., Liebert, J., & Stockman, H. S., Detection of the Hot White Dwarf in the Magnetic Nova V1500 Cygni with the Hubble Space Telescope. 1995, *Astrophysical Journal*, **441**, 414, DOI: 10.1086/175365

Shappee, B. J., Prieto, J. L., Grupe, D., et al., The Man behind the Curtain: X-Rays Drive the UV through NIR Variability in the 2013 Active Galactic Nucleus Outburst in NGC 2617. 2014, *Astrophysical Journal*, **788**, 48, DOI: 10.1088/0004-637X/788/1/48

Smak, J., Statistical analysis of outbursts and superoutbursts of VW Hyi. 1985, *Acta Astron.*, **35**, 357

Sosnovskij, A., Pavlenko, E., Pit, N., & Antoniuk, K., NY Her: possible discovery of negative superhumps. 2017, *Information Bulletin on Variable Stars*, **6216**, 1, DOI: 10.22444/IBVS.6216

Thorstensen, J. R., Alper, E. H., & Weil, K. E., A Trip to the Cataclysmic Binary Zoo: Detailed Follow-up of 35 Recently Discovered Systems. 2016, *Astronomical Journal*, **152**, 226, DOI: 10.3847/1538-3881/152/6/226

Uemura, M., Kato, T., Ishioka, R., et al., Superhump Evolution in the Ultrashort Period Dwarf Nova 1RXS J232953.9+062814. 2002, *Publications of the ASJ*, **54**, 599, DOI: 10.1093/pasj/54.4.599

Vogt, N., VW Hydri revisited : conclusions on dwarf nova outburst models. 1983, *Astronomy and Astrophysics*, **118**, 95

Warner, B., Cataclysmic variable stars. 1995, *Cambridge Astrophysics Series*, **28**

Warner, B. 2003, *Cataclysmic Variable Stars* (Cambridge University Press)

Whitehurst, R., Numerical simulations of accretion discs - I. Superhumps : a tidal phenomenon of accretion discs. 1988, *Monthly Notices of the RAS*, **232**, 35, DOI: 10.1093/mnras/232.1.35

Zemko, P., Kato, T., & Shugarov, S. Y., Detection of Change in Supercycles in ER Ursae Majoris. 2013, *Publications of the ASJ*, **65**, 54, DOI: 10.1093/pasj/65.3.54

Contrib. Astron. Obs. Skalnaté Pleso **51**, 163 – 174, (2021)
https://doi.org/10.31577/caosp.2021.51.2.163

# Photometric and period analysis of the eclipsing binary system V2783 Ori

**İ. Bulut**[1,3] **and A. Bulut**[2,3]

[1] *Department of Space Sciences and Technologies, Faculty of Arts and Sciences, Çanakkale Onsekiz Mart University, Terzioğlu Kampüsü, TR-17020, Çanakkale, Turkey TR-17020, Çanakkale, Turkey; (E-mail: ibulut@comu.edu.tr)*

[2] *Department of Physics, Faculty of Arts and Sciences, Çanakkale Onsekiz Mart University, Terzioğlu Kampüsü, TR-17020, Çanakkale, Turkey*

[3] *Astrophysics Research Centre and Observatory, Çanakkale Onsekiz Mart University, Terzioğlu Kampüsü, TR-17020, Çanakkale, Turkey*

Received: March 5, 2021; Accepted: May 7, 2021

**Abstract.** In this study we performed the first detailed photometric and period analysis of the recently discovered eclipsing binary star V2783 Ori. The analysis of the light curve has shown that the system is in a detached configuration, with the orbital eccentricity $e = 0.274 \pm 0.008$. The photometric mass ratio of V2783 Ori determined from the light curve analysis is $q = 0.734 \pm 0.015$. The absolute parameters of the system were obtained as a result of the light curve solution. Absolute parameters were found as follows: masses $M_1 = 1.80 \pm 0.01$ $M_\odot$, $M_2 = 1.32 \pm 0.01$ $M_\odot$, radii $R_1 = 2.19 \pm 0.10$ $R_\odot$, $R_2 = 1.91 \pm 0.10$ $R_\odot$, temperatures $T_1 = 8325 \pm 100$ K and $T_2 = 8300 \pm 100$ K. A comparison of these parameters with theoretical stellar models show that the secondary component is located inside the main-sequence band and still close to ZAMS, while the primary component is located in the middle of ZAMS-TAMS limits. The distance of the system determined from the absolute parameters, $d = 1064 \pm 150$ pc, takes into account the interstellar reddening.

The (O–C) diagram was discussed considering all reliable minima times found in the literature and new values for the parameters of the apsidal motion and light-time effect were found. The apsidal motion rate of V2783 Ori is $\dot{\omega} = 0.0063 \pm 0.0017$ deg cycle$^{-1}$, and it corresponds to an apsidal motion period of $U = 656 \pm 103$ yr. The third body orbital period is $10 \pm 2$ yr, its minimal mass is $0.82 \pm 0.11$ $M_\odot$.

**Key words:** photometric — stars: variables: binaries: eclipsing — stars: individual: V2783 Ori

## 1. Introduction

It is well known that in close binary systems of stars with eccentric orbits, the tidal and rotational distortions of the components from spherical symmetry lead

to secular changes in the position of the periastron.

Apsidal motion is the rotation of the major orbital axis of an eccentric orbital binary star in space. It is primarily caused by the effect of the tidal bulge due to the companion and the rotational distortions of the stars. Besides these contributions to the apsidal motion, there is also a general relativistic contribution. This contribution is often small.

Apsidal motion studies on the eclipsing binaries allow the determination of the observational internal constants of stars and the observational tests of General Relativity theory (Giménez 1985; Claret & Giménez 1993). The orbital elements of the binary stars with eccentric orbits have been used to constrain the timescales of synchronization and circularization predicted by the tidal theories (Zahn 2008). These studies depend on the number of such systems and the precision of their absolute and orbital parameters.

The star system V2783 Ori (GSC 0143-0226, HD 252984, $P = 4$ .21618, $V = 10^m.39$ ) is identified as a new eclipsing binary by Otero et al. (2004). They determined its period as 4.21618 days. The spectral type of this system was classified as A0 (according to Otero et al. (2004)). The ASAS light curve of V2783 Ori indicates that the orbit is eccentric, with the secondary minimum occurring at phase 0.54. The apsidal motion in the system was calculated by Bulut et al. (2017) who obtained its period to be $U = 415$ yr and the orbital eccentricity $e = 0.25$. The Gaia EDR3 gives a parallax of $0.876 \pm 0.035$ mas for the system, which means a distance of $1141 \pm 46$ pc (Gaia Collaboration et al. 2021).

There has been no photometric and spectroscopic study for V2783 Ori until now. In this paper, the detailed photometric and the orbital period study of V2783 Ori is presented.

## 2. Observational data

V2783 Ori was named as ASAS 061057+0621.1 in the ASAS catalogue of variable stars. We have taken from the ASAS-3 database (Pojmanski 2003) the $V$ photometric data of V2783 Ori observed between 2002, August, and 2009, November. About 476 observations of the system were made during the survey, of which 442 were recorded as being of good photometric quality; these data were used in the analysis. The light curve of the system is plotted in Figure 1. The phases are computed according to the following linear light elements given by Otero et al. (2004):

$$HJD\ (Min\ I) = 2412946.750 + 4^{\mathrm{d}}.21618\ \times E. \qquad (1)$$

## 3. Analysis of the light curves

For the analysis of the light curve of V2783 Ori we used the program PHOEBE (version 0.31a), which was developed by Prša & Zwitter (2005). This software is based on the Wilson-Devinney (W-D) method (Wilson & Devinney 1971). The program computes the light curves as a function of the following main parameters: orbital eccentricity ($e$), longitude of periastron ($\omega$), orbital inclination ($i$), surface temperature ($T_{1,2}$), dimensionless surface potentials ($\Omega_{1,2}$), mass ratio ($q = M_2/M_1$), relative luminosities ($L_{1,2}$), gravity darkening exponents ($g_{1,2}$), limb darkening coefficients ($x_{1,2}$) and bolometric albedos ($A_{1,2}$).

The detached binary mode (in W-D mode 2) was used with several assumptions. Some parameters of components should be fixed during the light-curve modeling. The corresponding linear limb-darkening coefficients were interpolated for the square root law from van Hamme's tables (van Hamme 1993). The values of gravity-darkening exponents ($g_{1,2} = 1.0$) and bolometric albedo coefficients ($A_{1,2} = 1.0$) were set at their suggested values for the radiative atmospheres (Lucy 1968).

The magnitudes and color indices in the literature can be used to estimate the mean effective temperature of the system for the combined light of the system. The results were collected in Table 1. We used the color/temperature calibrations of Casagrande et al. (2010) and Ramírez & Meléndez (2005) for the dwarf stars. The weighted average of the seven estimates is 8325 K. This value is adopted to be the mean of the effective temperature of the primary star in the analyses.

**Table 1.** Photometric indices and inferred mean effective temperature of V2783 Ori.

| Photometric Index | Value | $T$ (K) | References |
|---|---|---|---|
| Johnson $V$ | 10.39 ± 0.05 | | 1 |
| 2MASS $J$ | 10.003 ± 0.024 | | 2 |
| 2MASS $H$ | 10.008 ± 0.026 | | 2 |
| 2MASS $Ks$ | 9.985 ± 0.016 | | 2 |
| Johnson $B$ - $V$ | -0.04 ± 0.05 | 9210 ± 800 | 1 |
| Johnson/2MASS $V$ - $J$ | 0.387 ± 0.036 | 8254 ± 768 | 1, 2 |
| Johnson/2MASS $V$ - $H$ | 0.382 ± 0.039 | 8117 ± 829 | 1, 2 |
| Johnson/2MASS $V$ - $Ks$ | 0.387 ± 0.033 | 8343 ± 711 | 1, 2 |
| 2MASS $J$-$Ks$ | 0.018 ± 0.019 | 7750 ± 818 | 2 |

1: Høg et al. (2000), 2: Cutri et al. (2003)

As the spectroscopic value of the mass ratio is not known, we applied the $q$-search method with a step of 0.1 with trials, to find sensible photometric

estimates for the mass ratio. Figure 2 presents the sum of the squared residuals $\sum(O-C)^2$ for the tested mass ratios ($q$). It can be seen that the smallest value of squared residuals is achieved around $q = 0.75$. This value was used as the initial value of the mass radio in differential-corrections.

Considering the calculated apsidal motion period given in Table 3, the total change in the longitude of periastron during the observation time interval can be neglected. Therefore we assumed $\dot{\omega} = 0.0$ in the analyses.

The adjustable parameters are the temperature of secondary star ($T_2$), the orbital inclination ($i$), the orbital eccentricity ($e$), the longitude of periastron ($\omega$), the surface potentials ($\Omega_{1,2}$), the relative luminosity of primary star ($L_1$), and the mass ratio ($q$). The results of the light curve solution can be found in Table 2. For the parameters in the light curve fitting, the standard deviations of the differential corrections supplied by the W-D program were used as an error. The synthetic light curve and the observations are shown in Figure 1.

The analysis of the light curve suggests partial eclipses in both of the light curve minima. The depths of the primary and secondary minima are 0.581 mag and 0.523 mag in $V$, respectively. The duration of the minima are also, respectively, 4.84 hours for the primary and 9.29 hours for the secondary.

**Table 2.** Parameters of the light curves of V2783 Ori.

| Parameter | ASAS ($V$) |
|---|---|
| $T$ (HJD) | 24412949.828 ± 0.013 |
| $P$ (day) | 4.216180 ± 0.000001 |
| $i$ (deg) | 87.18 ± 0.09 |
| $e$ | 0.274 ± 0.008 |
| $\omega$ (deg) | 70.28 ± 0.70 |
| PSHIFT | 0.0213 ± 0.0004 |
| $T_1$ (K) | 8325 |
| $T_2$ (K) | 8300 ± 57 |
| $\Omega_1$ | 8.40 ± 0.11 |
| $\Omega_2$ | 8.22 ± 0.15 |
| $q$ | 0.734 ± 0.015 |
| $x_1$ | 0.503 |
| $x_2$ | 0.503 |
| $A_1 = A_2$ | 1.0 |
| $g_1 = g_2$ | 1.0 |
| $L_1$ ($L_1/L_{\rm Total}$) | 0.59 ± 0.11 |
| $L_2$ ($L_2/L_{\rm Total}$) | 0.41 |
| $r_{\rm mean,1}$ | 0.136 ± 0.002 |
| $r_{\rm mean,2}$ | 0.112 ± 0.002 |

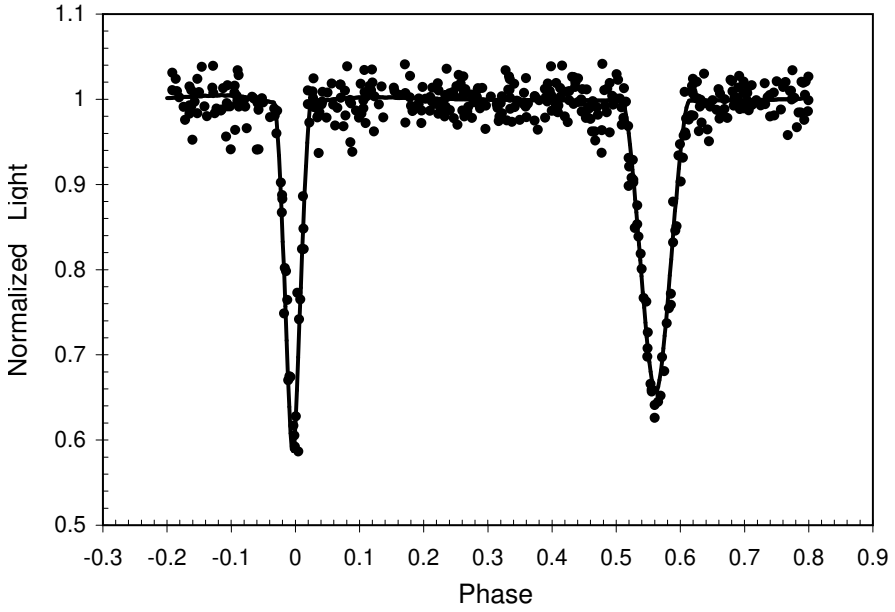


**Figure 1.** Light curves of V2783 Ori. The points are the individual observations. The solid lines are the synthetic light curves based on the parameters in Table 2.

## 4. (O–C) analysis

The orbital period variation of V2783 Ori was studied by means of an (O–C) diagram analysis. The minima times were taken from the modern database of the (O–C) Gateway (http://var2.astro.cz/ocgate/) (Paschke & Brat 2006). A total number of 25 photoelectric and CCD times of minimum light were collected, including 15 primary and 10 secondary eclipses. Those compiled minimum times spread over 18 years from 1999 to 2017. These minima times were used to study (O–C) residuals of V2783 Ori. The (O–C) values were computed with the linear ephemeris which was given in Eq.1.

The corresponding (O–C) curve is shown in Figure 3. It is clearly evident that the (O-C) diagram of V2783 Ori is represented by a sinusoidal variation superimposed on the apsidal motion effect. We assumed that the most likely cause of the sinusoidal variation could be an unseen third body in the system.

The calculations of the apsidal motion rate of the system were made with the computer program written by Zasche et al. (2009), which uses the method described by Giménez & Garcia-Pelayo (1983), with equations revised by Giménez

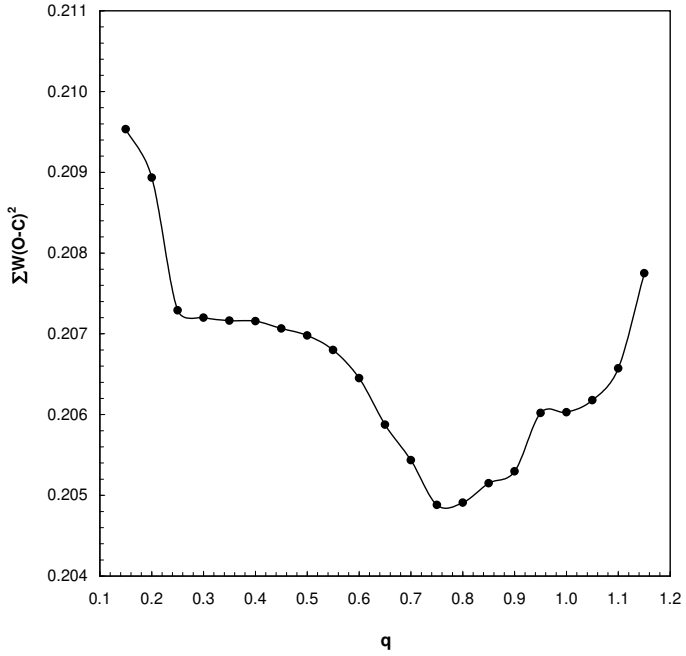


**Figure 2.** Sum of the squared residuals as a function of the mass ratio for V2783 Ori.

& Bastero (1995). The standard approach formulated by Irwin (1959) was used for the light-time effect resulting from the effect of the third body in the system.

Parameters are determined in the following procedures :

For the apsidal motion;

$T_\circ$: The zero epoch (HJD);

$\omega_\circ$: The position of the periastron at the zero epoch;

$P_a$: The anomalistic period;

$P_s$: The sidereal period;

e: The orbital eccentricity;

$\dot{\omega}$: The apsidal motion rate;

U: The apsidal motion period (U = 360 $P_a/\dot{\omega}$);

For the light-time effect

A: The observed semi-amplitude of the light-time curve;

$T_3$ : The time of the periastron passage of the third body;

$a_{12}$ sin $i_3$: The semi-major axis of the relative orbit of the eclipsing pair around the common center of mass;

$e_3$: The eccentricity of the third-body orbit;

$\omega_3$: The longitude of periastron of the third-body orbit.

The computed apsidal motion and the third body parameters with their

errors are presented in Table 3. The observational curves and the theoretical best fit curves, as well as the residuals, are plotted in Figures 3-4.

The apsidal motion rate ($\dot{\omega}$) obtained in this study appears to be statistically significant, 0.0063 ± 0.0017 deg cycle$^{-1}$. This corresponds to an apsidal period of $U = 656 \pm 103$ yr. Using the parameters of the hypothetical three-body orbit in Table 3, we derived that the mass of the third body in the system is 0.82 ± 0.11 $M_\odot$ for $i_3 = 90$ deg.

**Table 3.** Apsidal motion and third body parameters for V2783 Ori.

| Parameter | Unit | Value |
|---|---|---|
| $T_0$ | (HJD) | 2452946.879 ± 0.046 |
| $P_s$ | (day) | 4.21617 ± 0.00007 |
| $P_a$ | (day) | 4.21625 ± 0.00007 |
| $e$ | | 0.253 ± 0.016 |
| $\dot{\omega}$ | (deg/cycle) | 0.0063 ± 0.0017 |
| $\omega_0$ | (deg) | 64.3 ± 3.2 |
| $U$ | (yr) | 656 ± 103 |
| $A$ | (day) | 0.0092± 0.0046 |
| $T_3$ | (HJD) | 2454100± 2100 |
| $P_3$ | (yr) | 10± 2 |
| $e_3$ | | 0.262± 0.087 |
| $\omega_3$ | (deg) | 65.7 ± 2.3 |
| $a_{12} \sin i_3$ | (au) | 1.6± 0.8 |
| $f(M_3)$ | ($M_\odot$) | 0.043± 0.025 |
| $M_{3\,\mathrm{min}}$ | ($M_\odot$) | 0.82 ± 0.11 |

## 5. Conclusions and remarks

The light curve of the eclipsing binary V2783 Ori has been modeled using the W-D method. The analysis has shown that V2783 Ori is a detached binary system with a moderately eccentric orbit.

The absolute parameters of the system cannot be determined directly because no spectroscopic observations were available. But the absolute dimensions for V2783 Ori can be estimated from the empirical relations between temperature and stellar mass. According to the temperature of the primary component, its main sequence mass would be $M_1 = 1.80 \pm 0.01\ M_\odot$ (see Eker et al. (2015)). In this case the mass of the secondary component should be $M_2 = 1.32 \pm 0.01\ M_\odot$ using the mass ratio ($q = 0.734 \pm 0.015$) given in Table 2. The distance between the mass centers of the components would be calculated as $a = 16.1$

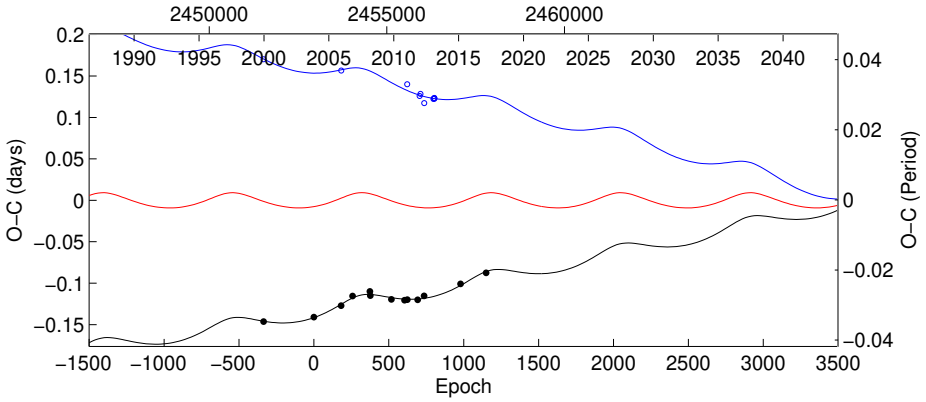


**Figure 3.** The complete (O–C) diagram for mid-eclipse times of V2783 Ori. The solid lines denote combination of the apsidal motion and the third-body LITE. Filled and open symbols represent the individual primary and secondary minima, respectively.

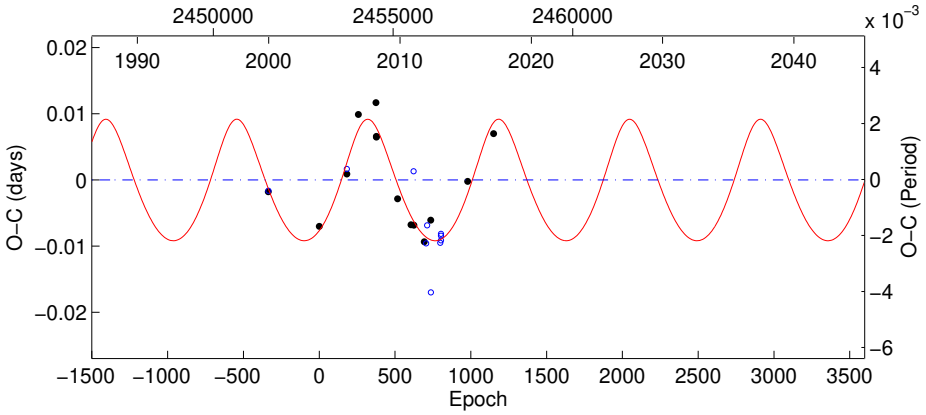


**Figure 4.** The (O–C) diagram of V2783 Ori after subtraction of apsidal motion.

$\pm$ 0.2 $R_{\odot}$ using Kepler's Third Law and the orbital period ($P = 4^d.21617$). By using definition of fractional radii as $r_{1,2} = R_{1,2}/a$ and the mean fractional radii from Table 2 as $r_1 = 0.136 \pm 0.002$ and $r_2 = 0.112 \pm 0.002$, the radius of the primary and secondary components $R_1 = 2.19 \pm 0.10\ R_{\odot}$, $R_2 = 1.91 \pm 0.10\ R_{\odot}$ can be obtained. The absolute dimensions are listed in Table 3. The bolometric corrections (BC) have been adopted from Flower (1996), together with $M_{\odot,bol} = 4.75$ , according to their effective temperatures.

**Table 4.** The absolute parameters of V2783 Ori.

| Parameter | Primary | Secondary |
|---|---|---|
| $M$ ($M_\odot$) | 1.80 ± 0.01 | 1.32 ± 0.01 |
| $R$ ($R_\odot$) | 2.19 ± 0.10 | 1.91 ± 0.10 |
| log $g$ (cgs) | 4.01 ± 0.10 | 4.00 ± 0.10 |
| $T$ (K) | 8325 ± 100 | 8300 ± 100 |
| log $L$ ($L_\odot$) | 1.61 ± 0.02 | 1.55 ± 0.02 |
| $M_{bol}$ | 0.80 ± 0.05 | 1.10 ± 0.06 |
| $a$ ($R_\odot$) | 16.1 ± 0.2 | |
| B.C. | -0.17 | -0.16 |
| $M_v$ | 0.97 ± 0.04 | 1.26 ± 0.04 |
| $d$ (pc) | 1064 ± 150 | |

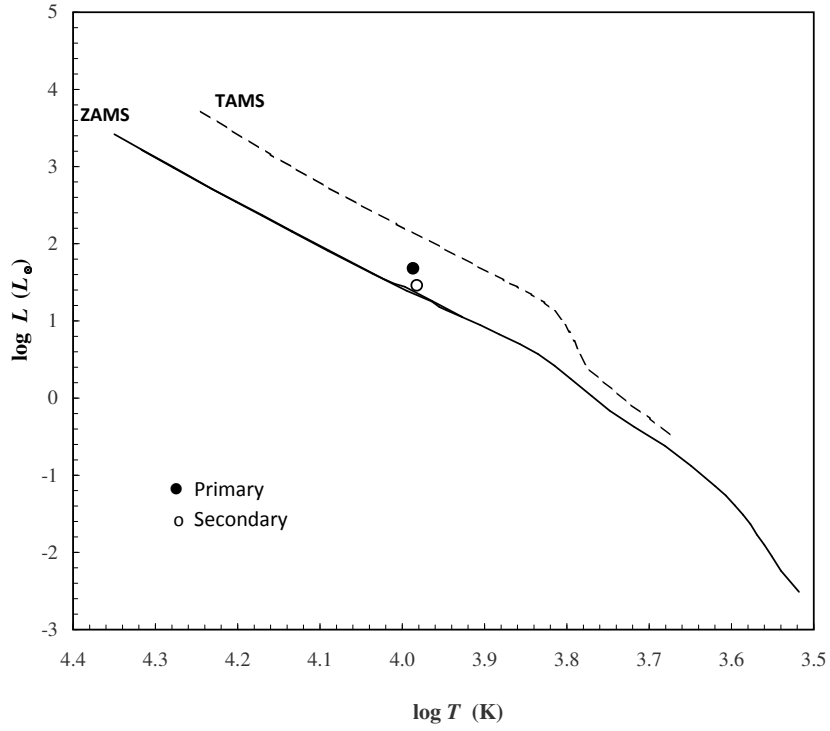


**Figure 5.** Locations of the components of V2783 Ori in the HR diagram. The ZAMS (lower) and the TAMS (upper) lines were taken from (Girardi et al. 2000) for the solar chemical composition. The filled and open symbols represent the primary and secondary stars, respectively.

Computed absolute elements of both the stars, reported in Table 4, are also used to estimate the evolutionary status of V2783 Ori by means of the log $T$-log $L$ (i.e. Hertzsprung-Russell) diagram (in Fig. 5). The Zero Age Main Sequence (ZAMS) and the Terminal Age Main Sequence (TAMS) were obtained from Girardi et al. (2000). As it can be seen from this figure, the primary component of the system is located almost in the middle of ZAMS-TAMS limits, while the secondary component is found to be closer to the ZAMS. According to the mass values of these stars, it seems that the more massive component is more evolved that the less massive one.

The estimate of the interstellar reddening was performed by using maps of dust infrared emission by Schlafly & Finkbeiner (2011). We obtained a colour excess of $E_{(B-V)} = 0.316 \pm 0.006$. Using the colour excess and the apparent visual magnitude of $V = 10.39$ at maximum light, we computed the distance to the V2783 Ori system to be $1064 \pm 150$ pc. This result agrees with the value of $1141 \pm 46$ pc obtained by the trigonometric parallax ($0.876 \pm 0.035$ mas) from Gaia EDR3 (Gaia Collaboration et al. 2021).

Analysing the (O-C) diagram, we solved the apsidal motion and the light-time effect (LITE) simultaneously. The apsidal motion rate ($\dot{\omega}$) obtained in this study appears to be statistically significant, $0.0063 \pm 0.0017$ deg cycle$^{-1}$. This corresponds to an apsidal period of $U = 656 \pm 103$ yr. The observational average value (log $k_{2,obs}$) of the internal structure constant can be calculated from the apsidal motion period with the absolute dimensions. We found the general relativistic contribution within the total apsidal motion rate, approximately 7.6% of the observed value. After making this correction, we calculated log $k_{2,obs} = 2.04$ with an assumption of the periastron-synchronization.

Using the standard solar composition (Y, Z) = (0.28, 0.02) models of Claret (2004), we obtained an average theoretical internal structure constant value $k_{2,teo} = 2.40$ by the interpolation. According to these results, the observational mean central density concentration for V2783 Ori seems to be smaller than that predicted by Claret (2004) models.

The invisible component around the V2783 Ori has a period of $P_3 = 10 \pm 2$ yr, an eccentricity of $e_3 = 0.262 \pm 0.087$, and its mass is $M_3 = 0.82 \pm 0.19$ $M_\odot$, which could be a main–sequence star. The third-body mass corresponds to a spectral type of about K5.5V, and the bolometric luminosity is calculated to be $L_3 = 0.36$ $L_\odot$ (see Eker et al. (2015); Pecaut & Mamajek (2013)), which contributes about 0.6 % to the total luminosity of V2783 Ori. This contribution is negligibly small.

Future spectroscopic observations will help to a more complete understanding of the system.

**Acknowledgements.** The author would like to thank an anonymous referee who provided valuable comments for improving the manuscript.

## References

Bulut, A., Bulut, I., Ciçek, C., & Erdem, A., Apsidal motion of two eclipsing binaries: V796 Cyg and V2783 Ori. 2017, in American Institute of Physics Conference Series, Vol. **1815**, *Turkish Physical Society 32nd International Physics Congress*, 080007

Casagrande, L., Ramírez, I., Meléndez, J., Bessell, M., & Asplund, M., An absolutely calibrated $T_{eff}$ scale from the infrared flux method. Dwarfs and subgiants. 2010, *Astronomy and Astrophysics*, **512**, A54, DOI: 10.1051/0004-6361/200913204

Claret, A., New grids of stellar models including tidal-evolution constants up to carbon burning. I. From 0.8 to 125 $M_{\odot}$ at Z=0.02. 2004, *Astronomy and Astrophysics*, **424**, 919, DOI: 10.1051/0004-6361:20040470

Claret, A. & Giménez, A., The apsidal motion test of the internal stellar structure: comparison between theory and observations. 1993, *Astronomy and Astrophysics*, **277**, 487

Cutri, R. M., Skrutskie, M. F., van Dyk, S., et al., VizieR Online Data Catalog: 2MASS All-Sky Catalog of Point Sources (Cutri+ 2003). 2003, *VizieR Online Data Catalog*, II/246

Eker, Z., Soydugan, F., Soydugan, E., et al., Main-Sequence Effective Temperatures from a Revised Mass-Luminosity Relation Based on Accurate Properties. 2015, *Astronomical Journal*, **149**, 131, DOI: 10.1088/0004-6256/149/4/131

Flower, P. J., Transformations from Theoretical Hertzsprung-Russell Diagrams to Color-Magnitude Diagrams: Effective Temperatures, B-V Colors, and Bolometric Corrections. 1996, *Astrophysical Journal*, **469**, 355, DOI: 10.1086/177785

Gaia Collaboration, Brown, A. G. A., Vallenari, A., et al., Gaia Early Data Release 3. Summary of the contents and survey properties. 2021, *Astronomy and Astrophysics*, **649**, A1, DOI: 10.1051/0004-6361/202039657

Giménez, A., General-relativistic periastron advances in eclipsing binary systems. 1985, *Astrophysical Journal*, **297**, 405, DOI: 10.1086/163539

Giménez, A. & Bastero, M., A Revision of the Ephemeris-Curve Equations for Eclipsing Binaries with Apsidal Motion. 1995, *Astrophysics and Space Science*, **226**, 99, DOI: 10.1007/BF00626903

Giménez, A. & Garcia-Pelayo, J. M., A New Method for the Analysis of Apsidal Motions in Eclipsing Binaries. 1983, *Astrophysics and Space Science*, **92**, 203, DOI: 10.1007/BF00653602

Girardi, L., Bressan, A., Bertelli, G., & Chiosi, C., Evolutionary tracks and isochrones for low- and intermediate-mass stars: From 0.15 to 7 $M_{sun}$, and from Z=0.0004 to 0.03. 2000, *Astronomy and Astrophysics, Supplement*, **141**, 371, DOI: 10.1051/aas:2000126

Høg, E., Fabricius, C., Makarov, V. V., et al., The Tycho-2 catalogue of the 2.5 million brightest stars. 2000, *Astronomy and Astrophysics*, **355**, L27

Irwin, J. B., Standard light-time curves. 1959, *Astronomical Journal*, **64**, 149, DOI: 10.1086/107913

Lucy, L. B., The Structure of Contact Binaries. 1968, *Astrophysical Journal*, **151**, 1123, DOI: 10.1086/149510

Otero, S. A., Wils, P., & Dubovsky, P. A., New Eclipsing Binaries Found in the NSVS Database I. 2004, *Information Bulletin on Variable Stars*, **5570**, 1

Paschke, A. & Brat, L., O-C Gateway, a Collection of Minima Timings. 2006, *Open European Journal on Variable Stars*, **23**, 13

Pecaut, M. J. & Mamajek, E. E., Intrinsic Colors, Temperatures, and Bolometric Corrections of Pre-main-sequence Stars. 2013, *Astrophysical Journal, Supplement*, **208**, 9, DOI: 10.1088/0067-0049/208/1/9

Pojmanski, G., The All Sky Automated Survey. The Catalog of Variable Stars. II. $6^{\rm h}$-$12^{\rm h}$ Quarter of the Southern Hemisphere. 2003, *Acta Astronomica*, **53**, 341

Prša, A. & Zwitter, T., A Computational Guide to Physics of Eclipsing Binaries. I. Demonstrations and Perspectives. 2005, *Astrophysical Journal*, **628**, 426, DOI: 10.1086/430591

Ramírez, I. & Meléndez, J., The Effective Temperature Scale of FGK Stars. II. $T_{eff}$:Color:[Fe/H] Calibrations. 2005, *Astrophysical Journal*, **626**, 465, DOI: 10.1086/430102

Schlafly, E. F. & Finkbeiner, D. P., Measuring Reddening with Sloan Digital Sky Survey Stellar Spectra and Recalibrating SFD. 2011, *Astrophysical Journal*, **737**, 103, DOI: 10.1088/0004-637X/737/2/103

van Hamme, W., New Limb-Darkening Coefficients for Modeling Binary Star Light Curves. 1993, *Astronomical Journal*, **106**, 2096, DOI: 10.1086/116788

Wilson, R. E. & Devinney, E. J., Realization of Accurate Close-Binary Light Curves: Application to MR Cygni. 1971, *Astrophysical Journal*, **166**, 605, DOI: 10.1086/150986

Zahn, J. P., Tidal dissipation in binary systems. 2008, in EAS Publications Series, Vol. **29**, *EAS Publications Series*, ed. M. J. Goupil & J. P. Zahn, 67–90

Zasche, P., Liakos, A., Niarchos, P., et al., Period changes in six contact binaries: WZ And, V803 Aql, DF Hya, PY Lyr, FZ Ori, and AH Tau. 2009, *New Astronomy*, **14**, 121, DOI: 10.1016/j.newast.2008.06.002

PRÁCE ASTRONOMICKÉHO OBSERVATÓRIA
NA SKALNATOM PLESE
LI, číslo 2

| | |
|---|---|
| Zostavovateľ: | RNDr. Richard Komžík, CSc. |
| Vedecký redaktor: | RNDr. Augustín Skopal, DrSc. |
| Vydal: | Astronomický ústav SAV, Tatranská Lomnica |
| IČO vydavateľa: | 00 166 529 |
| Periodicita: | 3-krát ročne |
| ISSN (on-line verzia): | 1336-0337 |
| CODEN: | CAOPF8 |
| Rok vydania: | 2021 |
| Počet strán: | 78 |

Contributions of the Astronomical Observatory Skalnaté Pleso are processed using
LaTeX 2ε CAOSP DocumentClass file 3.08 ver. 2020.